

**Chemical Interactions of Hydraulic Fracturing Biocides with Natural Pyrite**

Submitted in partial fulfillment of the requirements for

the degree of

Doctor of Philosophy

in

Civil and Environmental Engineering

Nizette A. Consolazio

B.S.E., Chemical and Biological Engineering, Princeton University  
M.S., Civil and Environmental Engineering, Carnegie Mellon University

Carnegie Mellon University  
Pittsburgh, PA

September, 2017

© Nizette A. Consolazio, 2017  
All Rights Reserved

## **Acknowledgements**

This work was initially performed as part of the National Energy Technology Laboratory's Regional University Alliance (NETL-RUA) under the RES contract DE-FE0004000. Subsequent support for tuition and research was provided by the Oak Ridge Associated Universities (ORAU) Oak Ridge Institute for Science and Education (ORISE) Fellowships (2013 & 2015), as well as the Athanasios Karamalidis Discretionary Funds. Additional funding was awarded by the Carnegie Mellon University (CMU) College of Engineering Dean's Fellowship (2013); Scott Institute ProSEED/EQT Energy Seed Grant (2016); the Anchor QEA Scholarship Fund (2016); and the CMU Provost Graduate Student Grant (2017).

I would like to thank my advisors Dr. Athanasios Karamalidis (committee chair) and Dr. Gregory Lowry. I could not have asked for two better experts in to guide me through this work. Dr. Karamalidis has always been ready to answer my questions, talk me through a procedure, and walk with me through the long process of organizing my thoughts and words. There has never been a detail that was too small for his time. Dr. Lowry has always challenged me to think bigger, write better and do more. He is a true role model and teacher. Together, they have encouraged me to grow and inspire me to never stop learning.

I would also like to thank my committee members for their guidance and support. Dr. Alexandra Hakala has never ceased to lend her support to this work. I am grateful for her ideas and her broad knowledge of the field which has been a welcome counterbalance to the minutiae of my work. Despite his extremely busy schedule, Dr. Dave Dzombak has been always been willing to offer valuable insights on this project. His work on pyrite has been invaluable in the

conducting and designing of experiments and has helped me to piece together the “why” behind the “what”.

I am so grateful for all the peers who have walked with me at CMU: Eric McGivney, Aniela Burant, Clint Noack, Lauren Bergman, Adam Cadwallader, Joe Moore, Megan Leitch, Hari Parthasarathy, Kai Chucherdwatanasak, Corey Harper, Kedar Perkins, Erin Dauson, Djuna Gulliver, Eleanor Spielman-Sun, Pengyun Wang, Alex Bertuccio, Ann Johannson, Tyrica Terry, Yajie Guo, Greg Healy, Alexia Michel. There is not enough space to mention how you have all contributed to my experience over the last four years. It has been an honor to have learnt from you all. You give me hope that the future will be bright. The only downside is that I will miss those days we spent together, doing problem sets, in Journal Club, discussing experiments and just being friends.

There is no way I would have navigated this PhD without the unfailing support of Maxine Leffard and Ron Ripper. Maxine’s patience has always been a refuge. Even when that I had not followed up on her last several emails or when she was tired, she has never had anything less than a smile for me. The Hauck labs would crumble without Ron. All of the analytical instruments would cease to function, and there would be no monthly donuts. I am grateful for them both for showing us all what it means to work from the heart.

And most important of all, I would like to thank my family. Adjani Peralta is a sister to me, always there for me, even when we were separated by half the globe. I am grateful for my aunt and cousins here in the US with me, who constantly remind me of who I am and the strength that we all share. My parents Nigel Edwards and Germaine Suzette De Silva have given me so much love and support over the years. Words cannot express how much I love them. And finally, I would like to thank Justin, my husband. He has shared with me his infectious love of life, laughter and learning. But more than anything he has taught me the deepest lesson of all by embodying the words of Thich Nhat Hanh, “Happiness is available. Please help yourself.”

## **Abstract**

In conjunction with horizontal drilling, hydraulic fracturing or fracking has enabled the recovery of natural gas from low permeable shale formations. In addition to water, these fracking fluids employ proppants and up to 38 different chemical additives to improve the efficiency of the process.

One important class of additives used in hydraulic fracturing is biocides. When applied appropriately, they limit the growth of harmful microorganisms within the well, saving energy producers 4.5 billion dollars each year. However, biocides or their harmful daughter products may return to the surface in produced water, which must then be appropriately stored, treated and disposed of.

Little is known about the effect of mineral-fluid interactions on the fate of the biocides employed in hydraulic fracturing. In this study, we employed laboratory experiments to determine changes in the persistence and products of these biocides under controlled environments. While many minerals are present in shale formations, pyrite,  $\text{FeS}_{2(s)}$  is particularly interesting because of its prevalence and reactivity. The  $\text{Fe}^{\text{II}}$  groups on the face of pyrite may be oxidized to form  $\text{Fe}^{\text{III}}$  phases. Both of these surfaces have been shown to be reactive with organic compounds. Chlorinated compounds undergo redox reactions at the pyrite-fluid interface, and sulfur-containing compounds undergo exceptionally strong sorption to both pristine and oxidized pyrite. This mineral may significantly influence the degradation of biocides in the Marcellus Shale. Thus, the overall goal of this study was to understand the effect of pyrite on biocide reactivity in hydraulic fracturing, focusing on the influence of pyrite on specific functional groups.

The first specific objective was to demonstrate the effect of pyrite and pyrite reaction products on the degradation of the bromine-containing biocide, DBNPA. On the addition of pyrite to DBNPA, degradation rates of the doubly brominated compound were found to increase significantly. DBNPA is proposed to undergo redox reactions with the pyrite surface, accepting two-electrons from pyrite, and thus becoming reduced. The primary product is the monobrominated analogue of DBNPA, 2-monobromo-3-nitrilopropionamide (or MBNPA). The surface area-normalized first-order initial degradation rate constant was found to be  $5.1 \text{ L}\cdot\text{m}^{-2}\cdot\text{day}^{-1}$ . It was also determined that the dissolution and oxidation products of pyrite,  $\text{Fe}^{\text{II}}$ ,  $\text{S}_2\text{O}_3^{2-}$  and  $\text{SO}_4^{2-}$  are unlikely to contribute to the reduction of the biocide. Taken together, the results illustrate that a surface reaction with pyrite has the ability to reduce the persistence of DBNPA, and as a consequence change the distribution of its reaction products.

The second objective was to quantify the influence of water chemistry and interactions with pyrite on the degradation of the sulfur-containing biocide. Dazomet readily hydrolyzes in water due to the nucleophilic attack of hydroxide ( $\text{OH}^-$ ) anions. Thus the half-life of dazomet during the shut-in phase of hydraulic fracturing will decrease with increasing pH: 8.5 hours at pH 4.1 to 3.4 hours at pH 8.2. Dazomet degradation was rapidly accelerated upon exposure to the oxidized pyrite surface, reacting five times faster than hydrolysis in the absence of pyrite at a similar pH. The products measured were identical to those identified on hydrolysis (methyl isothiocyanate and formaldehyde) and no dissolved iron was detected in solutions. This suggests that the dithiocarbamate group in dazomet was able to chemisorb onto the oxidized pyrite surface, shifting the electron density of the molecule which resulted in accelerated hydrolysis of the biocide.

The third objective explored the reactivity of various biocide functional groups due to the addition of pyrite. Several elimination mechanisms were identified, and tied to the reactivity of the specific functional group involved. The addition of pyrite led to accelerated degradation of

dibromodicyanobutane. This is because the bromine (-Br) group is easily reduced. For methylene bis(thiocyanate), hydrolysis was a noteworthy elimination mechanism since the thiocyanate (-SCN) functionality is a good leaving group. Benzisothiazolinone and methyl isothiazolinone were stable at low pH due to the stabilizing donor-acceptor interactions between the organic biocides' carbonyl ( $-C=O$ ) groups and salts in the solution.

This body of work has illustrated that pristine pyrite can undergo redox reactions with brominated biocides used in hydraulic fracturing, reducing their persistence and altering the product distribution. This will change the efficacy and the risks associated with the use of these biocides in shales containing pyrite, particularly at lower pH where organic compounds are more stable to hydrolysis. However, at higher pH hydrolysis becomes more important, and additional studies will need to be conducted to investigate the pyrite contribution under these conditions. Conversely, the  $Fe^{III}$  surface groups on oxidized pyrite can catalyze the hydrolysis of dazomet and may do so for other labile, sulfur-containing biocides as well. Overall, this research has shown that the physicochemical properties (such as the acid dissociation constant and the standard reduction potential) that govern the environmental reactivity of a molecule can be used to anticipate its reactivity in hydraulic fracturing.

# Table of Contents

<b>Acknowledgements</b> .....	<b>iii</b>
<b>Abstract</b> .....	<b>v</b>
<b>List of Tables</b> .....	<b>xiii</b>
<b>List of Figures</b> .....	<b>xv</b>
<b>Chapter 1 Introduction, Problem Identification, and Research Objectives</b> .....	<b>1</b>
1.1 Introduction .....	2
1.2 Problem Identification .....	4
1.3 Research Objectives .....	6
1.4 Thesis Organization .....	9
1.5 References .....	10
<b>Chapter 2 Review of mineral and biocide properties influencing biocide sorption and transformation in the Marcellus Shale</b> .....	<b>14</b>
2.1 Abstract .....	15
2.2 Introduction .....	17
2.3 Common biocides used in the Marcellus Shale .....	19
2.3.1 Physical and chemical properties of biocides .....	19
2.3.2 Mechanisms for sorption .....	25
2.4 Mineralogy of the Marcellus Shale.....	28

2.5	Quartz.....	29
2.5.1	Sorption to quartz .....	30
2.5.2	Transformation due to quartz.....	31
2.6	Clays .....	31
2.6.1	Sorption to clays.....	33
2.6.2	Transformation with clays .....	35
2.7	Carbonates .....	37
2.7.1	Sorption to carbonates .....	38
2.7.2	Transformation with carbonates.....	40
2.8	Sulfides.....	40
2.8.1	Sorption to pyrite .....	42
2.8.2	Transformation with pyrite.....	44
2.9	Organic matter .....	45
2.9.1	Sorption to kerogen.....	46
2.9.2	Transformation with kerogen .....	48
2.10	Perspective on Mineral-Fluid Interactions of Biocides .....	48
2.11	References .....	52
<b>Chapter 3</b>	<b>Pyrite-induced reduction of organobromide biocides: Case Study of DBNPA.....</b>	<b>62</b>
3.1	Abstract .....	63
3.2	Introduction .....	64
3.3	Background on DBNPA.....	66

3.4	Methods.....	68
3.4.1	Materials .....	68
3.4.2	Pyrite preparation .....	69
3.4.3	Batch experiments .....	69
3.4.4	Analytical Methods .....	70
3.5	Results.....	70
3.5.1	Effect of pyrite loading on the rate of degradation.....	70
3.5.2	Change in DBNPA reaction products due to pyrite .....	73
3.5.3	Effect of Fe <sup>II</sup> .....	74
3.5.4	Effect of other salts .....	75
3.5.5	Effect of sulfur oxyanions .....	78
3.6	Discussion .....	79
3.7	References.....	82
<b>Chapter 4</b>	<b>Abiotic degradation of dazomet: hydrolysis and degradation with pyrite .....</b>	<b>85</b>
4.1	Abstract .....	86
4.2	Introduction .....	87
4.3	Methods and Materials .....	88
4.3.1	Chemicals .....	88
4.3.2	Batch reactors .....	89
4.3.3	Pyrite preparation .....	90
4.3.4	Dazomet reaction rate analysis .....	90
4.3.5	Dazomet reaction products.....	91

4.4	Results.....	92
4.4.1	Effect of pH on the removal of dazomet .....	92
4.4.2	Effect of dissolved species on the removal of dazomet.....	93
4.4.3	Effect of dissolved species on the removal of dazomet.....	94
4.4.4	Effect of temperature on the removal of dazomet .....	95
4.4.5	Catalysis due to oxidized and unoxidized pyrite.....	98
4.4.6	Analysis of hydrolysis products .....	99
4.5	Discussion .....	101
4.6	References .....	106
<b>Chapter 5</b>	<b>Pyrite-induced reduction of four hydraulic fracturing biocides: the effect of selected functional groups on reactivity .....</b>	<b>110</b>
5.1	Abstract .....	111
5.2	Introduction .....	112
5.3	Methods and Materials .....	115
5.3.1	Materials .....	115
5.3.2	Preparation of pyrite .....	115
5.3.3	Batch experiments .....	116
5.3.4	Analysis of dibromodicyanobutane. ....	116
5.3.5	Analysis of methylene bis(thiocyanate) .....	117
5.3.6	Analysis of benzisothiazolinone and methyl isothiazolinone .....	117
5.4	Results.....	118
5.4.1	Degradation of DBDCB.....	118
5.4.2	Degradation of MBT.....	120

5.4.3	Degradation of the isothiazoliones: BIT and MIT .....	121
5.5	Discussion .....	122
5.6	References .....	125
<b>Chapter 6</b>	<b>Conclusions and recommendations for future work .....</b>	<b>127</b>
6.1	Overall conclusions .....	128
6.2	Summary of novel contributions.....	131
6.3	Suggestions for future work .....	132
6.4	References .....	137
<b>Appendix A</b>	<b>Supporting information for Chapter 3 .....</b>	<b>139</b>
<b>Appendix B</b>	<b>Supporting information for Chapter 4 .....</b>	<b>145</b>
<b>Appendix C</b>	<b>Supporting information for Chapter 5 .....</b>	<b>150</b>
<b>Appendix D</b>	<b>Structure-reactivity relationships to predict pyrite induced reduction of organic compounds.....</b>	<b>153</b>
D.1	Background on structure-activity relationships .....	154
D.2	References .....	157

## List of Tables

Table 2-1. The common name, CAS number, structural and physical properties of biocides selected for this study. ....	20
Table 2-2. The number of biocides containing at least one of functional groups and structural arrangements identified.....	24
Table 2-3. Organic functional groups and organic compounds shown to chemisorb onto carbonates, pristine pyrite, and oxidized pyrite surfaces .....	50
Table 3-1. Zero- and first-order degradation rates for experiments containing 5, 10 and 15 g/L of pyrite. ....	72
Table 3-2. Constants for complexation with OH <sup>-</sup> (log *K <sub>1</sub> ) and NH <sub>3</sub> (log K <sub>NH3</sub> ) for divalent metal ions considered in this study. ....	78
Table 4-1. Pseudo first-order rate constant for the hydrolysis of dazomet under varying, pH, temperature dissolved iron (II), dazomet concentration, dissolved sodium and oxygen removal, along with the corresponding calculated lifetimes.....	97
Table 4-2. The key physicochemical properties and biodegradability of biocides used in hydraulic fracturing operations.....	101
Table 5-1. The abbreviation, structural and physical properties of biocides selected for this chapter.. ....	113
Table 5-2. The functional groups of DBDCB and MBT, and the acid dissociation constant (pK <sub>a</sub> ) of the conjugate acids.....	123
Table 5-3. The functional groups of DBDCB and MBT, and the standard redox potential for the corresponding dimer.....	123
Table A-1. Data for Figures 3-2 and 3-4 .....	140
Table A-2. Data for Figure 3-5.....	141

Table A-3. Data for control/blank and NaCl samples in Figures 3-6, 3-7, and 3-8 .....	142
Table A-4. Data for Figures 3-6 and 3-7 .....	143
Table A-5. Data for Figure 3-8 .....	144
Table B-1. Data for Figure 4-2 .....	146
Table B-2. Data for Figure 4-3 .....	147
Table B-3. Data for Figure 4-4 .....	148
Table B-4. Data for Figure 4-6 .....	149
Table C-1. Data for Figure 5-1 .....	151
Table C-2. Data for Figure 5-3 .....	152
Table C-3. Data for Figure 5-4 .....	152

## List of Figures

Figure 1-1. Flowchart illustrating the relationships between research goals, objectives and tasks completed in the dissertation. ....	7
Figure 2-1. Heat map displaying the reactivity of each biocide and the occurrence of each identified functional group and structural arrangement. ....	23
Figure 2-2. Illustration of possible sorption mechanisms of organic biocides onto mineral surfaces .....	26
Figure 2-3. (a) Classification of biocide used in the Marcellus Shale according to dissociation in aqueous solutions. (b) Changes in net charge of cationic, neutral, basic and acidic biocides with pH. ....	28
Figure 2-4. Flow chart classifying the major minerals of Marcellus Shale minerals. ....	29
Figure 2-5. (a) Molecular structure of carbosulfan, indicating points of sorption to clay surfaces (b) Molecular structure of primicarb.....	37
Figure 2-6. Molecular structures of pyrite collectors and biocides with similar-sulfur-containing groups. ....	43
Figure 2-7. Reductive dechlorination of chlorinated ethenes by pyrite. ....	44
Figure 2-8. A summary of physisorption mechanisms controlling the sorption of the assigned biocide classes to quartz, clays and carbonates.....	49
Figure 3-1. Reaction scheme illustrating two proposed degradation pathways for the biocide DBNPA. Base-catalyzed hydrolysis (Pathway 1) leads to dibromoacetonitrile (DBAN). Reduciton by nucleophilic elimination (Pathway 2) leads to monobromonitrilopropiamide (MBNPA). ....	68
Figure 3-2. Fraction of DBNPA remaining as a function of time (h), in aqueous suspensions of 0 g/L, 5 g/L, 10 g/L and 15 g/L of pyrite (FeS <sub>2</sub> ).. ....	71

Figure 3-3. The effect of pyrite concentration on the pseudo-first order degradation rate of DBNPA.....	73
Figure 3-4. Measured monobromonitrilopropiamide (MBNPA) concentrations as a function of DBNPA converted in 0 g/L, 5 g/L, 10 g/L and 15 g/L of pyrite.....	74
Figure 3-5. The concentration of DBNPA as a function of time (h) in the presence and absence of equal moles of FeCl <sub>2</sub> .....	75
Figure 3-6. Fraction of DBNPA remaining as a function of time (h), in the presence of 1 mM CuCl <sub>2</sub> , 1 mM NiCl <sub>2</sub> , 2 mM NaCl and control (containing no chloride salt). ....	76
Figure 3-7. Measured monobromonitrilopropiamide (MBNPA) and dibromoacetoneitrile (DBAN) concentrations in the presence of 1 mM CuCl <sub>2</sub> , 1 mM NiCl <sub>2</sub> , 2 mM NaCl and control (containing no chloride salt).....	77
Figure 3-8. Fraction of DBNPA remaining as a function of time (h), in the presence of 1 mM Na <sub>2</sub> S <sub>2</sub> O <sub>3</sub> , 1 mM Na <sub>2</sub> SO <sub>4</sub> , 2 mM NaCl and control (containing no sodium salt).....	79
Figure 3-9. Proposed two-electron pathway for the reduction of DBNPA to MBNPA, highlighting the anionic intermediate.....	80
Figure 4-1. Structures of the key hydrolysis and metabolized products of dazomet as reported by Roberts and Hudson (1999).....	88
Figure 4-2. (a) The hydrolytic degradation of dazomet as a function of time (h), at pH 3.4, 4.1, 8.2 and 9.5 according to pseudo-first order kinetics (b) Dazomet half-life as a function of pH, calculated from the data in (a).....	93
Figure 4-3. The degradation of dazomet as a function of time (h) in the presence of 0 mM, 0.4 mM and 0.8 mM dissolved Fe <sup>II</sup> according to pseudo-first order kinetics.....	94
Figure 4-4. Temperature dependence of the degradation of dazomet as a function of time (h), conducted at four temperatures (34°C, 49°C and 57°C). ....	96

Figure 4-5. Plot of $\ln k$ as a function of $1000/T$ to estimate the activation energy of dazomet hydrolysis.....	97
Figure 4-6. Fraction of dazomet remaining as a function of time (h), in aqueous suspensions of 0 g/L pyrite, 20 g/L unoxidized (acid washed) pyrite and 20 g/L of pyrite ( $\text{FeS}_2$ ).....	99
Figure 4-7. Dazomet degradation and production of major hydrolysis products formaldehyde (HCHO), hydrogen sulfide, and methyl isothiocyanate as a function of time (h).....	100
Figure 4-8. Projected percentage decrease and increase of dazomet half-lives due to varying compositions of dissolved $\text{Fe}^{\text{II}}$ , temperature and pH. ....	102
Figure 4-9. Comparison of hydrolysis half-lives determined in this study to those in previously published results as a function of pH. ....	103
Figure 4-10. The structure of dazomet, the Marcellus Shale biocide of interest and a generic xanthate, a common collector used for the flotation of pyrite. ....	104
Figure 5-1. Fraction of DBDCB remaining as a function of time (h), in aqueous suspensions of 0 g/L, 5 g/L, 10 g/L and 15 g/L of pyrite ( $\text{FeS}_2$ ). ....	119
Figure 5-2. EI-MS spectrum of the main product of DBDCB, 2-methyleneglutaronitrile (or 2-methylenepentanedinitrile). ....	120
Figure 5-3. Fraction of MBT remaining as a function of time (h), in aqueous suspensions of 0 g/L and 100 g/L of pyrite ( $\text{FeS}_2$ ).....	121
Figure 5-4. Fraction of MIT and BIT remaining as a function of time (h), in aqueous suspensions of 0 g/L and 100 g/L of pyrite ( $\text{FeS}_2$ ). ....	122
Figure D-1. Best fit for the Langmuir-Hinshelwood (LH) reduction rate constant of chlorinated ethenes with pyrite as a function the $E_{\text{LUMO}}$ of the chlorinated ethenes (AM1 semi-empirical method). ....	155

**Chapter 1**      **Introduction, Problem Identification, and  
Research Objectives**

## **1.1 Introduction**

Hydraulic fracturing (fracking) and horizontal drilling have enabled the extraction of natural gas from low permeable shales, allowing the US to tap into reserves of 176 trillion cubic feet of natural gas (US EIA, 2016a). Although hydraulic fracturing has been around since the 1940s (Montgomery & Smith, 2010; Yan, et al., 2011), the successful incorporation of horizontal drilling has resulted in its recent increase in productivity and popularity. Once considered an “unconventional” form of resource extraction, this technology is quickly becoming the norm. In 2016 alone 6,900 wells were fractured in shale formations across the country, generating 17 trillion cubic feet of natural gas (US EIA, 2017). The technology has brought about substantial benefits to the US: significantly lower natural gas prices and a decrease in dependence on coal (Loomis and Haefele, 2017). By the year 2040, shale gas production is expected to triple, accounting for over 50% of US gas production (US EIA, 2016b).

To access the natural gas in the low permeable shale, the technique relies upon greatly increasing the exposed surface area within the gas reservoir. Energy producers capitalize on horizontal drilling, which can extend 1 or 2 miles from the vertical well-bore (Yan et al., 2011). Following this, roughly 1.5 million gallons of fracking fluid are pumped into each well at pressures exceeding the tensile strength of the rock. In addition to water, these fracking fluids employ proppants and up to 38 different chemical additives such as corrosion inhibitors, friction reducers, surfactants and biocides (U.S. EPA, 2015). These chemical additives are employed at concentrations of about 1% to improve the recovery of natural gas of the fracking fluid. The fluid is held in the well for a few days to a month. The high pressures result in fractures throughout the formation, which allow the natural gas to flow (King, 2012; Carter et al., 2011; Fakcharoenphol et al., 2013). Some fraction of this water, along with chemical residues, returns to the surface as flowback water, along with native formation water.

Collectively, this is termed produced water, which is considered a waste. This waste stream must then be disposed of, or if economically infeasible, primed for reuse (Shaffer et al., 2013).

It follows that sourcing fresh water for fracking fluids and treating waste water from the process are two of the biggest issues related to the technology. Hydraulic fracturing requires large amounts of water and this may add pressure to already water-stressed regions (Walker et al., 2017; Vengosh et al., 2014). In addition, the well generates produced water over the course of its lifetime and is the largest waste stream associated with gas production (Judd et al., 2014). Calculations suggest that 150 billion gallons of water is produced from unconventional oil and gas extraction each year (Thiel et al., 2015). This produced water contains high concentrations of dissolved solids, pH ranging from 5.1 to 8.4 and can also contain the residuals of chemicals used in the fracking fluid (Luek and Gonsior, 2017; Barbot et al., 2013; Orem et al., 2014; Gregory et al., 2011). Typically, this produced water is deposited into regulated Class II deep well injection sites. Recently, due to a combination of high costs of fresh water and limited options for safe disposal of produced water, the latter is reused: treated, blended with fresh surface water and pumped back into the shale (Shaffer et al., 2013; Akyon et al., 2015).

Biocides form a vital class of chemical additives in the hydraulic fracturing water cycle as they control the growth of bacteria within the well. Bacteria can be harmful as they may generate hydrogen sulfide ( $H_2S$ ) which increases production costs, and cause microbially induced corrosion (MIC) of materials within the well. The successful use of biocides saves energy producers 4.5 billion dollars each year (Javaherdashti, 1999; Adesina et al., 2015). They are critical for keeping wells in service for their expected lifetime of 15 years or longer (O'Sullivan and Paltsev, 2012). Biocides are used to sterilize the surface water that is needed for fracking and added to the well for long-term disinfection. They may also be mixed into produced water while stored in holding ponds and before being pumped back into the shale for reuse (BASF, 2000). This work investigates the reactivity of selected biocides used in hydraulic fracturing.

## 1.2 Problem Identification

It is clear that fracking has been beneficial for the US economy. However, questions still linger over the environmental impact of chemical usage. Exposure to these chemicals may occur under one of two circumstances: either due to spills of chemicals at the surface prior to injection; or due to inadequate storage and disposal of flowback water. While the former can be prevented by following industry best practices, the risks due to flowback fluid can only be managed by thorough characterization of this waste stream. Studies have shown that this fluid contains hazardous substance that may adversely affect human and ecological health (McKenzie et al., 2012; Ferrar et al. 2013; Zhang et al., 2015). In addition to changes in pH and salinity, research has shown that many of the organic compounds in the initial fracturing fluid do not return in produced water, suggesting that adsorption or chemical transformations may take place in the subsurface (Carter et al., 2013). This study will investigate some of these reactions and aid decision makers in adopting best practices for produced water reuse and disposal.

While the behavior of many biocides has been studied under surface conditions, little is known about the effect of mineral-fluid interactions on the fate of these compounds (Kahrilas et al, 2015). For biocides, this is particularly important for two main reasons. First, an understanding of sorption and transformation reactions will contribute to our knowledge of the efficacy of these biocides under specific formation conditions. Second, identifying these reactions and their corresponding reaction products will also aid in pinpointing biocides or harmful daughter products returning to the surface in produced water. By developing a more fundamental understanding of biocide reactivity, energy producers can improve the efficacy of microbial treatments while limiting adverse effects of this burgeoning technology.

Many studies have attempted to investigate mineral-fluid interactions by comparing the components of produced water to that of the fracking fluid (Orem et al., 2014; Ferrer and Thurman, 2015; Hoelzer et al., 2016). However, these matrices are challenging to analyze and

thus, researchers find it difficult to elucidate specific mechanisms in this way. The most promising approach is to perform laboratory experiments to determine changes under a controlled environment. Several studies have also looked at core samples testing various formation conditions (Tasker et al., 2016; Paukert Vankeuren et al., 2017; Marcon et al., 2017; Harrison et al., 2017). These have generated much needed information regarding changes to porosity and mineral surfaces, but offer little insight into the behavior of biocides.

While many minerals are present in shale formations, this research will focus on pyrite,  $\text{FeS}_{2(s)}$  because of its prevalence and reactivity. In the first coordination sphere, the Fe atoms are surrounded by six S neighbors, in a distorted octahedral arrangement. The Fe ions should be considered to be in a low spin divalent state rather than in tetravalent state as the stoichiometry would suggest. Pyrite formation naturally occurs under oxygen-depleted conditions (Berner, 1984), which also support the accumulation of organic matter, the ultimate source of natural gas. Consequently pyrite is often prevalent in black shales, occurring at up to 24 vol% in some parts of the Marcellus Shale, which is currently the largest producer of shale gas in the world (Wang & Carr, 2012, US EIA, 2016b). Pyrite also is present in other producing shale formations throughout the United States (Chermak and Schreiber, 2014; Wang et al., 2016), Canada (Haeri-Ardakani et al., 2015; Dong et al., 2015; Van de Wetering et al., 2016) and China (Zeng et al., 2016; Cai et al., 2009; Guo et al., 2016).

Of equal significance is the reactivity of pyrite. Pyrite plays a catalytic role in the degradation of various organic pollutants. Pyrite induces chemical transformation, either due to the redox activity of the sulfur dimers ( $\text{S}_2$ ) (Luther, 1987; Lee and Batchelor, 2002); the production of highly reactive hydroxyl radicals ( $\cdot\text{OH}$ ) due to a Fenton-like mechanism (Borda et al. 2003; Pham et al., 2009; Wang et al., 2012; Dhanasekara et al., 2015); or as a source of ferrous ( $\text{Fe}^{\text{II}}$ ), hydrogen ( $\text{H}^+$ ) and sulfate ( $\text{SO}_4^{2-}$ ) ions on dissolution (Zhang et al., 2014).

Additionally, the oxidation of pyrite changes the surface groups at the mineral-fluid interface. In aqueous, air-saturated solutions, pyrite is oxidized to form mainly ferric (hydroxy)sulfate and at pH greater than 4, Fe<sup>III</sup> oxyhydroxide forms on the surface as well (Todd et al., 2002; Dos Santos et al., 2016). These iron oxide surfaces can catalyze the hydrolysis of organic compounds due to the formation of complexes that allow for hydrolytic attack (Torrents and Stone, 1991). As the largest source of iron in shale formations (Jew et al., 2017), pyrite stands to be the greatest contributor of dissolved Fe<sup>II</sup> and Fe<sup>III</sup> in flowback waters. Thus, both pristine pyrite and the oxidation of this mineral may significantly influence the degradation of biocides in the Marcellus Shale.

### **1.3 Research Objectives**

The overall goal of this study is to understand the effect of pyrite on biocide reactivity in hydraulic fracturing. Although biocides are often considered a coherent class of compounds, they exhibit widely differing chemical properties. Consequently, an initial study was done to characterize the reactivity of the various biocides used in hydraulic fracturing and to place the reactivity of pyrite within context of the many interactions that may occur downhole. This initial review to explore significant sorption and transformation mechanisms that occur at the mineral-fluid interface was done by tackling three tasks: (i) to determine the physical and chemical properties of biocides used in hydraulic fracturing; (ii) to present the physical and chemical properties of major minerals in the Marcellus Shale and (iii) to anticipate the sorption and transformation mechanisms that occur at the mineral-fluid interface.

This review prompted the three main experimental objectives as illustrated in Figure 1-1 and described in detail, below.

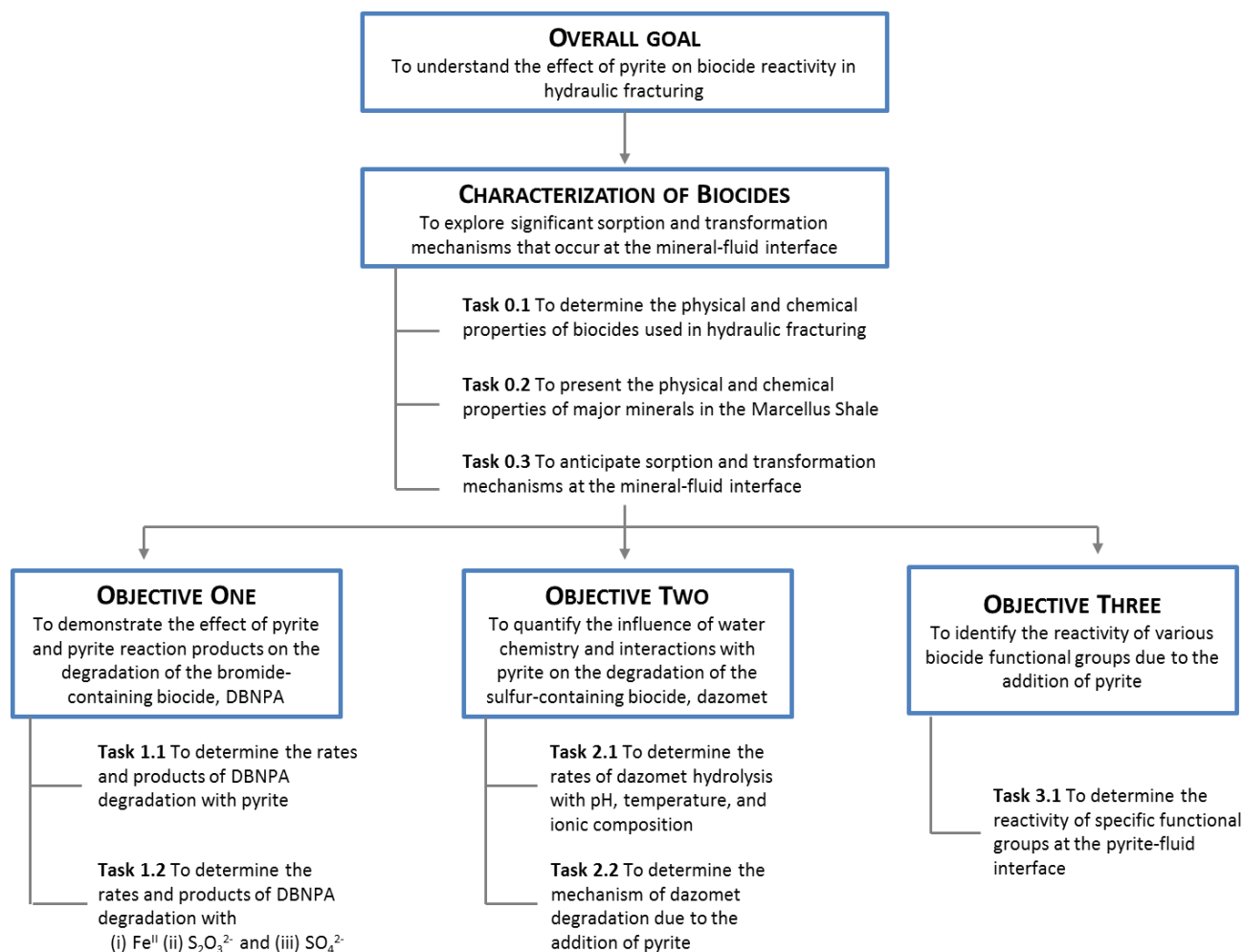


**Figure 1-1. Flowchart illustrating the relationships between research goals, objectives and tasks completed in the dissertation.**

*Objective 1. To demonstrate the effect of pyrite and pyrite reaction products on the degradation of the bromine-containing biocide, DBNPA.*

Organobromides have proven to be an effective class of disinfectants and have been successfully applied to hydraulic fracturing. These biocides attribute some of their efficacy to the ability of the hydrophobic bromine group to partition into bacterial cell membranes, disrupting normal cellular function. Studies have shown that the dehalogenation of organobromides can be catalyzed by bacterial electron mediators, but no studies have yet assessed whether pyrite can also reduce these compounds.

This study puts forward the hypothesis that pyrite can reduce brominated compounds, just as observed with their chlorinated counterparts. To test this, DBNPA is used as a model compound to explore the effect of pyrite on the persistence of brominated biocides. This is done by exploring two tasks: Task 1.1 is to determine the rates and products of DBNPA degradation with pyrite; and Task 1.2 is to determine the rates and products of DBNPA degradation with (i)  $\text{Fe}^{\text{II}}$ , the redox-active pyrite hydrolysis product of pyrite and (ii)  $\text{S}_2\text{O}_3^{2-}$  and  $\text{SO}_4^{2-}$ , nucleophilic pyrite oxidation products.

*Objective 2. To quantify the influence of water chemistry and interactions with pyrite on the degradation of the sulfur-containing biocide, dazomet.*

Dazomet is one of the most-commonly used biocides for hydraulic fracturing, and one of the many sulfur-containing biocides reported. Chemically, it falls under the group of dithiocarbamates, a sulfur analog to carbamates or urethanes. It rapidly hydrolyses in water to form methyl isothiocyanate (MITC), formaldehyde and other compounds. Manufacturers recommend using dazomet at concentrations between 200 and 1000 mg/L in fracking fluids and 150 and 200 mg/L in produced water that will be stored or reused (BASF, 2000). Its degradation product hexahydro-1,3,5-trimethyl-1,3,5-triazine-2-thione has been measured in produced water at concentrations between 0.01 and 1.6 mg/L (Orem et al., 2014).

While pyrite can bind to a range of compounds, sulfur-containing species are particularly likely to approach the surface (Bebié and Schoonen, 2000). This study proposes that the reactivity of dazomet will change at the water-mineral interface. In order to assess this difference, it was important to also understand the influence of temperature and water chemistry. This was done by accomplishing the following tasks: Task 2.1 is to determine the rates of dazomet hydrolysis with pH, temperature, and ionic composition; and Task 2.2 is to determine the mechanism of dazomet degradation due to the addition of pyrite.

*Objective 3. To identify the reactivity of various biocide functional groups due to the addition of pyrite.*

While the initial objectives have targeted the degradation of more reactive compounds, this objective targets the degradation of more recalcitrant biocides. Four biocides are investigated with very different functional groups: dibromodicyanobutane, methylene bis(thiocyanate) and two isothiazolinones – benzisothiazolinone and methyl isothiazolinone. The result of this work is to identify functional groups relevant to biocides that are responsible for the reduction of these biocides with pyrite. This was accomplished by the completion of Task 3.1: to determine the reactivity of specific functional groups at the pyrite-fluid interface.

#### **1.4 Thesis Organization**

This dissertation consists of six chapters. Chapter 1 discusses the motivation, problem identification and research objectives. Chapter 2 presents a review of the state of knowledge of significant sorption and transformation mechanisms that occur between major shale minerals and organic compounds at the mineral-fluid interface. Chapter 3, 4 and 5 describe the methods and materials, results and discussion for objectives 1, 2 and 3, respectively. These chapters progress from specific case studies of biocides to more general research generating fundamental understanding of pyrite-organic reactions. Lastly, chapter 6 summarizes the conclusions, novel contributions and suggestions for future work.

## 1.5 References

- Adesina, A., Y., Kayode, A., Faisal, M.A.-A., 2015. Microbiologically Influenced Corrosion (MIC) Challenges in Unconventional Gas Fields. Presented at the Corrosion, NACE International, p. 15.
- Akyon, B., Stachler, E., Wei, N., Bibby, K., 2015. Microbial Mats as a Biological Treatment Approach for Saline Wastewaters: The Case of Produced Water from Hydraulic Fracturing. *Environmental Science & Technology* 49, 6172–6180. doi:10.1021/es505142t
- Analysis of Hydraulic Fracturing Fluid Data from the FracFocus Chemical Disclosure Registry (No. EPA/601/R-14/003), 2015. . U.S. Environmental Protection Agency (EPA).
- Barbot, E., Vidic, N.S., Gregory, K.B., Vidic, R.D., 2013. Spatial and Temporal Correlation of Water Quality Parameters of Produced Waters from Devonian-Age Shale following Hydraulic Fracturing. *Environmental Science & Technology* 47, 2562–2569. doi:10.1021/es304638h
- BASF, 2000. Water and oilfield biocides.
- Bebié, J., Schoonen, M.A.A., 2000. Pyrite surface interaction with selected organic aqueous species under anoxic conditions. *Geochemical Transactions* 1, 47. doi:10.1039/b005581f
- Berner, R.A., 1984. Sedimentary pyrite formation: An update. *Geochimica et Cosmochimica Acta* 48, 605–615. doi:10.1016/0016-7037(84)90089-9
- Cai, C., Li, K., Anlai, M., Zhang, C., Xu, Z., Worden, R.H., Wu, G., Zhang, B., Chen, L., 2009. Distinguishing Cambrian from Upper Ordovician source rocks: Evidence from sulfur isotopes and biomarkers in the Tarim Basin. *Organic Geochemistry* 40, 755–768. doi:10.1016/j.orggeochem.2009.04.008
- Carter, K.E., Hakala, J.A., Hammack, R.W., 2013. Hydraulic Fracturing and Organic Compounds – Uses, Disposal and Challenges. Presented at the SPE Eastern Regional Meeting, Society of Petroleum Engineers, Pittsburgh, PA.
- Carter, K.M., Harper, J.A., Schmid, K.W., Kostelnik, J., 2011. Unconventional natural gas resources in Pennsylvania: The backstory of the modern Marcellus Shale play. *Environmental Geosciences* 18, 217–257. doi:10.1306/eg.09281111008
- Chermak, J.A., Schreiber, M.E., 2014. Mineralogy and trace element geochemistry of gas shales in the United States: Environmental implications. *International Journal of Coal Geology* 126, 32–44. doi:10.1016/j.coal.2013.12.005
- Dong, T., Harris, N.B., Ayranci, K., Twemlow, C.E., Nassichuk, B.R., 2015. Porosity characteristics of the Devonian Horn River shale, Canada: Insights from lithofacies classification and shale composition. *International Journal of Coal Geology* 141–142, 74–90. doi:10.1016/j.coal.2015.03.001
- Dos Santos, E.C., de Mendonça Silva, J.C., Duarte, H.A., 2016. Pyrite Oxidation Mechanism by Oxygen in Aqueous Medium. *The Journal of Physical Chemistry C* 120, 2760–2768. doi:10.1021/acs.jpcc.5b10949
- Drilling productivity report for key tight oil and shale gas regions. August 2017, 2017. . U.S. Energy Information Administration (EIA).
- Fakcharoenphol, P., Torcuk, M.A., Wallace, J., Bertonecello, A., Kazemi, H., Wu, Y.-S., Honarpour, M., 2013. Managing Shut-in Time to Enhance Gas Flow Rate in Hydraulic Fractured Shale Reservoirs: A Simulation Study. Society of Petroleum Engineers. doi:10.2118/166098-MS
- Ferrer, I., Thurman, E.M., 2015. Analysis of hydraulic fracturing additives by LC/Q-TOF-MS. *Analytical and Bioanalytical Chemistry* 407, 6417–6428. doi:10.1007/s00216-015-8780-5

- Ferrar, K.J., Michanowicz, D.R., Christen, C.L., Mulcahy, N., Malone, S.L., Sharma, R.K., 2013. Assessment of Effluent Contaminants from Three Facilities Discharging Marcellus Shale Wastewater to Surface Waters in Pennsylvania. *Environmental Science & Technology* 47, 3472–3481. doi:10.1021/es301411q
- Gregory, K.B., Vidic, R.D., Dzombak, D.A., 2011. Water Management Challenges Associated with the Production of Shale Gas by Hydraulic Fracturing. *Elements* 7, 181–186. doi:10.2113/gselements.7.3.181
- Guo, L., Jiang, Z., Liang, C., 2016. Mineralogy and shale gas potential of lower silurian organic-rich shale at the southeastern margin of sichuan basin, South China. *Oil Shale* 33, 1. doi:10.3176/oil.2016.1.01
- Haeri-Ardakani, O., Sanei, H., Lavoie, D., Chen, Z., Jiang, C., 2015. Geochemical and petrographic characterization of the Upper Ordovician Utica Shale, southern Quebec, Canada. *International Journal of Coal Geology* 138, 83–94. doi:10.1016/j.coal.2014.12.006
- Harrison, A.L., Jew, A.D., Dustin, M.K., Thomas, D.L., Joe-Wong, C.M., Bargar, J.R., Johnson, N., Brown, G.E., Maher, K., 2017. Element release and reaction-induced porosity alteration during shale-hydraulic fracturing fluid interactions. *Applied Geochemistry* 82, 47–62. doi:10.1016/j.apgeochem.2017.05.001
- Hoelzer, K., Sumner, A.J., Karatum, O., Nelson, R.K., Drollette, B.D., O'Connor, M.P., D'Ambro, E.L., Getzinger, G.J., Ferguson, P.L., Reddy, C.M., Elsner, M., Plata, D.L., 2016. Indications of Transformation Products from Hydraulic Fracturing Additives in Shale-Gas Wastewater. *Environmental Science & Technology* 50, 8036–8048. doi:10.1021/acs.est.6b00430
- International energy outlook, 2016. Chapter 3. Natural gas (No. DOE/EIA-0484(2016)), 2016. . U.S. Energy Information Administration (EIA).
- Javaherdashti, R., 1999. A review of some characteristics of MIC caused by sulfate-reducing bacteria: past, present and future. *Anti-Corrosion Methods and Materials* 46, 173–180. doi:10.1108/00035599910273142
- Jew, A.D., Dustin, M.K., Harrison, A.L., Joe-Wong, C.M., Thomas, D.L., Maher, K., Brown, G.E., Bargar, J.R., 2017. Impact of Organics and Carbonates on the Oxidation and Precipitation of Iron during Hydraulic Fracturing of Shale. *Energy & Fuels* 31, 3643–3658. doi:10.1021/acs.energyfuels.6b03220
- Judd, S., Qiblawey, H., Al-Marri, M., Clarkin, C., Watson, S., Ahmed, A., Bach, S., 2014. The size and performance of offshore produced water oil-removal technologies for reinjection. *Separation and Purification Technology* 134, 241–246. doi:10.1016/j.seppur.2014.07.037
- Kahrilas, G.A., Blotvogel, J., Stewart, P.S., Borch, T., 2015. Biocides in Hydraulic Fracturing Fluids: A Critical Review of Their Usage, Mobility, Degradation, and Toxicity. *Environmental Science & Technology* 49, 16–32. doi:10.1021/es503724k
- King, G.E., 2012. Hydraulic Fracturing 101: What Every Representative, Environmentalist, Regulator, Reporter, Investor, University Researcher, Neighbor, and Engineer Should Know About Hydraulic Fracturing Risk. Presented at the SPE Hydraulic Fracturing Technology Conference, Society of Petroleum Engineers, The Woodlands, TX, pp. 34–42.
- Loomis, J., Haeefe, M., 2017. Quantifying Market and Non-market Benefits and Costs of Hydraulic Fracturing in the United States: A Summary of the Literature. *Ecological Economics* 138, 160–167. doi:10.1016/j.ecolecon.2017.03.036
- Marcon, V., Joseph, C., Carter, K.E., Hedges, S.W., Lopano, C.L., Guthrie, G.D., Hakala, J.A., 2017. Experimental insights into geochemical changes in hydraulically fractured Marcellus Shale. *Applied Geochemistry* 76, 36–50. doi:10.1016/j.apgeochem.2016.11.005
- McKenzie, L.M., Witter, R.Z., Newman, L.S., Adgate, J.L., 2012. Human health risk assessment of air emissions from development of unconventional natural gas resources. *Science of The Total Environment* 424, 79–87. doi:10.1016/j.scitotenv.2012.02.018

- Montgomery, C.T., Smith, M.B., 2010. Hydraulic Fracturing: History Of An Enduring Technology. *Journal of Petroleum Technology* 62, 26–40. doi:10.2118/1210-0026-JPT
- Orem, W., Tatu, C., Varonka, M., Lerch, H., Bates, A., Engle, M., Crosby, L., McIntosh, J., 2014. Organic substances in produced and formation water from unconventional natural gas extraction in coal and shale. *International Journal of Coal Geology* 126, 20–31. doi:10.1016/j.coal.2014.01.003
- O’Sullivan, F., Paltsev, S., 2012. Shale gas production: potential versus actual greenhouse gas emissions. *Environmental Research Letters* 7, 044030. doi:10.1088/1748-9326/7/4/044030
- Paukert Vankeuren, A.N., Hakala, J.A., Jarvis, K., Moore, J.E., 2017. Mineral Reactions in Shale Gas Reservoirs: Barite Scale Formation from Reusing Produced Water As Hydraulic Fracturing Fluid. *Environmental Science & Technology* 51, 9391–9402. doi:10.1021/acs.est.7b01979
- Shaffer, D.L., Arias Chavez, L.H., Ben-Sasson, M., Romero-Vargas Castrillón, S., Yip, N.Y., Elimelech, M., 2013. Desalination and Reuse of High-Salinity Shale Gas Produced Water: Drivers, Technologies, and Future Directions. *Environmental Science & Technology* 47, 9569–9583. doi:10.1021/es401966e
- Srinivasan, K., Krishnamurthy, J., Williams, R., Dharwadkar, P., Izykowski, T., Moore, W.R., 2016. Eight-Plus Years of Hydraulic Fracturing in the Williston Basin: What Have We Learned? *Society of Petroleum Engineers*. doi:10.2118/179156-MS
- Tasker, T.L., Piotrowski, P.K., Dorman, F.L., Burgos, W.D., 2016. Metal Associations in Marcellus Shale and Fate of Synthetic Hydraulic Fracturing Fluids Reacted at High Pressure and Temperature. *Environmental Engineering Science* 33, 753–765. doi:10.1089/ees.2015.0605
- Thiel, G.P., Tow, E.W., Banchik, L.D., Chung, H.W., Lienhard, J.H., 2015. Energy consumption in desalinating produced water from shale oil and gas extraction. *Desalination* 366, 94–112. doi:10.1016/j.desal.2014.12.038
- Todd, E., Sherman, D., Purton, J., 2003. Surface oxidation of pyrite under ambient atmospheric and aqueous (pH = 2 to 10) conditions: electronic structure and mineralogy from X-ray absorption spectroscopy. *Geochimica et Cosmochimica Acta* 67, 881–893. doi:10.1016/S0016-7037(02)00957-2
- Torrents, A., Stone, A.T., 1991. Hydrolysis of phenyl picolinate at the mineral/water interface. *Environmental Science & Technology* 25, 143–149. doi:10.1021/es00013a016
- U.S. Crude Oil and Natural Gas Proved Reserves, Year-end 2015, 2016. . U.S. Energy Information Administration (EIA), Washington, DC.
- Van de Wetering, N., Sanei, H., Mayer, B., 2016. Organic matter characterization in mixed hydrocarbon producing areas within the Duvernay Formation, Western Canada Sedimentary Basin, Alberta. *International Journal of Coal Geology* 156, 1–11. doi:10.1016/j.coal.2016.01.012
- Vengosh, A., Jackson, R.B., Warner, N., Darrah, T.H., Kondash, A., 2014. A Critical Review of the Risks to Water Resources from Unconventional Shale Gas Development and Hydraulic Fracturing in the United States. *Environmental Science & Technology* 48, 8334–8348. doi:10.1021/es405118y
- Walker, E.L., Anderson, A.M., Read, L.K., Hogue, T.S., 2017. Water Use for Hydraulic Fracturing of Oil and Gas in the South Platte River Basin, Colorado. *JAWRA Journal of the American Water Resources Association* 53, 839–853. doi:10.1111/1752-1688.12539
- Wang, G., Carr, T.R., 2012. Methodology of organic-rich shale lithofacies identification and prediction: A case study from Marcellus Shale in the Appalachian basin. *Computers & Geosciences* 49, 151–163. doi:10.1016/j.cageo.2012.07.011

- Wang, L., Burns, S., Giammar, D.E., Fortner, J.D., 2016. Element mobilization from Bakken shales as a function of water chemistry. *Chemosphere* 149, 286–293.  
doi:10.1016/j.chemosphere.2016.01.107
- Yan, T., Li, W., Bi, X., 2011. An experimental study of fracture initiation mechanisms during hydraulic fracturing. *Petroleum Science* 8, 87–92. doi:10.1007/s12182-011-0119-z
- Zeng, J., Jia, W., Peng, P., Guan, C., Zhou, C., Yuan, X., Chen, S., Yu, C., 2016. Composition and pore characteristics of black shales from the Ediacaran Lantian Formation in the Yangtze Block, South China. *Marine and Petroleum Geology* 76, 246–261.  
doi:10.1016/j.marpetgeo.2016.05.026
- Zhang, T., Hammack, R.W., Vidic, R.D., 2015. Fate of Radium in Marcellus Shale Flowback Water Impoundments and Assessment of Associated Health Risks. *Environmental Science & Technology* 49, 9347–9354. doi:10.1021/acs.est.5b01393
- Zhang, Y., Zhang, K., Dai, C., Zhou, X., 2014. Performance and mechanism of pyrite for nitrobenzene removal in aqueous solution. *Chemical Engineering Science* 111, 135–141.  
doi:10.1016/j.ces.2014.02.029

**Chapter 2      Review of mineral and biocide properties  
influencing biocide sorption and transformation in the  
Marcellus Shale**

The information presented in this chapter will appear as a publication in a peer-reviewed journal with the tentative title "Review of mineral and biocide properties influencing biocide sorption and transformation in the Marcellus Shale" by Nizette Consolazio, Gregory V. Lowry, J. Alexandra Hakala and Athanasios K. Karamalidis.

## 2.1 Abstract

Biocides are being used as chemical additives in hydraulic fracturing fluids to control microbial activity in the subsurface. When biocides are released into the subsurface, their fate is controlled by sorption to solids and/or heterogeneous electron transfer (redox) reactions at the mineral-fluid interface. This Chapter reviews the literature and synthesizes data and information from various fields to identify the major minerals that may impact biocide sorption and reactivity. To achieve this goal, the chemical and physical properties of quartz, illite, chlorite, pyrite, calcite and dolomite are presented and their reactions with organic compounds similar to biocides are identified. Although biocides are often thought of as a coherent group of chemical compounds, they are structurally diverse and possess various chemical reactive groups. However, certain properties are common across the chemical structures. Oxygen-containing groups dominate the class and the carbonyl ( $-C=O$ ) substructure is integrated into many biocides. The biocides are also classified according to their charge in water and any surfactant-like properties: cationic biocides (with surfactants placed within their own separate group), acidic, basic, and neutral biocides. Cationic surfactant biocides were shown to sorb to every mineral due to multiple mechanisms for sorption. Clays, because of their negative surface charge and comparatively high surface area, make excellent sorbents of positively charged biocides (cationic and basic biocides). Despite the high concentrations in shale formations, the sorption to organic matter is expected to be limited due to the very polar groups found in biocides. Pyrite stands as the mineral most likely to cause transformation of biocides due to its ability to reduce halogenated organic compounds and initiate Fenton-like reactions which generate non-specific hydroxyl radicals. Carbonate minerals act as physisorption sites for negatively charged biocides and potential chemisorption sites for biocides possessing a carbonyl

group adjacent to another electronegative group. However, the rapid dissolution of this mineral limits its persistence at the mineral-fluid interface.

## 2.2 Introduction

During the shut-in phase of hydraulic fracturing, the reactions that take place at the mineral-fluid interface play an important role in the fate of the minerals, fluid and the dissolved species. The introduction of hydraulic fracturing fluid into newly fractured shale formations leads to chemical disequilibrium (Harrison et al., 2017). When the thermodynamic equilibrium at the interface is disturbed, matter and energy are transferred through chemical reactions to establish a new chemical equilibrium (Hinman, 2013). At the micro level, these heterogeneous processes amount to the attachment and detachment of fluid molecules to mineral surfaces. At the macroscopic level, they have shaped the planet, responsible for the distribution of nutrients, the concentration of CO<sub>2</sub> in the atmosphere, and the geochemical cycling of the elements (Teng, 2005). An understanding of these reactions is vital in order to predict the long-term effects of this anthropogenic activity over across temporal and spatial scales (Brantley et al., 2008).

The impact of the hydraulic fracturing fluid on the mineral surface has been the subject of much interest, as research in this field can help to maximize well productivity. This is particularly true during the shut-in phase of the hydraulic fracturing process where the fluid interacts with the formation for days to weeks (Paukert Vankeuren et al., 2017; Fakcharoenphol et al., 2013). In fact, fracking fluids are designed to interact with, and change the properties of, formation minerals. Acids cause dissolution of some rocks and initiate fractures. Antiscalants inhibit the thermodynamically favored precipitation of minerals. Surfactants reduce the surface tension at the mineral-fluid interface, altering the wettability of the rock.

This chapter focuses on the effect of the mineral surface on the fate and transport of biocides. This study proposes that this can be done by identifying and categorizing the common biocides used, as well as the minerals found in the Marcellus Shale, the largest producing shale gas formation. By understanding the properties of each these components, it is possible to

anticipate how they may interact. The environment of the system is also influential. In this study, the range of pH of the fluid at the mineral interface was assumed to be equal to that recorded for produced water, i.e. 5.2 to 8.9 (Hayes, 2009). The effect of ionic strength is also considered as the median salinity of the Marcellus Shale is 250,000 mg/L (Rowan et al., 2011). Temperature is also an important factor as it spans a wide range within the formation, 27 - 93°C, averaging 61°C (Dilmore et al., 2015).

This review draws from the great quantity of previously documented data that exists for organic compounds of comparable physicochemical properties, including research from the fields of geochemistry, soil science, mining engineering and environmental science. Although both inorganic and organic biocides are used, the fate of the latter is more complex as they undergo a wider variety of transformation and sorption. When released into the subsurface, their fate is controlled by sorption to solids and heterogeneous electron transfer (redox) reactions (Martin et al., 2015; Grundl and Sparks, 1999). The rate of reaction at the mineral-fluid interface is also promoted by the increased surface area of the induced fractures (Walton and Woocay, 2013). The sorption of these biocides will define the ultimate fate, bioavailability and toxicity of these biocides.

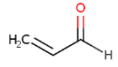
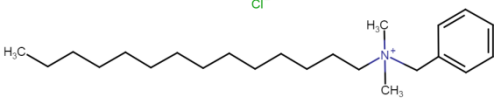
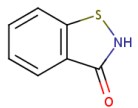
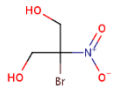
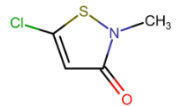
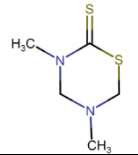
The goal of this chapter is to establish a qualitative picture of the environmental fate of the organic biocides at the mineral-fluid interface within the Marcellus Shale. The initial task of this review was to summarize the physical and chemical properties of biocides used in hydraulic fracturing. Then, the balance of the review presents the chemical and physical properties of each major mineral component of the Marcellus Shale and identifies published literature on the reactions of organic compounds similar to the biocides. The final task is to then anticipate sorption and transformation mechanisms at the mineral-fluid interface. This approach will consequently identify reactions of interest for more focused study.

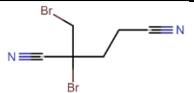
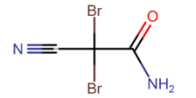
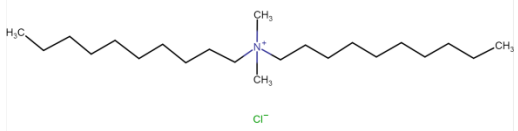
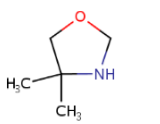
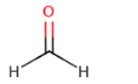
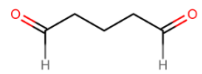
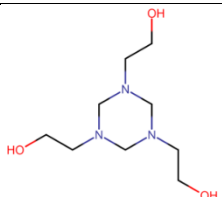
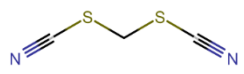
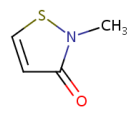
## **2.3 Common biocides used in the Marcellus Shale**

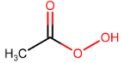
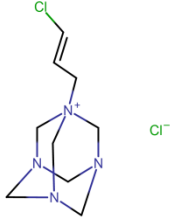
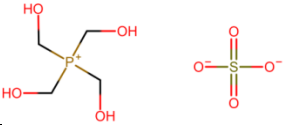
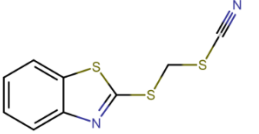
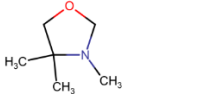
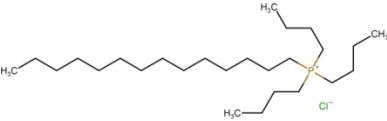
### *2.3.1 Physical and chemical properties of biocides*

Many states, including Pennsylvania have adopted FracFocus, the hydraulic fracturing chemical registry for the disclosure of the chemical additives used for hydraulic fracturing. Forty-five unique compounds have been reported for use in biocidal formulations (Kahrilas et al., 2015; Rogers et al., 2015; Stringfellow et al., 2014; Carter et al., 2013; Elsner and Hoelzer, 2016). Of these, 22 biocides were organic compounds identified by the US Environmental Protection Agency (EPA) as “active ingredients” (Office of Pesticides and Toxic Substances, 1992). Table 2-1 lists the identifiers, structures, reactive functional groups, and key physicochemical properties (solubility, log P and polar surface area, PSA) of biocides reportedly used in the Marcellus Shale.

**Table 2-1. The common name, CAS number, structural and physical properties of biocides selected for this study. Note: log P is the logarithm of the partitioning between octanol and water and PSA is the polar surface area of the compound, as modeled by SciFinder.**

Biocide name (CAS#)	Structure	Reactive groups	MW (g/mol)	Physical properties	Ionization
Acrolein (107-02-8)		Alkene, C=C Aldehyde, C=O	56.06	Solubility: 66.2 g/L Log P: 0.263 PSA: 17.1 A <sup>2</sup>	none
Alkyl dimethyl benzyl ammonium chloride (For example , 139-08-2)		Long carbon chain Phenyl ring Quaternary ammonium ion, N <sup>+</sup> R <sub>4</sub> Long carbon chain	368.04	-	Dissociates
Benzisothiazolinone (2634-33-5)		Phenyl ring Carboxamide, - C(=O)N(R <sub>2</sub> ) Sulfide, -S-	151.19	Solubility: 0.56 g/L Log P: 1.953 PSA: 54.4 A <sup>2</sup>	pK <sub>a</sub> (acidic) = 10.19 pK <sub>a</sub> (basic) = -1.97
Bronopol (52-51-7)		Bromide, -Br Alcohol, -OH Nitro, -NO <sub>2</sub>	199.99	Solubility: 86 g/L Log P: 1.150 PSA: 86.3 A <sup>2</sup>	pK <sub>a</sub> (acidic) = 12.02
1-Bromo- 3-chloro-5,5- dimethylhydantoin (16079-88-2)		Chloride, -Cl Bromide, -Br Aminal - C(NR <sub>2</sub> )(NR <sub>2</sub> ) Carboxamide, - C(=O)N(R <sub>2</sub> )	241.47	Solubility: 7.2 g/L Log P: 1.134 PSA: 40.6 A <sup>2</sup>	pK <sub>a</sub> (basic) = -3.44
Chloromethyl- isothiazolinone (26172-55-4)		Alkene, C=C Sulfide, -S- Chloride, -Cl Carboxamide, - C(=O)N(R <sub>2</sub> )	149.60	Solubility: 10 g/L Log P: 0.487 PSA: 45.6 A <sup>2</sup>	pK <sub>a</sub> (basic) = -4.06
Dazomet (533-74-4)		Aminal, - C(NR <sub>2</sub> )(NR <sub>2</sub> ) Dithiocarbamate, N(R <sub>2</sub> )C(=S)SR	162.28	Solubility: 4.9 g/L Log P: 0.639 PSA: 63.9 A <sup>2</sup>	pK <sub>a</sub> (basic) = 4.04

Dibromodicyanobutane (35691-65-7)		Bromide, -Br Nitrile, -C≡N	265.93	Solubility: 0.82 g/L Log P: 1.515 PSA: 47.6 A <sup>2</sup>	none
Dibromonitrilo propamide (DBNPA) (10222-01-2)		Bromide, -Br Nitrile, -C≡N Amide, -C(=O)N(R <sub>2</sub> )	241.87	Solubility: 4.1 g/L Log P: 1.061 PSA: 66.9 A <sup>2</sup>	pK <sub>a</sub> (acidic) = 11.72 pK <sub>a</sub> (basic) = -1.87
Didecyl dimethyl ammonium chloride (7173-51-5)		Long carbon chain Quaternary ammonium ion, N <sup>+</sup> R <sub>4</sub>	362.083	Solubility: 0.65g/L Log P: 2.59	dissociates
Dimethyloxazolidine (51200-87-4)		Hemiaminal, -C(OH)(NR <sub>2</sub> )-	101.15	Solubility: 256 g/L Log P: 0.237 PSA: 21.3A <sup>2</sup>	pK <sub>a</sub> (basic) = 8.41
Formaldehyde, paraformaldehyde (50-00-0)		Aldehyde, C=O	30.03	Solubility: 198 g/L Log P: 0.350 PSA: 17.1 A <sup>2</sup>	none
Glutaraldehyde (111-30-8)		Aldehyde, C=O	100.12	Solubility: 19 g/L Log P: -0.264 PSA: 34.1 A <sup>2</sup>	none
Grotan or Actane (4719-04-4)		Alcohol, -OH Aminal, -C(NR <sub>2</sub> )(NR <sub>2</sub> )	219.28	Solubility: 1000 g/L Log P: -1.270 PSA: 70.4 A <sup>2</sup>	pK <sub>a</sub> (acidic) = 14.16 pK <sub>a</sub> (basic) = 5.44
Methylene bis(thiocyanate) (6317-18-6)		Thiocyanate, -SC≡N	130.19	Solubility: 23 g/L Log P: 0.630 PSA: 98.2 A <sup>2</sup>	none
Methyl isothiazolinone (2682-20-4)		Alkene, C=C Sulfide, -S- Carboxamide, -C(=O)N(R <sub>2</sub> )	115.15	Solubility: 24 g/L Log P: 0.119 PSA: 45.6 A <sup>2</sup>	pK <sub>a</sub> (basic) = -2.03

Peracetic acid (79-21-0)		Peroxyacid, - C(=O)OOH	76.05	Solubility: 389 g/L Log P: -0.301 PSA: 46.5 A <sup>2</sup>	pK <sub>a</sub> (acidic) = 8.08
Quaternium-15 or CTAC (4080-31-3)		Long carbon chain Alkene, C=C Chloride, -Cl Alcohol, -OH Aminal, - C(NR <sub>2</sub> )(NR <sub>2</sub> )	251.155	Solubility: 127.2 g/L Log P: -0.1 PSA: 9.7 A <sup>2</sup>	97.8% dissociated
Tetrakis hydroxymethyl phosphonium sulfate (55566-30-8)		Alcohol, -OH Phosphonium, P <sup>+</sup> R <sub>4</sub>	406.276	Solubility: 1000 g/L Log P: -20.39	Dissociates
Thiocyanomethyl thiobenzothiazole (21564-17-0)		Phenyl ring Imine, -C=NR Sulfide, -S- Thiocyanate, -SC≡N	238.35	Solubility: 0.076 g/L Log P: 3.120 PSA: 116 A <sup>2</sup>	pK <sub>a</sub> (basic) = -0.09
Trimethyloxazolidin e (75673-43-7)		Hemiaminal, -C(OH) (NR <sub>2</sub> )-	115.17	Solubility: 250 g/L Log P: 0.387 PSA: 12.5 A <sup>2</sup>	pK <sub>a</sub> (basic) = 7.58
Tributyl tetradecyl phosphonium chloride (81741-28-8)		Long carbon chain Phosphonium, P <sup>+</sup> R <sub>4</sub>	435.158		Dissociates

Although biocides are often thought of as a coherent group of chemical compounds, they are structurally diverse with a range of chemical functional groups. While many heteroatoms are represented (for example: halogens, sulfur, nitrogen), oxygen-containing groups dominate the class. In particular, the carbonyl functionality (C=O) is integrated into many biocides, either as the simple aldehyde group or in more complex arrangements such as carboxamides, -C(=O)N(R<sub>2</sub>). There is also an assortment of structures: ten biocides exhibit ring structures and three possess aromatic (phenyl) rings; four possess long alkyl chains consisting of 8 or more carbon atoms. Figure 2-1 presents the number of biocides possessing at least one of the functional groups identified, highlighting the most common functional groups and the most reactive compounds. Table 2-2 presents the data in table form.

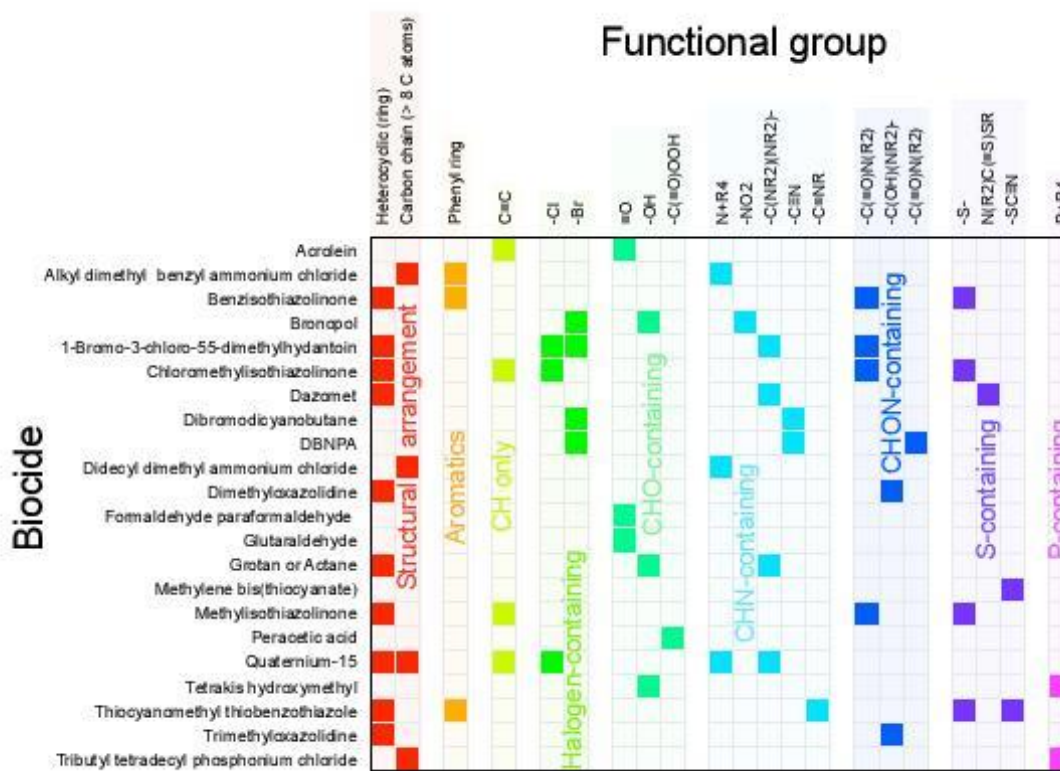


Figure 2-1. Heat map displaying the reactivity of each biocide and the occurrence of each identified functional group and structural arrangement.

**Table 2-2. The number of biocides containing at least one of functional groups and structural arrangements identified. Functional groups are classified according to type.**

		Number of Biocides	Example biocide
Structural arrangement	Heterocyclic (ring)	10	Dimethyloxazolidine
	Carbon chain (> 8 C atoms)	4	Didecyl dimethyl ammonium chloride
Aromatics	Phenyl ring	3	Benzisothiazolinone
CH only	Alkene C=C	4	Acrolein
Halogen-containing	Chloride -Cl	3	Chloromethyl isothiazolinone
	Bromide -Br	4	1-Bromo-3-chloro-5,5-dimethylhydantoin
CHO-containing	Aldehyde =O	3	Glutaraldehyde
	Alcohol -OH	3	Grotan or Actane
	Peroxyacid -C(=O)OOH	1	Peracetic acid
CHN-containing	Ammonium N <sup>+</sup> R <sub>4</sub>	4	Quaternium-15
	Nitro -NO <sub>2</sub>	2	Bronopol
	Aminal -C(NR <sub>2</sub> )(NR <sub>2</sub> )-	4	Quaternium-15
	Nitrile -C≡N	2	Dibromodicyanobutane
	Imine -C=NR	1	Thiocyanomethyl thiobenzothiazole
CHON-containing	Carboxamide -C(=O)N(R <sub>2</sub> )	4	Benzisothiazolinone
	Hemiaminal -C(OH)(NR <sub>2</sub> )-	2	Trimethyloxazolidine
	Amide -C(=O)N(R <sub>2</sub> )	1	DBNPA
S-containing	Sulfide -S-	4	Methylisothiazolinone
	Dithiocarbamate N(R <sub>2</sub> )C(=S)SR	1	Dazomet
	Thiocyanate -SC≡N	2	Methylene bis(thiocyanate)
P-containing	Phosphonium P <sup>+</sup> R <sub>4</sub>	2	Tributyl tetradecyl phosphonium chloride

These numerous functional groups ultimately determine their toxicity and physical behavior in the environment. For example, C=O-containing compounds in particular are often

electrophilically-active substances that can react with nucleophilic groups in bacteria (Bieleman, 2000). Each biocide is either charged or possesses highly polar groups which are exemplified by their significant polar surface areas (PSA). This accounts for their appreciable solubility which ranges from sparingly soluble at 0.076 g/L to essentially miscible in water at 1000 g/L. Hydrophobic moieties such as Br and phenyl rings greatly increase the hydrophobicity of some compounds: only the biocides containing these groups have octanol/water partition coefficients ( $K_{ow}$ ) greater than 100. Nitrogen-containing functional groups are also more likely than others to be positively charged. Biocides with quaternary ammonium (or quaternary phosphonium) groups are positively charged at all pHs. The biocides with a basic pKa between 5.2 - 8.9 (i.e. dazomet, grotan, di- and tri-methyl oxazolidine) all contain nitrogen within their structure. These varied groups undergo different chemical reactions (for example hydrolysis or nucleophilic substitution) leading to a wide range of persistence in the environment.

### *2.3.2 Mechanisms for sorption*

Given the diverse properties of biocides, various mechanisms exist to explain the sorption of these biocides molecules from solution to the mineral surface. To approach a charged mineral surface, a biocide must first displace the water molecule previously sorbed to the surface. Thus, highly polar chemicals can usually compete with the water molecules. Adsorption may occur by either chemisorption, the formation of specific bonds between biocide and mineral surface; or physisorption, which relies on intermolecular forces such as hydrogen bonding or electrostatic attractions to provide the attraction between the biocide and surface. Ion exchange occurs when a charged biocide displaces a similarly charged ion from the surface of the mineral. The adsorption of compounds to mineral surfaces of similar charge may occur through “bridging”. Here, an intermediary ion of opposite charge first sorbs to the surface, changing the apparent surface charge and causing a mutual electrostatic attraction for the

chemical and mineral surface. By contrast if the biocide dissolves into the bulk mineral phase, absorption occurs. These mechanisms are summarized in Figure 2-2. Although these definitions are useful in principle, in practice, it may be difficult to distinguish between specific mechanisms. In fact, in heterogeneous systems, multiple sorption mechanisms may be occurring simultaneously.

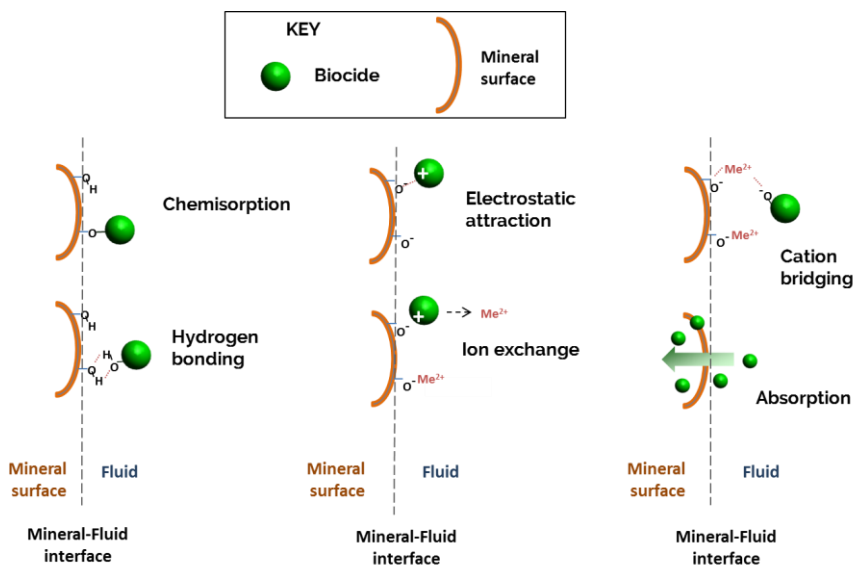
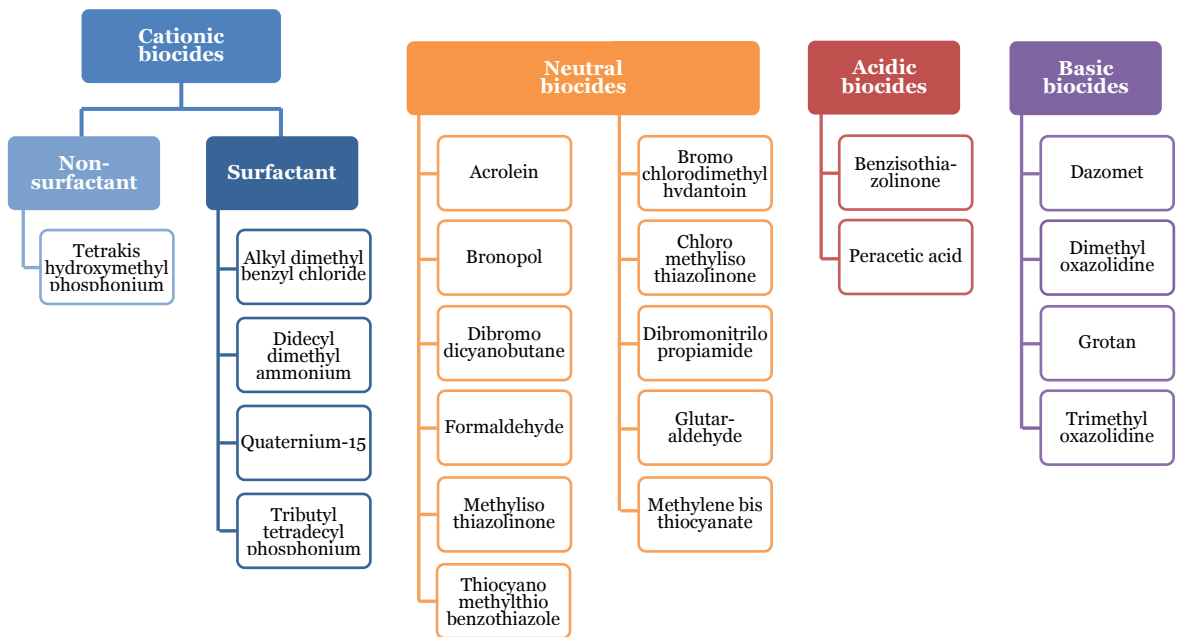


Figure 2-2. Illustration of possible sorption mechanisms of organic biocides onto mineral surfaces

Due to their amphiphilic nature, the sorption of cationic surfactant biocides can occur via two mechanisms and result in pronounced effects on the wettability and electrostatic properties of the mineral. Here, surfactants are defined as possessing a charged hydrophilic group (head) and a hydrophobic group or tail consisting of at least 8 carbon atoms. The first sorption mechanism is the electrostatic sorption of the charged head to the oppositely charged mineral surface. The hydrophobic chains which extend into the fluid can then stabilize other surfactant chains to form hemimicelles. The hydrophobic chains may also sequester other apolar compounds to the surface (Fuerstenau and Jia, 2004; Somasundaran and Zhang, 2006; Scheider et al., 1994). If the solid surface is itself hydrophobic, then the long hydrophobic chains adsorb, leaving the charged head to interact with the fluid.

Thus, to facilitate the discussion of mineral-fluid interactions, the biocides were also classified according to their charge in water and any surfactant-like properties, Figure 2-3a. Five main groups are represented: cationic biocides (with surfactants placed within their own separate group), acidic, basic, and neutral biocides. Figure 2-3b demonstrates visually how pH affects the overall charge of selected groups. Of the 22 biocides, the largest class was that of neutral biocides, i.e. compounds with no ionizable functional groups within 2 pH units from the pH range for produced water (pH 5.2 - 8.9). Interestingly, all of the surfactant biocides were cationic and several of the biocides possess a permanent positive charge or acquire one at low pH (basic biocides). No anionic biocides were identified. Positively charged biocides may be particularly useful as they are electrostatically attracted to the negatively charged bacterial cell walls (Carmona-Ribeiro and de Melo Carrasco, 2013). Several biocides dissociate into an inorganic anion and an organic cation. Only the latter was considered for this study.



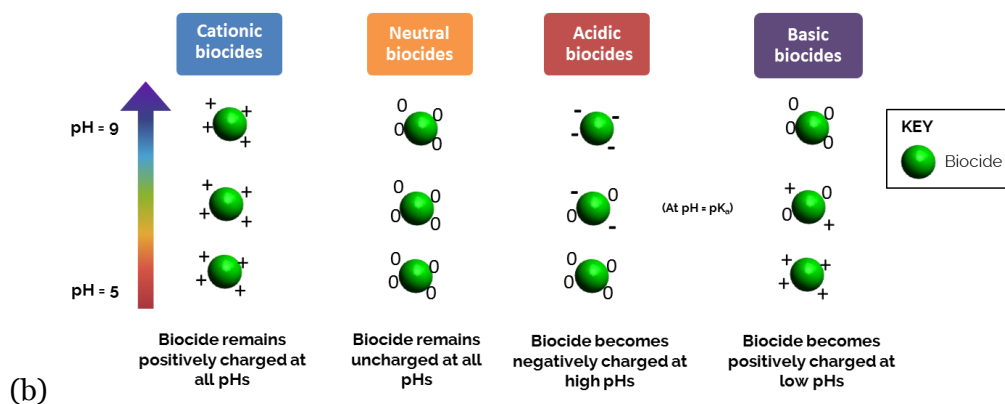
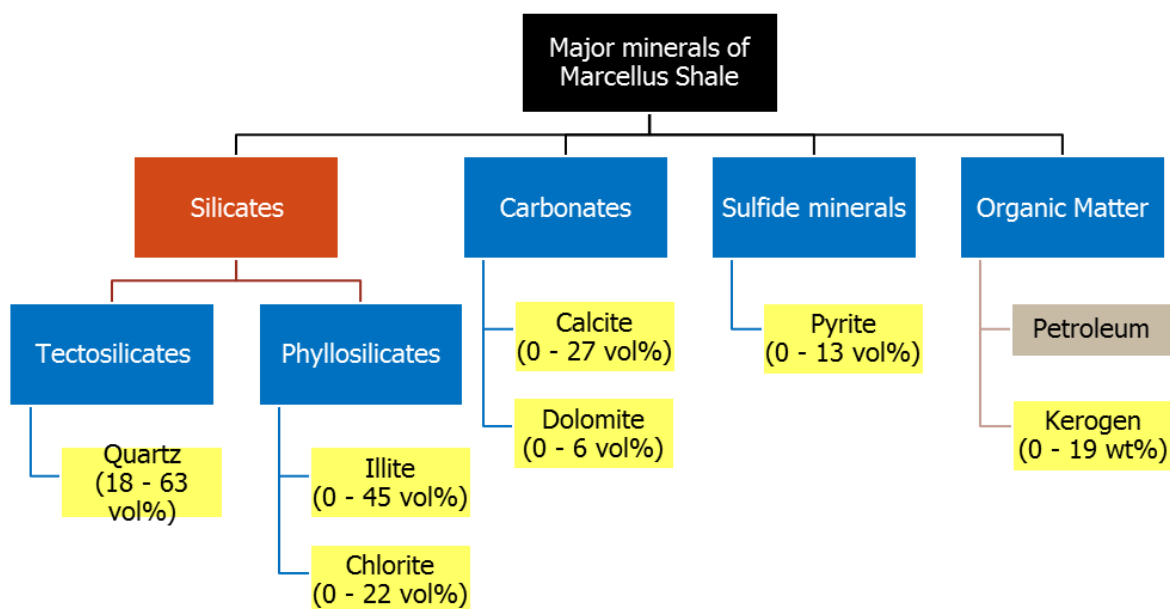


Figure 2-3. (a) Classification of biocide used in the Marcellus Shale according to dissociation in aqueous solutions. The biocides were compiled from Kahrilas et al., 2015, Rogers et al., 2015, Stringfellow et al., 2014, Carter et al., 2013 and Elsner and Hoelzer, 2016. The physical properties were estimated from the Chemical Abstracts Service, SciFinder (2017) and the PubChem compound database (2017). (b) Changes in net charge of cationic, neutral, basic and acidic biocides with pH.

## 2.4 Mineralogy of the Marcellus Shale

Extending southwest from New York state through Pennsylvania into West Virginia, the Marcellus Shale covers 50,000 square miles (Bruner and Smosna, 2011). It is the lowest unit of the clastic sedimentary layers in the Middle Devonian which accumulated 390 – 360 million years ago (Soeder, 2010). In 2015, proved reserves in the Marcellus Shale stood at 72.7 trillion cubic feet in 2016 (US EIA, 2016).

Shale is a highly consolidated composite of clay-sized particles and rock types (Figure 2-4). The characteristic dark color of black shales stems from compositions of organic carbon greater than 2% (Nijenhuis et al., 1999). The mineralogy of the Marcellus Shale consists predominantly of quartz,  $\text{SiO}_2$ ; illite,  $\text{KAl}_2(\text{AlSi}_3\text{O}_{10})(\text{OH})_2$ ; chlorite,  $(\text{Al,Fe,Mg})_6(\text{Al,Si})_4\text{O}_{10}(\text{OH})_8$ ; calcite,  $\text{CaCO}_3$ ; dolomite,  $\text{CaMg}(\text{CO}_3)_2$ ; and pyrite,  $\text{FeS}_2$  (Wang and Carr, 2012; Roen, 1984; Emmanuel, 2014; Fortson, 2012; Chalmers et al., 2012; Curtis et al., 2010, Tiab and Donaldson, 2004). In a typical sample, the phyllosilicates (quartz and clays) make up the largest portion of the shale matrix although the distribution varies widely between samples.



**Figure 2-4. Flow chart classifying the major minerals of Marcellus Shale minerals. The major groupings used in this review are shown in blue and the minerals investigated in detail are highlighted in yellow. The values in parentheses indicate the 25th to 75th percentiles corresponding minerals as determined by XRD and geochemical data (Wang and Carr, 2012)**

Mineral surfaces are charged in aqueous solutions, and the sign and magnitude of this charge is dependent on, among other factors, pH. At the water interface, the unsatisfied groups on the edges of the crystals are hydrolyzed resulting in the loss of gain of a proton ( $H^+$ ). This charge can be described as the point of zero charge (PZC) or pH at which the mineral surface is uncharged. It may also be quantified as the isoelectric point (IEP) or the pH at which there is a net neutral electric field. Although PZC and IEP are sometimes used interchangeably, the latter shifts if specific sorption of potential determining ions (PDIs) occurs. The mineral surface will be negatively charge at any pH higher than the IEP, and positively charged when the pH falls below.

## 2.5 Quartz

Quartz ( $SiO_2$ ) is the largest, single component of shale samples, accounting for approximately 40 vol% (Roen, 1984; Wang and Carr, 2012; Emmanuel, 2014). Its prevalence

and persistence are in part due to its low solubility and high stability which comes from its three-dimensional network of SiO<sub>2</sub> groups (Morey et al., 1962; Knauss and Wolery, 1988). Quartz also has very low surface areas: even finely ground powders have surface areas of less than 1 m<sup>2</sup>/g (Klimesch et al., 1996; Meloni et al., 2012). At the quartz-water interface, the silanol ( $\equiv\text{Si-OH}$ ) groups hydrolyze to form Si-O<sup>-</sup> groups. With an IEP below 2 (Kosmulski, 2014), a clean quartz surface is always negatively charged at the pH range observed in the Marcellus Shale. The structure of clays is unlikely to be affected by the hydraulic fracturing fluid.

### *2.5.1 Sorption to quartz*

The sorption of biocides to quartz is likely to be predicted by charge. In particular, positively charged biocides can displace water molecules within the diffuse layer to adsorb onto the negative surface of quartz. The influence of ionic strength, pH and temperature has been shown with methylene blue, a cationic organic dye (Jada and Ait Akbour, 2014). Increasing the ionic strength of the solution reduced sorption, due to an increased competition for surface sites. This competition is more pronounced with larger, loosely hydrated cations, as they can bind more tightly to the quartz surface. As pH is increased, the quartz surface becomes more negatively charged, enhancing sorption. Although an increase in temperature often leads to a decrease in sorption (Goss, 1992), the opposite was found to be true for methylene blue. This is likely due to compound-specific changes in the planarity of with temperature (Fontecha-Cámara et al., 2006). Basic biocides which dissociate at higher pH will likely sorb to the surface.

The sorption of cationic surfactant biocides may lead to the apparent sorption of less polar, neutral biocides. Cationic surfactants such as dodecylammonium chloride and dodecylpyridinium chloride have been shown to sorb onto the quartz surface (Li, 1958; Fuerstenau and Jia, 2004). At low concentrations of surfactants, the positively charged hydrophobic head approach the quartz surface, leaving the hydrophobic tail to interact with the

surrounding fluid. Consequently, this leads to further sorption of surfactants as the hydrophobic alkyl tails undergo favorable interactions. Alternatively, the small apolar molecules may partition from the surrounding fluid to these hydrophobic chains at the surface (Schieder et al., 1994).

In general, neutral biocides cannot compete with water molecules and dissolved cations sorbed on the quartz surface. Extremely hydrophobic, insoluble compounds such as PAHs have been shown to gain thermodynamic stability by sorbing to the vicinal water near the quartz surface (Müller et al., 2007). However, compounds with a log  $K_{ow}$  less than 2 will not undergo significant sorption to quartz surface (Barrett et al., 1994). This suggests that the only neutral biocide that may sorb to quartz is thiocyanomethyl thiobenzothiazole ( $K_{ow}$  of  $10^{3.1}$ ) although its relatively high solubility will combat this effect. At very high ionic strengths, cation bridging may become possible, resulting in the partitioning of negatively charged biocides to the quartz surface.

### *2.5.2 Transformation due to quartz*

The transformation of biocides due to quartz is not likely. Quartz is extremely stable hence unreactive due to its three dimensional silica structure. Although the generation of quartz dust is known to produce highly redox active hydroxyl ( $\bullet OH$ ) radicals (Narayanasamy and Kubicki, 2005), this is likely negligible in aqueous systems.

## **2.6 Clays**

Clay minerals are pervasive throughout the Marcellus Shale formation: one study reports clay minerals in every sample tested (Emmanuel, 2014; Hosterman and Whitlow, 1981). The two most detected clays are illite,  $KAl_2(AlSi_3O_{10})(OH)_2$  and chlorite  $(Al,Fe,Mg)_6(Al,Si)_4O_{10}(OH)_8$  with

median values of 30 vol% and 8 vol% respectively. The structures of these clays lend tremendous insight into their influence of the movement of organics in the subsurface.

Illite and chlorite are both 2:1 clays, comprising layers of octahedral aluminum oxide sheets each sandwiched between two layers of tetrahedral aluminum oxide sheets. These tetrahedral-octahedral-tetrahedral (TOT) layers are slightly negatively charged due to the presence of electron donating oxygen atoms on the surface (Hsu, 1999). The unbound  $\equiv\text{Al-OH}$  (PZC of 8.5) and  $\equiv\text{Si-OH}$  (PZC of 2) groups on the edges of the crystals hydrolyze in water, resulting in modest, but noticeable pH dependent positive and negative charges (Sposito and Grasso, 1999; Wainippee et al., 2013). Isomorphic substitutions on the surface of the TOT sheets result in a larger permanent charges. Here, cations with lower charges such as  $\text{Al}^{3+}$ ,  $\text{Fe}^{2+}$  or  $\text{Mg}^{2+}$  replace those with higher charges, ( $\text{Si}^{4+}$  or  $\text{Al}^{3+}$ ) (Sposito and Grasso, 1999; Schwarzenbach et al., 2003). These negatively charged TOT sheets are balanced by a positively charged interlayer. In illite, this consists of poorly hydrated potassium ions. In chlorites, this is a brucite-like ( $\text{Mg}^{2+}$ ,  $\text{Fe}^{3+}$ )(OH)<sub>6</sub> layer. In other clays such as smectite or montmorillonite, water can enter these sheets, forcing the layers apart when wet. However, illite and to a greater extent chlorite are considered “non-swelling” clays due to the strong electrostatic forces holding the layers together (Foster, 1954).

These structural properties result in the observable characteristics of these clays. Illite possesses an IEP of 2.8 (Nagaraj and Ravishankar, 2007; Hu et al., 2003), and for chlorite, this lies between 2 and 2.5 (Tan et al., 2013; Alvarez-Silva 2010). The ability of clays to attract positively charged species is measured as the cation exchange capacity or CEC. Unlike many other clays, the major clays in the Marcellus Shale possess relatively low surface areas and CECs. Chlorite has a surface area of 10 to 40 m<sup>2</sup>/g. Illite’s is slightly higher, at 65 to 100 m<sup>2</sup>/g. By contrast, montmorillonite has a surface area between 600 to 800 m<sup>2</sup>/g. This difference stems from increased access to the interlayer surface area of the latter (Bailey and White, 1964;

Antognozzi et al., 2006; Altin et al., 1999; Burgos et al., 2002). Thus while montmorillonite clays boasts CEC values between 80 and 150 meq per 100 gram clay, the CEC of illite and chlorite lie between 10 and 40 meq per 100 gram clay. Illite and chlorite are hence much less reactive than kaolinite and montmorillonite clays and are consequently featured less often in scientific studies. Acid treatment may alter the structure of clays, usually increasing the available surface area for adsorption (Jozefaciuk and Matyka-Sarzynska, 2006; Jozefaciuk and Bowanko, 2002). The hydraulic fracturing fluid on the other hand has been shown to have little effect on the structure of these clays (Dieterich et al., 2016).

### *2.6.1 Sorption to clays*

Clays are excellent adsorbents for cationic and basic biocides such as the tetrakis hydroxymethyl phosphonium cation and dimethyloxazolidine. Due to the permanent negative surface charge on the TOT layers, cationic biocides are electrostatically adsorbed to clay minerals (Koppelman, 1980; Siobhán and Roubaud, 1997; Cornejo, et al., 2008, Bansal and Bansal, 1980). This sorption is comparable to that experienced with (but may decrease on the addition of) natural organic matter (NOM) (Droge and Goss, 2013; Bansal and Bansal, 1980). In addition, the dissociated water molecules that are sorbed to the negatively charged TOT sheets can behave as proton donor sites resulting in clay minerals surfaces 2 to 4 pH units below the pH of the bulk fluid (Stevens, 1998; Bhattacharyya and Gupta 2008; Bailey et al., 1968). The presence of these acidic sites on the surface of clay favors the protonation and adsorption of basic compounds such as atrazine (Herwig, et al., 2001). As ionic strength increases, sorption is expected to decrease as inorganic cations compete for limited sorption sites on the clay surface (Fil et al. 2016; Droge and Goss, 2013). The effect of temperature is more difficult to predict as it can affect the rate of sorption, desorption and solubility of the organic compound, all which affect overall affinity to the clay surface (Fil et al. 2016; Bansal and Bansal, 1980; Adeyemo et al.,

2017). By comparing the sorption of a wide variety of cationic amines ( $-N^+R_4$ ) Droge and Goss (2013) found that in general, sorption increased as the size of the molecule increased and as the order of the amine increased. However, the addition of other polar groups decreased sorption. This suggests that the sorption of the cationic biocide tetrakis hydroxymethyl phosphonium and the basic biocide grotan will be tempered due to their multiple polar groups.

Similarly, the sorption of cationic surfactants such as the quaternary ammonium surfactants (alkyl dimethyl benzyl ammonium chloride and didecyl dimethyl ammonium chloride) is favorable, enhanced by hydrophobic interactions. Fourier transform infrared spectroscopy (FTIR) shows that sorption initially occurs via electrostatic attraction and, if possible hydrogen bonding (Huang et al., 2013). In a study investigating the sorption of octadecyltrimethylammonium bromide, a cationic surfactant onto illite, it was estimated that surfactant sorption exceeded the CEC of the clay by 410% (Sánchez-Martín et al., 2008). Langmuir type graphs indicate that the hydrophobic attractions are equally as favorable as electrostatic ones: there was no plateau or break in the isotherm to indicate a switch from monolayer electrostatic attraction to sorption of hemicelles. At lower concentrations, cationic surfactants on the surface of clay may increase the sorption of neutral species (Sánchez-Martín et al., 2006; Laha et al., 2009; Klumpp et al., 1993).

The effect of pH is complex due to the pH dependence of both the molecule and the clay surface. For example, we consider the amphoteric pesticide oxamyl (Bansal and Bansal, 1980). At low pH, some fraction of the compound exists in the protonated form which favors sorption onto the clay. As the pH increases, the clay become more negatively charged, resulting in an overall increase in sorption. However, as the pH is further increased, the organic compounds in turn became deprotonated, losing their affinity for the clay surfaces. Studies investigating the ability of cationic surfactants to adsorb to illite for the recovery of useful mineral ores show that as pH increases, sorption generally decreases (Deng et al., 2016; Xia et al., 2009). This is due to

enhanced competition with the solution cations or protonation of the surfactant. The result is that affinity for positively charged biocides will peak around neutral pH.

Due to the negatively charged surface, the sorption of any anionic biocides is expected to be limited. Although negatively charged pesticides are not usually well retained, sorption may occur via one or both of two mechanisms (Errais et al., 2012; Cornejo et al., 2008). The first is the use of an electrolyte cation as a bridge or intermediate. Experiments with salicylic acid (a negatively charged organic molecule) and illite illustrate that as  $\text{Na}^+$  concentration is increased, sorption also increases due to more “bridging” cations. The second is sorption to the unbound  $\equiv\text{Al-OH}_2$  and  $\equiv\text{Al-OH}$  groups at the clay edges via ligand exchange. In this case, increasing pH leads to a decrease in the sorption of deprotonated (negatively charged) salicylic ions as fewer easily exchangeable  $\equiv\text{Al-OH}_2$  become available (Kubicki et al., 1997).

The sorption of neutral biocides is also predicted to be limited, except in the case of bronopol. Because all the biocides surveyed are polar and soluble, they are expected to partition weakly (if at all) to clay surfaces due a combination of van der Waals forces and H-bonding (Herwig et al., 2001; Weber, 1970; Hermosin et al., 1982; Laird 1996; Lagaly, 2001). Nitro aromatic compounds (NACs) have been shown to strongly sorb to illite clays (Haderlein et al., 1996). This sorption is due to limited solubility of NACs in water and the presence of electron-withdrawing aromatic nitro groups which chemisorb to the electron-rich siloxanes oxygen atoms on the illite TOT sheets. Although none of the biocides are NACs, bronopol does have a nitro group which may enhance its sorption.

### *2.6.2 Transformation with clays*

Illite and chlorite may contribute to the reduction of reducible biocides due to the redox properties of structural iron. Illites and chlorite clays possess structural  $\text{Fe}^{\text{III}}$  and  $\text{Fe}^{\text{II}}$  (Seabaugh et al., 2006; Jaisi et al., 2007). The latter has to potential to contribute some redox activity.

Smectite clays, particularly those with high amounts of iron have been shown to reduce NACs and polychlorinated alkanes (Hofstetter et al., 2003; Neumann et al., 2009). The fraction of redox-active species was found to depend on the total Fe content; the layer charge; and molecular scale Fe–O bond lengths of the clay (Gorski et al., 2013). Little research has investigated the phenomenon with chlorite and illite clays, but experiments illustrating the microbial reduction of Fe<sup>III</sup> in these minerals suggest that the structural iron may be accessible to chemical redox activity (Jaisi et al., 2007). However, this is likely to be limited by illite and chlorite's non-expanding structure and relatively few structural defects which may increase the reaction surface area (Seabaugh et al., 2006).

Illite may catalyze the hydrolysis of some hydrolysable biocides such as DBNPA. In experiments investigating the effect of clay minerals on carbamates, Wei et al. (2001) found that illite, along with other clay minerals could hydrolyze the pesticides carbosulfan and aldicarb. Interestingly, montmorillonite was shown to inhibit the degradation of chlorpropham, and had no significant effect on other carbamate pesticides carbofuran and primicarb. Despite having similar reactive groups (that is, the carbamate functionality, -NHC(O)O-) the effect of clays varied widely. The difference in reactivity was attributed instead to the structural properties of each of these related pesticides. Chlorpropham hydrolysis was inhibited due to its ability to penetrate into and be protected by the interlayer spaces of montmorillonite. Because illite and chlorite are non-expanding clays, they are unlikely to inhibit the catalysis of biocides in this way. Carbosulfan and aldicarb were both hydrolyzed, because only these pesticides possessed a carbonyl functionality and nitrogen-containing group separated by a flexible aliphatic chain of one or two atoms. Figure 2-5 contrasts the structures of carbosulfan and primicarb. This allowed the sorption of carbosulfan to the clay surface, where it was hydrolyzed either due to the surface acidity of the clays or the formation of surface chelates which promote the attack of H<sub>2</sub>O molecules. As DBNPA also has a carbonyl group separated from a nitrogen-containing group,

enhanced sorption of illite is likely, but experimental work will need to be done to determine whether illite can catalyze this reaction. The addition of other organic compounds or salts is likely to decrease this catalysis.

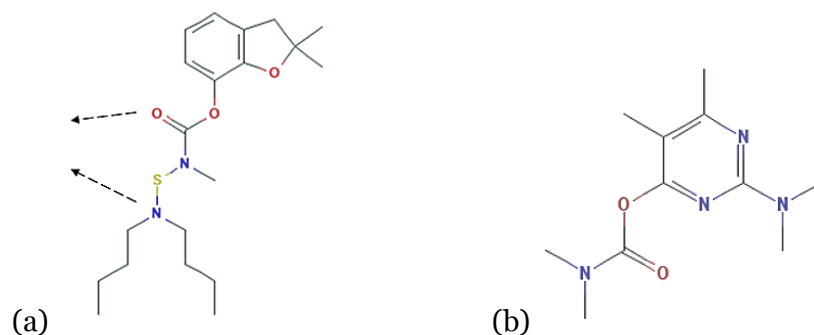


**Figure 2-5. (a) Molecular structure of carbosulfan, indicating points of sorption to clay surfaces as suggested in Wei et al., 2001 (b) Molecular structure of primicarb**

## 2.7 Carbonates

Calcite minerals in sedimentary rocks originate from the exoskeletons of marine animals and the direct precipitation of the mineral. Dolomite is generally authigenic (Emmanuel 2014). Calcite and dolomite are usually present at low levels in black shales (3 vol% and 2 vol% in the Marcellus Shale, respectively) but have been detected at concentrations greater than 90 vol% (Wang and Carr, 2012). Many more studies have been conducted on calcite than dolomite, leading to a larger repository of data, but in aqueous systems, both minerals react in a similar manner (Pokrovsky et al., 1999). Carbonate dissolution is accelerated in acidic solutions. At 25°C and pH of 7, calcite and dolomite dissolution rates lie at  $10^{-7}$  and  $10^{-10}$  mmol  $\text{cm}^{-2}$   $\text{s}^{-1}$ , respectively. Decreasing the pH drastically increases dissolution rates by 2 – 3 orders of magnitude (Plummer et al., 1979; Morse and Arvidson, 2002). Hydrochloric acid may be used by operators to chemically initiate fracturing of the formation (King, 2012). This acid

preferentially dissolves these soluble minerals. Because of their rapid dissolution the abundance of carbonates in hydraulically fractured shale is expected to be much lower than that of pristine shale samples. The carbonate also acts as a buffer, so that shales with higher carbonate concentrations generate produced water with higher pH (Paukert Vankeuren et al., 2017; Harrison et al., 2017; Marcon et al., 2017).

In water, calcite surface groups react with the divalent cations,  $Me^{2+}$ , and  $CO_3^{2-}/HCO_3^-$  to develop the overall surface charge. As the  $Me^{2+}$  concentrations in solution increase, the surface of the carbonate becomes more positively charged. And as  $CO_3^{2-}/HCO_3^-$  concentrations increase, the surface becomes more negative. Thus, the point of zero charge (PZC) of the carbonate system depends on the pH, partial pressure of  $CO_2$  and the  $Me^{2+}$  potential determining ions (PDIs) in solution (Moulin and Roques, 2003; Vdović, 2001). In light of the best estimates for calcite and dolomite isoelectric points (IEPs), the carbonates would be positively charged for most pHs of interest (Ma et al., 2013; Pokrovsky et al., 1999; Kosmulski, 2009).

### 2.7.1 Sorption to carbonates

The sorption of biocides with carboxyl functional groups,  $-C(O)OH$ , can occur by the substitution of the carboxyl group for the  $CO_3$  group in carbonates. The chemisorption of acidic amino acids, humic acids and fulvic acids (all negatively charged organics in aqueous solution) has been well investigated in the literature. These organic compounds react with  $CO_3^{2-}$  ions in calcite and dolomite (Morse, 1986; Carter, 1978). Computer simulations have been employed to discern the effects of the carbonyl ( $-C=O$ ) group and hydroxyl ( $-OH$ ) group. The results suggest that in addition to carboxylic acids, hydroxy aldehydes (compound containing non-adjacent carbonyl and hydroxyl groups) and amides ( $-C(=O)NR_2$ ) could undergo significant chemisorption with calcite (de Leeuw and Cooper, 2003). This idea is supported by many studies investigating the sorption of various pesticides onto calcite: only pesticides with these

groups exhibited measureable sorption (Clausen et al., 2001; Kovaios et al., 2006; Gülüt and Sayin, 1998). Thus unlike the previous minerals, the sorption of biocides to carbonates introduces the need to consider the specific functional groups of the biocides. An interesting sorbate would be peracetic acid. It dissociates to form a negatively charged compound which possesses both the carbonyl and hydroxyl groups which favor sorption onto calcite. This also suggests that there may some affinity for biocides containing amine groups such as DBNPA; biocides with multiple carbonyl groups such as glutaraldehyde; and biocides with a carbonyl group adjacent to another electronegative group such as bromochlorodimethylhydantoin or any of the isothiazolinones.

Ionic strength, in general, was found to decrease sorption. In some cases,  $Mg^{2+}$  ions were theorized to complex with the organic compound, resulting in decreased sorption on the carbonate surface (Lahann and Campbell, 1980). In others, negatively charged orthophosphate was found to displace fatty acids from the surface (Zullig and Morse, 1988). Because most studies focused on the reactions taking place in surface waters, the effect of temperature or pH has been largely ignored (Morse, 1986).

The sorption of positively charged surfactant biocides to calcite is also likely to be appreciable although the mechanism for this unlikely interaction is not yet clear. Although carbonates are positively charged in the pH range of natural systems, studies have reported the sorption of cationic surfactants such as cetylpyridinium chloride and dodecyltrimethylammonium bromide (Ma et al., 2013, Durán-Álvarez et al., 2016). Multiple explanations have been proposed. Undetectable sorption onto synthetic calcite suggest that Si and Al impurities or sorbed natural organic matter may provide additional negative sites for cationic sorption (Moulin and Roques, 2003). Alternatively, the sorption of cationic surfactants may take place at the negatively charged surface groups on the calcite surface, which exist despite a net positive charge. Theoretical and computational models using

dodecyltrimethylammonium bromide have led to a third explanation. This cationic surfactant possesses a relatively “soft” (viz. large and polarizable) headgroup. This results in a diffuse positive charge that is partly spread onto the surfactant’s aliphatic, hydrophobic tail. Density Functional Theory (DFT) models illustrate that the flexible surfactant can undergo rearrangement in solution due to both anionic bridging and hydrophobic chain-chain interactions to aggregate onto the calcite surface (Vlachy et al., 2009; Durán-Álvarez et al., 2016). Considering these arguments, it is highly likely that sorption of alkyl dimethyl benzyl ammonium chloride, quaternium-15 and didecyl dimethyl ammonium chloride will occur. By extension, the sorption of tributyl tetradecyl phosphonium chloride is also likely. The polarizability of phosphonium surfactants should be greater than that of corresponding ammonium surfactants leading to even more favorable interactions with carbonate minerals.

### *2.7.2 Transformation with carbonates*

While carbonates are themselves transformed due to dissolution and precipitation reactions, there is very little research highlighting the role of calcite and dolomite in redox reactions. While Nefso et al. (2005), show that of six mineral surfaces, only calcite and siderite were able to reduce trinitrotoluene, TNT, the reduction was occurred due the presence of  $\text{Fe}^{2+}$ , this activity was attributed to the higher final pH rather than the carbonate structure.

## **2.8 Sulfides**

Pyrite ( $\text{FeS}_2$ ) is the most frequently detected sulfide in the Marcellus Shale and is often associated with organic matter in black shales (Curtis et al., 2010). Pyrite formation occurs during the early stages of burial via the reaction of iron minerals and  $\text{H}_2\text{S}$  from to the respiration of sulfate-reducing bacteria under oxygen-depleted conditions (Berner, 1984). These conditions also support the accumulation of organic matter, the ultimate source of natural gas. Thus, pyrite

is often associated with black shales, occurring at average concentrations of 4 vol% but has been measured at up to 24 vol% in some parts of the Marcellus Shale (Wang and Carr, 2012). Pyrite aggregates into framboids, forming thin bands averaging 5  $\mu\text{m}$  throughout the shale (Chalmers et al., 2012; Roen, 1984; Curtis et al., 2010; Emmanuel, 2014; Lash and Blood, 2014).

The pyrite surface presents two distinct surface sites: those centered around the Fe atoms and those on the  $\text{S}_2$  dimer. While the iron sites tend to be hydrophilic, the thiol surface sites are more hydrophobic. Under anoxic conditions and in the absence of PDIs, the PZC of all metal sulfides including pyrite lie between 0.6 and 3.0. Solutions containing  $\text{Fe}^{2+}$  will result in an increase in isoelectric potential (IEP) (Weerasooriya and Tobschall, 2005; Bebié et al., 1998). In acidic ( $\text{pH} < 5$ ) anoxic solutions, pyrite dissolves to release  $\text{Fe}^{2+}$  into solution (Weerasooriya and Tobschall, 2005). Parthasarathy et al. (2015) showed that pyrite dissolution may be enhanced by the presence of that are cations such as  $\text{Na}^+$  (which preferentially coordinate with the  $\text{S}_2$  dimer) but suppressed by the presence of  $\text{Cl}^-$ .

Pyrite surfaces are quite complex and continually evolving in aqueous solution. Because  $\text{FeS}_2$  is a semiconductor, it can undergo electrochemical reactions. The surface of pyrite is quite reactive: it rapidly oxidizes in air and in oxygenated aqueous solutions. In water, pyrite generates  $\text{H}^+$  ions and ferric iron ( $\text{Fe}^{3+}$ ) which further fuels pyrite oxidation (Chandra and Gerson, 2010). In aqueous, air-saturated solutions, the pyrite surface is oxidized to form mainly ferric (hydroxy)sulfate and at pH greater than 4,  $\text{Fe}^{\text{III}}$  oxyhydroxide forms on the surface as well (Todd et al., 2002; Dos Santos et al., 2016). This rapid oxidation of pyrite may be the cause of misestimated IEP: studies reporting values between 5.5 and 6.8 (as summarized by Kosmulski, 2009) may be measuring the IEP of the corresponding, and often present, iron oxide (Weerasooriya and Tobschall, 2005). Experiments confirm that if even in fracking fluids with low levels of oxygen are used, pyrite will be oxidized and dissolved, especially at higher pH. The

result is that the surface becomes oxidized with a corresponding release of Fe<sup>III</sup> cations and sulfate anions (Jew et al., 2017; Harrison et al., 2017; Marcon et al., 2017).

### 2.8.1 Sorption to pyrite

Evidence points to the ability of pyrite to chemisorb to a wide variety of organic biocides. In fact, there is little correlation between the charge of the pyrite surface and sorption of organic compounds (Murphy and Strongin, 2009). In a study designed to probe the effects of carboxyl (-C(O)OH), sulfonate (-SO<sub>3</sub>-), hydroxyl (OH) and carbonothioyl or thiourea (-C(=S)R) functional groups, Boulton et al. (2001) concluded that each of these groups were able to undergo specific interactions to the pyrite surface. In oxygen rich solutions, this adsorption occurs on the oxidized pyrite sites (Mu et al., 2016). Under anoxic conditions, Bebié and Schoonen (2000) observed that a diverse group of 12 cationic, anionic, zwitterionic and neutral biogenic molecules could all chemisorb to pyrite sites due to the distinct physicochemical properties of the iron-centered and the sulfide-centered surface groups. In both studies, even anionic compounds were able to overcome electrostatic repulsion of the negatively charged surface to bind with the pyrite surface. Metal ions Fe<sup>2+</sup> and Cu<sup>2+</sup> often caused an increase in the magnitude of the interaction between organics and pyrite (Bebié and Schoonen, 2000). Particularly strong interaction is predicted for biocides with multiple electronegative functional groups such as grotan but further experimental work is needed to investigate this.

The sorption of biocides with sulfur containing groups such as dazomet and benzisothiazolinone also stand out as being very likely to sorb to oxidized pyrite. In the aforementioned study, Bebié and Schoonen (2000) noted a particularly strong interaction of cysteine under anoxic conditions, which contains a thiol (-SH) group, possibly due to an enhanced affinity to iron sites. Practices in mineral engineering echo this finding. Xanthates, sulfur analogues of carbonate ester salts, are extensively used to alter the hydrophobicity of

pyrite. Other sulfur containing compounds such as dithiophosphates, thiocarbamates and benzothiozoles have also been used (Bradshaw and O'Connor, 1994). Chemisorption of xanthates occurs under oxygen-saturated conditions via the interaction of the negatively charged sulfur group with any oxidized iron-centered (sulfur deficient) surface sites (Wang, 1995; Ahmed, 1978). The molecular structures of established pyrite collectors and sulfur-containing biocides are presented in Figure 2-6 to illustrate the possibility of sorption of dazomet and benzisothiazolinone.

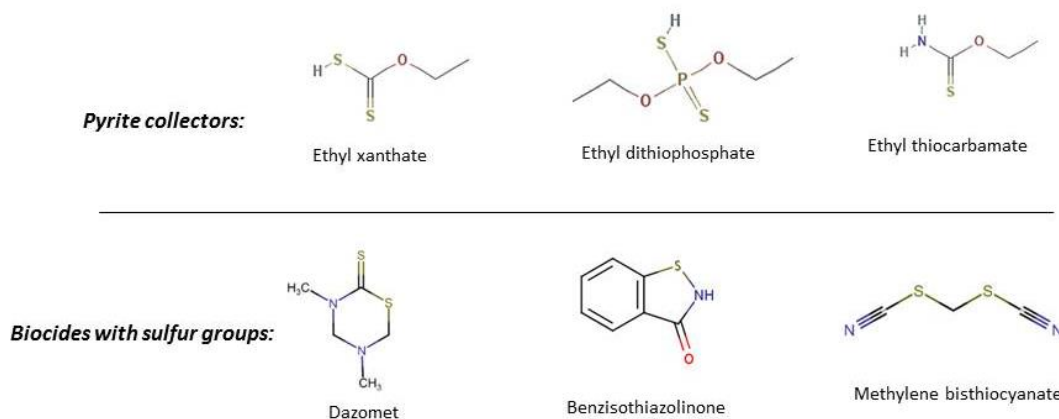


**Figure 2-6. Molecular structures of pyrite collectors and biocides with similar-sulfur-containing groups.**

The sorption of the cationic surfactant biocides should occur at any pH as they can sorb to both the hydrophobic and hydrophilic sites. Bae et al. (2012) looked at the adsorption of the cationic surfactant cetylpyridinium chloride onto pyrite, varying pH and the solution ionic strength. Because the experiment was conducted under aerobic conditions they measured a PZC value of 6.25. They found that adsorption occurred under two regimes. Below the PZC, the surfactant sorbed due to hydrophobic interactions such that the aliphatic tails were towards the pyrite surface. However, above the PZC, the hydrophilic heads were sorbed towards the surface and the formation of micelles was observed. This is likely to be an electrostatic attraction, as increasing ionic strength decreased sorption.

## 2.8.2 Transformation with pyrite

Pyrite is redox active, as demonstrated by its oxidation in oxic aqueous solutions. This redox activity may result in the reduction of halogenated biocides such as dibromodicyanobutane, dibromonitrilopropionamide (DBNPA) and 1-Bromo-3-chloro-5,5-dimethylhydantoin. Molecular orbital theory indicates that electrons may be transferred between the sulfur dimer of pyrite and the highest occupied molecular orbitals (HOMO) or lowest unoccupied molecular orbitals (LUMO) of the approaching compound (Luther, 1987). Specifically, pyrite can reduce compounds with  $\pi$  or  $\pi^*$  LUMO symmetry and oxidize compounds with  $\sigma^*$  HOMO symmetry. This hypothesis was used to explain the reductive dechlorination of recalcitrant pollutants such as trichloroethene (TCE) under anoxic conditions (Weerasooriya and Dharmasena, 2001). Degradation rates were independent of pH below 5.5. However, above this pH, degradation increased significantly, probably due a greater prevalence of hydrophobic  $S_2$  sites, which interact favorably with the hydrophobic TCE molecules ( $\log K_{ow} \approx 2.4$ ). Lee and Batchelor (2002) also showed that pyrite could dechlorinate a range of chlorinated ethylenes (tetrachloroethylene, trichloroethylene, TCE, *cis*-dichloroethylene, *cis*-DCE, and vinyl chloride, VC), Figure 2-7. Extending this argument predicts that redox activity is likely with that biocides which possess double and triple bonds (that is,  $\pi$  bonding) and good leaving groups (such as halogens).

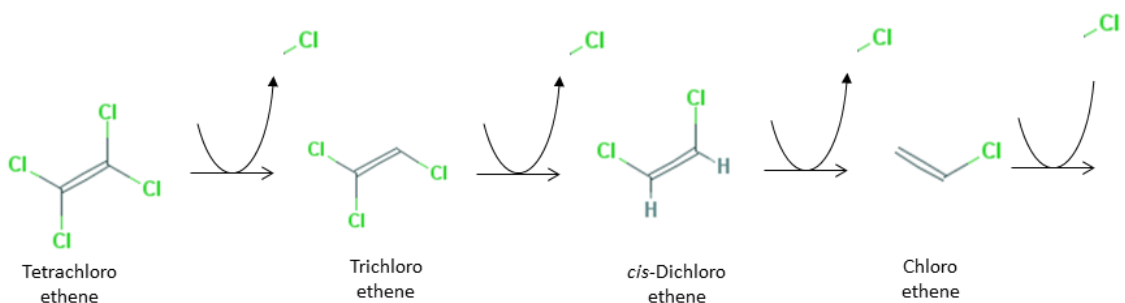


Figure 2-7. Reductive dechlorination of chlorinated ethylenes by pyrite, as proposed by Lee and Batchelor (2002).

Another mechanism for the degradation of any organic biocide due to pyrite lies in the formation of reactive hydroxyl radicals ( $\cdot\text{OH}$ ) in aqueous solutions. Borda et al. (2002) hypothesized that the conversion of  $\equiv\text{Fe}^{\text{III}}$  defect sites to  $\equiv\text{Fe}^{\text{II}}$  produces hydroxyl radicals which can then combine to form  $\text{H}_2\text{O}_2$ . Both of these species are extremely reactive and non-specific oxidants. Using the pyrite as an iron source, dissolved  $\text{Fe}^{2+}$  ions in conjunction with  $\text{H}_2\text{O}_2$  can then initiate a Fenton-like mechanism to oxidize organic compounds. Pham et al. (2008; 2009) illustrated that in the presence of dissolved oxygen, TCE could be oxidized with pyrite to produce organic acids and  $\text{CO}_2$ . This Fenton-like reaction is dependent on both temperature and pH. For example, lactate oxidation was fastest in the pH range of 4.5 to 6. Under basic conditions  $\text{H}_2\text{O}_2$  decomposes and the ferric sites become hydroxylated, reducing the production of hydroxyl radicals. Increasing the temperature increased the rate of lactate oxidation with pyrite, up to  $60^\circ\text{C}$  at which increased  $\text{H}_2\text{O}_2$  degradation diminished the oxidation of lactate (Wang et al., 2012). This reaction was found to decline with the addition of hydroxyl radical scavengers such as ethanol (Zhang et al., 2015). The production of hydrogen peroxide has also been noted in mineral engineering and is affected by the grinding method used prior to floatation (Javadi Nooshabadi and Hanumantha Rao, 2014; Moslemi and Gharabaghi, 2017; Peng and Grano, 2010). This mechanism is highly dependent on the concentration of oxygen in the fracking fluid, but the production of in situ hydroxyl radicals due to defects at the surface may result in non-specific oxidation of biocides.

## **2.9 Organic matter**

Organic matter in sediments is often a major factor controlling the adsorption of nonionic organic compounds. The nature of sorption depends heavily on the structure of the organic matter (Schwarzenbach et al., 2003; Grathwohl, 1990; Huang et al., 2003). At 4 to 19 wt% in the Marcellus Shale, the organic carbon originated from phytoplankton and higher plant

material remains that escaped remineralization in the water column during sedimentation (Werne et al., 2002; Lash and Blood, 2014). On burial, it was then subjected to increasing heat and pressure resulting in kerogen and, over time, oil and natural gas (Killops and Killops, 2005). Of these forms of organic matter, kerogen is the largest by several orders of magnitude (Vandenbroucke and Largeau, 2007). The kerogen of the Marcellus Shale is classified as type II kerogen as it was formed under marine settings (Bruner and Smosna, 2011; Killops and Killops, 2005).

Kerogen is operationally defined as the organic component of sedimentary rocks that is insoluble in typical solvents. Thus, elucidation of its structure must be implied from converging lines of evidence: its lack of solubility; a range of analytical techniques; and theoretical understanding of kerogen formation (Cao et al., 2013; Longbottom et al., 2016). Kerogen is proposed to be a condensed, three-dimensional organic macromolecule or geopolymer of molecular weight between 5,000 – 10,000 Da (Vandenbroucke and Largeau, 2007). Initially, type II kerogen has both structurally flexible aliphatic groups and rigid aromatic groups. As it matures, the latter begins to dominate the structure and the polar oxygen- and nitrogen-containing functional groups are lost (Behar and Vandenbroucke, 1987; Killops and Killops, 2005).

### *2.9.1 Sorption to kerogen*

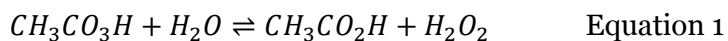
The sorption of positively charged surfactant biocides to kerogen is highly favorable due to multiple augmenting mechanisms of sorption. Sorption to organic matter is described by a dual mode model: the sum of linear absorption into the aliphatic portions and nonlinear adsorption onto relatively planar, aromatic surface. In kerogen, the latter can result in partitioning coefficients several orders of magnitude higher than predicted by  $k_d$  (Cornelissen et al., 2005; Allen-King et al., 2002). In the field however, this sorption is attenuated due to

polycyclic aromatic hydrocarbons (PAHs) such as naphthalene and phenanthrene that are naturally present in the shale (Cornelissen et al., 2005; Orem et al., 2014). Organic biocides must also be capable of displacing these PAHs previously sorbed to kerogen. Positively charged surfactants appear to be the best suited for this as they can undergo hydrophobic interaction with the aliphatic and aromatic components of kerogen, electrostatic bonding and even hydrogen bonding (Keiluweit and Kleber, 2009; Zhang and He, 2011; Edwards et al., 1994). An increase in temperature is likely to decrease sorption to organic matter (Zhang et al., 2009). The sorption of surfactant biocides also results in a subsequent increase in partitioning of apolar compounds, but a decrease in the partitioning of hydrophilic biocides. This is due to an increase in hydrophobic sorption sites (Zhang and He, 2011; Edwards et al., 1994; Tao et al., 2006).

Because of the numerous polar groups observed on other biocides, kerogen is unlikely to be a significant factor controlling their transport. Of these, the biocides benzisothiazolinone and thiocyanomethyl thiobenzothiazole are most likely to be influenced by kerogen due to aromatic moieties in their structure. Experiments with highly polar but aromatic 1,3,5-trinitrobenzene (TNB) illustrate that the aromatic rings in black carbon to sediments were responsible for 34-54% of sorption due to highly favorable interactions of the aromatic groups (Shi et al., 2010; Keiluweit and Kleber, 2009). For kerogen with the specific thermal history of the Marcellus Shale (type II kerogen with a reflectance of vitrinite, RO, between 1.1 and 2%) the most significant factor controlling sorption is adsorption in the kerogen pores. Partitioning into aliphatic moieties and onto external aromatic surfaces is less important (Yang et al., 2004; Bruner and Smosna, 2011, Ran et al., 2004). Thus, the biocides with aromatic groups are likely to partition, but larger biocides such thiocyanomethyl thiobenzothiazole will be sterically inhibited. The acid treatments used in hydraulic fracturing are unlikely to affect the sorption of biocides to kerogen as experiments show that treating unoxidized sediments with acids had no effect on the partitioning of organic compounds to the sediments (Jeong et al., 2008).

### 2.9.2 Transformation with kerogen

Kerogen is considered fairly inert as the most reactive components have long been degraded (Philip and Calvin, 1976). Kerogen reduces strong oxidizing agents, and is slowly oxidized in air (Saxby, 1976; Durand and Nicaise, 1980). Of the biocides listed, peracetic acid is the most likely to be affected by this property of kerogen. In water, peracetic acid exists in equilibrium with acetic acid and hydrogen peroxide (equation 1). The latter is reduced by kerogen. The law of mass action will ultimately lead to a decrease in the parent compound, peracetic acid.



### 2.10 Perspective on Mineral-Fluid Interactions of Biocides

When compiled, a variety of experimental studies from diverse fields have advanced our understanding of interactions between minerals surfaces and organic compounds. By focusing on the structure and reactivity of biocides and minerals, this review offers general approaches to anticipate the sorption and transformation mechanisms of biocides, and has identified specific processes that may occur.

Of the groups of biocides studied, positively charged biocides (cationic and basic biocides) are the most likely to physisorb to the Marcellus Shale. Despite widely differing structures, most of the minerals surveyed were negatively charged in aqueous solutions, in particular the most prevalent minerals: quartz and clays minerals. The surface area of illite and chlorite is 2 – 3 orders of magnitude greater than that of quartz, so these clay minerals are likely to be much better sorbents. The extent of sorption is a strong function of pH, which affects the charge of minerals and basic biocides. Cationic biocides were shown to sorb to every mineral due to multiple mechanisms for sorption. This is consistent with the studies showing significant

losses of cationic surfactants when exposed to shale minerals (Zhou et al., 2016). These biocides, in significant concentrations, can also change the wettability of the shale, allowing the incorporation of neutral biocides (Zelenev et al., 2011). In the absence of cationic biocides, neutral biocides are unlikely to sorb due to their high hydrophilicities (as in Tasker et al., 2016). Of the minerals investigated, illite is likely the most responsible for physisorption in the shale. However, many more experimental studies are needed to better characterize the interactions of this mineral with organic compounds in shale formations. These results are summarized in Figure 2-8.

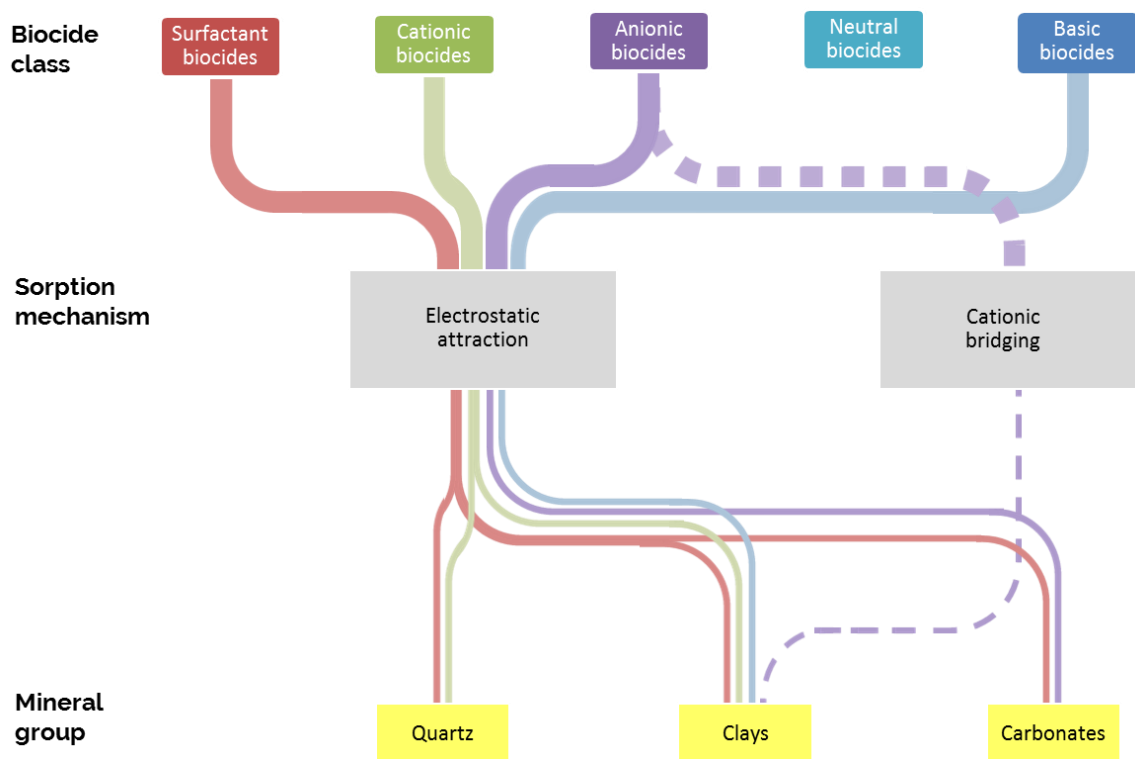
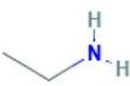
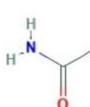
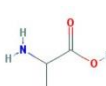
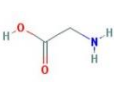
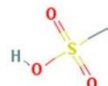
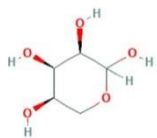
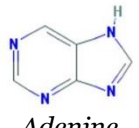
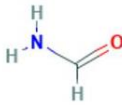
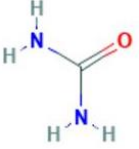
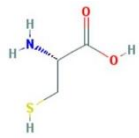
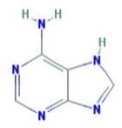


Figure 2-8. A summary of physisorption mechanisms controlling the sorption of the assigned biocide classes to quartz, clays and carbonates.

Chemisorption of biocides is predicted by the presence of specific functional groups. In carbonate minerals, the interaction between calcite and dolomite  $\text{CO}_3$  groups and carbonyl containing functional groups was the primary driver for chemisorption. But, the rapid

dissolution of this mineral limits chemisorption onto the surface. With pyrite, the chemisorption of multiple functional groups in both oxic and anoxic environments has been observed (Table 2-3). It must be noted that although the interaction of pyrite with multiple groups has been illustrated, the extent of this reaction has not been measured and as such, it is difficult to translate these interactions in to what is observed on a macroscopic level. However, a key finding is that pyrite sorption can occur, regardless of the charge of the biocide or pyrite surface.

**Table 2-3. Organic functional groups and organic compounds shown to chemisorb onto carbonates, pristine pyrite, and oxidized pyrite surfaces (de Leeuw and Cooper, 2003; Bebié and Schoonen, 2000; Mu et al., 2016).**

<b>Carbonates</b>	<b>(Unoxidized) Pyrite</b>		<b>Oxidized Pyrite</b>
 <p>Compounds containing hydroxyl and carboxyl groups</p>	 <p>Acetate</p>	 <p>Ethylamine</p>	 <p>Compounds containing carboxyl group</p>
 <p>Compounds containing hydroxyl and amine groups</p>	 <p>Alanine</p>	 <p>Glycine</p>	 <p>Compounds containing sulfonate group</p>
	 <p>D-Ribose</p>	 <p>Adenine</p>	 <p>Compounds containing hydroxyl group</p>
	 <p>Formamide</p>	 <p>Carbamide</p>	 <p>Compounds containing thiourea group</p>
	 <p>L-cysteine</p>	 <p>Purine</p>	

The transformation of biocides is largely predicted by the presence of specific functional groups. The reduction of halogenated biocides is expected to occur due to the presence of pyrite.

Although oxidation of the pyrite surface will lower the number of reactive S<sub>2</sub> sites, experiments suggest that this may still allow for reaction (Harrison et al., 2017; Kriegman-King and Reinhard, 1994). Hydrolysable biocides, those containing amide groups and (thio)carbamate groups are anticipated to be catalyzed due to the presence of clay minerals. Pyrite is the largest source of inorganic iron in shale formations and, in the presence of Fe<sup>2+</sup> may also initiate Fenton-like reactions which generate non-specific hydroxyl radicals. These characteristics make pyrite the mineral most likely to induce transformations of biocides in shale formations

## 2.11 References

- Adeyemo, A.A., Adeoye, I.O., Bello, O.S., 2017. Adsorption of dyes using different types of clay: a review. *Applied Water Science* 7, 543–568. doi:10.1007/s13201-015-0322-y
- Ahmed, S.M., 1978. Electrochemical studies of sulphides, I. The electrocatalytic activity of galena, pyrite and cobalt sulphide for oxygen reduction in relation to xanthate adsorption and flotation. *International Journal of Mineral Processing* 5, 163–174. doi:10.1016/0301-7516(78)90013-3
- Altin, O., Özbelge, H.Ö., Dogu, T., 1999. Effect of pH in an Aqueous Medium on the Surface Area, Pore Size Distribution, Density, and Porosity of Montmorillonite. *Journal of Colloid and Interface Science* 217, 19–27. doi:10.1006/jcis.1999.6271
- Alvarez-Silva, M., Uribe-Salas, A., Mirnezami, M., Finch, J.A., 2010. The point of zero charge of phyllosilicate minerals using the Mular–Roberts titration technique. *Minerals Engineering* 23, 383–389. doi:10.1016/j.mineng.2009.11.013
- Antognozzi, M., Wotherspoon, A., Hayes, J.M., Miles, M.J., Szczelkun, M.D., Valdrè, G., 2006. A chlorite mineral surface actively drives the deposition of DNA molecules in stretched conformations. *Nanotechnology* 17, 3897–3902. doi:10.1088/0957-4484/17/15/047
- Bae, S., Mannan, M.B., Lee, W., 2012. Adsorption of cationic cetylpyridinium chloride on pyrite surface. *Journal of Industrial and Engineering Chemistry* 18, 1482–1488. doi:10.1016/j.jiec.2012.02.010
- Bailey, G.W., White, J.L., 1964. Soil-Pesticide Relationships, Adsorption and Desorption of Organic Pesticides by Soil Colloids, with Implications Concerning Pesticide Bioactivity. *Journal of Agricultural and Food Chemistry* 12, 324–332. doi:10.1021/jf60134a007
- Bailey, G.W., White, J.L., Rothberg, T., 1968. Adsorption of Organic Herbicides by Montmorillonite: Role of pH and Chemical Character of Adsorbate. *Soil Science Society of America Journal* 32, 222. doi:10.2136/sssaj1968.03615995003200020021x
- Bansal, O.P., Bansal, V., 1980. Influence of time, pH, temperature, organic matter and exchangeable cations on the adsorption of oxamyl on illites and kaolinites. *The Journal of Agricultural Science* 94, 557. doi:10.1017/S0021859600028562
- Barrett, M.H., Williamson, D.J., Lerner, D.N., 1994. A continuous flow method for calculating adsorption isotherms of organic pollutants onto aquifer materials. *Journal of Contaminant Hydrology* 15, 15–25. doi:10.1016/0169-7722(94)90008-6
- Bebié, J., Schoonen, M.A., Fuhrmann, M., Strongin, D.R., 1998. Surface charge development on transition metal sulfides: an electrokinetic study. *Geochimica et Cosmochimica Acta* 62, 633–642.
- Bebié, J., Schoonen, M.A.A., 2000. Pyrite surface interaction with selected organic aqueous species under anoxic conditions. *Geochemical Transactions* 1, 47. doi:10.1039/b005581f
- Berner, R.A., 1984. Sedimentary pyrite formation: An update. *Geochimica et Cosmochimica Acta* 48, 605–615. doi:10.1016/0016-7037(84)90089-9
- Bhattacharyya, K.G., Gupta, S.S., 2008. Adsorption of a few heavy metals on natural and modified kaolinite and montmorillonite: a review. *Adv Colloid Interface Sci* 140, 114–131. doi:10.1016/j.cis.2007.12.008
- Bieleman, J. (Ed.), 2000. Additives for coatings. Wiley-VCH, Weinheim ; New York.
- Borda, M.J., Elsetinow, A.R., Strongin, D.R., Schoonen, M.A., 2003. A mechanism for the production of hydroxyl radical at surface defect sites on pyrite. *Geochimica et Cosmochimica Acta* 67, 935–939. doi:10.1016/S0016-7037(02)01222-X

- Boulton, A., Fornasiero, D., Ralston, J., 2001. Selective depression of pyrite with polyacrylamide polymers. *International Journal of Mineral Processing* 61, 13–22. doi:10.1016/S0301-7516(00)00024-7
- Bradshaw, D.J., O'Connor, C.T., 1994. The flotation of pyrite using mixtures of dithiocarbamates and other thiol collectors. *Minerals Engineering* 7, 681–690. doi:10.1016/0892-6875(94)90099-X
- Brantley, S.L., Kubicki, J.D., White, A.F. (Eds.), 2008. *Kinetics of water-rock interaction*. Springer Verlag, New York.
- Bruner, K., R., Smosna, R., 2011. A Comparative Study of the Mississippian Barnett Shale, Fort Worth Basin, and Devonian Marcellus Shale, Appalachian Basin (No. DOE/NETL-2011/1478). U.S. Department of Energy, National Energy Technology Laboratory, Pittsburgh, PA.
- Burgos, W.D., Pisutpaisal, N., Mazzaresse, M.C., Chorover, J., 2002. Adsorption of Quinoline to Kaolinite and Montmorillonite. *Environmental Engineering Science* 19, 59–68. doi:10.1089/10928750252953697
- Cao, X., Yang, J., Mao, J., 2013. Characterization of kerogen using solid-state nuclear magnetic resonance spectroscopy: A review. *International Journal of Coal Geology* 108, 83–90. doi:10.1016/j.coal.2011.12.001
- Carmona-Ribeiro, A., de Melo Carrasco, L., 2013. Cationic Antimicrobial Polymers and Their Assemblies. *International Journal of Molecular Sciences* 14, 9906–9946. doi:10.3390/ijms14059906
- Carter, K.E., Hakala, J.A., Hammack, R.W., 2013. Hydraulic Fracturing and Organic Compounds – Uses, Disposal and Challenges. Presented at the SPE Eastern Regional Meeting, Society of Petroleum Engineers, Pittsburgh, PA.
- Carter, P.W., 1978. Adsorption of amino acid-containing organic matter by calcite and quartz. *Geochimica et Cosmochimica Acta* 42, 1239–1242. doi:10.1016/0016-7037(78)90117-5
- Chalmers, G.R., Bustin, R.M., Power, I.M., 2012. Characterization of gas shale pore systems by porosimetry, pycnometry, surface area, and field emission scanning electron microscopy/transmission electron microscopy image analyses: Examples from the Barnett, Woodford, Haynesville, Marcellus, and Doig units. *AAPG Bulletin* 96, 1099–1119. doi:10.1306/10171111052
- Chandra, A.P., Gerson, A.R., 2010. The mechanisms of pyrite oxidation and leaching: A fundamental perspective. *Surface Science Reports* 65, 293–315. doi:10.1016/j.surfrep.2010.08.003
- Clausen, L., Fabricius, I., Madsen, L., 2001. Adsorption of pesticides onto quartz, calcite, kaolinite, and alpha-alumina. *J. Environ. Qual.* 30, 846–857.
- Cornejo, J., Celis, R., Pavlovic, I., Ulibarri, M.A., 2008. Interactions of pesticides with clays and layered double hydroxides: a review. *Clay Minerals* 43, 155–175. doi:10.1180/claymin.2008.043.2.01
- Cornelissen, G., Gustafsson, Ö., Bucheli, T.D., Jonker, M.T.O., Koelmans, A.A., van Noort, P.C.M., 2005. Extensive Sorption of Organic Compounds to Black Carbon, Coal, and Kerogen in Sediments and Soils: Mechanisms and Consequences for Distribution, Bioaccumulation, and Biodegradation. *Environmental Science & Technology* 39, 6881–6895. doi:10.1021/es050191b
- Curtis, M.E., Ambrose, R.J., Sondergeld, C.H., Rai, C.S., 2010. Geochemical and spatial investigation of uranium in the Marcellus Shale, in: *Geochemical and Spatial Investigation of Uranium in the Marcellus Shale*. Geochemical and spatial investigation of uranium in the Marcellus Shale, Calgary, Alberta, Canada.

- de Leeuw, N.H., Cooper, T.G., 2004. A Computer Modeling Study of the Inhibiting Effect of Organic Adsorbates on Calcite Crystal Growth. *Crystal Growth & Design* 4, 123–133. doi:10.1021/cg0341003
- Deng, L., Wang, S., Zhong, H., Liu, G., 2016. A novel surfactant 2-amino-6-decanamidohexanoic acid: Flotation performance and adsorption mechanism to diaspore. *Minerals Engineering* 93, 16–23. doi:10.1016/j.mineng.2016.04.002
- Dieterich, M., Kutchko, B., Goodman, A., 2016. Characterization of Marcellus Shale and Huntersville Chert before and after exposure to hydraulic fracturing fluid via feature relocation using field-emission scanning electron microscopy. *Fuel* 182, 227–235. doi:10.1016/j.fuel.2016.05.061
- Dilmore, R., Bruner, K., Wyatt, C., Romanov, V., Goodman, A., Hedges, S., McIntyre, D., Crandall, D., Gill, M., Disenhof, C., Jinesh, J., Lopano, C., Aminian, K., Zamirian, M., Mashayekhi, A., Sanguinito, S., Mroz, T., Soeder, D., 2015. Experimental Characterization of Marcellus Shale Outcrop Samples, and their Interactions with Carbon Dioxide and Methane, NETL Technical Report Series. U.S. Department of Energy, National Energy Technology Laboratory, Morgantown, WV.
- Dos Santos, E.C., de Mendonça Silva, J.C., Duarte, H.A., 2016. Pyrite Oxidation Mechanism by Oxygen in Aqueous Medium. *The Journal of Physical Chemistry C* 120, 2760–2768. doi:10.1021/acs.jpcc.5b10949
- Droge, S.T.J., Goss, K.-U., 2013. Sorption of Organic Cations to Phyllosilicate Clay Minerals: CEC-Normalization, Salt Dependency, and the Role of Electrostatic and Hydrophobic Effects. *Environmental Science & Technology* 47, 14224–14232. doi:10.1021/es403187w
- Durán-Álvarez, A., Maldonado-Domínguez, M., González-Antonio, O., Durán-Valencia, C., Romero-Ávila, M., Barragán-Aroche, F., López-Ramírez, S., 2016. Experimental–Theoretical Approach to the Adsorption Mechanisms for Anionic, Cationic, and Zwitterionic Surfactants at the Calcite–Water Interface. *Langmuir* 32, 2608–2616. doi:10.1021/acs.langmuir.5b04151
- Durand, B., Nicaise, G., 1980. Procedures for kerogen isolation, in: Durand, B. (Ed.), *Kerogen: Insoluble Organic Matter from Sedimentary Rocks*. Editions technip, Paris, p. 19.
- Edwards, D.A., Adeel, Z., Luthy, R.G., 1994. Distribution of Nonionic Surfactant and Phenanthrene in a Sediment/Aqueous System. *Environmental Science & Technology* 28, 1550–1560. doi:10.1021/es00057a027
- Elsner, M., Hoelzer, K., 2016. Quantitative survey and structural classification of hydraulic fracturing chemicals reported in unconventional gas production. *Environmental Science & Technology* 50, 3290–3314. doi:10.1021/acs.est.5b02818
- Emmanuel, O.O., 2014. Geologic characterization and the recognition of cyclicity in the Middle Devonian Marcellus Shale, Appalachian Basin, NE USA. Colorado School of Mines, Golden, CO.
- Errais, E., Duplay, J., Elhabiri, M., Khodja, M., Ocampo, R., Baltenweck-Guyot, R., Darragi, F., 2012. Anionic RR120 dye adsorption onto raw clay: Surface properties and adsorption mechanism. *Colloids and Surfaces A: Physicochemical and Engineering Aspects* 403, 69–78. doi:10.1016/j.colsurfa.2012.03.057
- Fakcharoenphol, P., Torcuk, M.A., Wallace, J., Bertonecello, A., Kazemi, H., Wu, Y.-S., Honarpour, M., 2013. Managing Shut-in Time to Enhance Gas Flow Rate in Hydraulic Fractured Shale Reservoirs: A Simulation Study. Society of Petroleum Engineers. doi:10.2118/166098-MS
- Fil, B.A., Korkmaz, M., Özmetin, C., 2016. Application of Nonlinear Regression Analysis for Methyl Violet (MV) Dye Adsorption from Solutions onto Illite Clay. *Journal of Dispersion Science and Technology* 37, 991–1001. doi:10.1080/01932691.2015.1077455

- Fontecha-Cámara, M.A., López-Ramón, M.V., Álvarez-Merino, M.A., Moreno-Castilla, C., 2006. About the endothermic nature of the adsorption of the herbicide diuron from aqueous solutions on activated carbon fiber. *Carbon* 44, 2335–2338. doi:10.1016/j.carbon.2006.05.031
- Fortson, L., 2012. Geochemical and spatial investigation of uranium in the Marcellus Shale. State University of New York at Buffalo, Buffalo, NY.
- Foster, M.D., 1954. The Relation Between Composition and Swelling in Clays. *Clays and Clay Minerals* 3, 205–220. doi:10.1346/CCMN.1954.0030117
- Fuerstenau, D.W., Jia, R., 2004. The adsorption of alkylpyridinium chlorides and their effect on the interfacial behavior of quartz. *Colloids and Surfaces A: Physicochemical and Engineering Aspects* 250, 223–231. doi:10.1016/j.colsurfa.2004.04.090
- Gorski, C.A., Klüpfel, L.E., Voegelin, A., Sander, M., Hofstetter, T.B., 2013. Redox Properties of Structural Fe in Clay Minerals: 3. Relationships between Smectite Redox and Structural Properties. *Environmental Science & Technology* 47, 13477–13485. doi:10.1021/es403824x
- Goss, K.U., 1992. Effects of temperature and relative humidity on the sorption of organic vapors on quartz sand. *Environmental Science & Technology* 26, 2287–2294. doi:10.1021/es00035a030
- Grathwohl, P., 1990. Influence of organic matter from soils and sediments from various origins on the sorption of some chlorinated aliphatic hydrocarbons: implications on Koc correlations. *Environmental Science & Technology* 24, 1687–1693. doi:10.1021/es00081a010
- Grundl, T.J., Sparks, D.L., 1999. Kinetics and Mechanisms of Reactions at the Mineral-Water Interface: An Overview, in: Sparks, D.L., Grundl, T.J. (Eds.), *Mineral-Water Interfacial Reactions*. American Chemical Society, Washington, DC, pp. 2–11. doi:10.1021/bk-1998-0715.ch001
- Gülüt, K.Y., Sayin, M., 1998. Sorption of Aldicarb Sulfoxide by Samples of Some Calcareous Soils From Turkey. *Turkish Journal of Agriculture and Forestry* 22, 419–424.
- Haderlein, S.B., Weissmahr, K.W., Schwarzenbach, R.P., 1996. Specific Adsorption of Nitroaromatic Explosives and Pesticides to Clay Minerals. *Environmental Science & Technology* 30, 612–622. doi:10.1021/es9503701
- Harrison, A.L., Jew, A.D., Dustin, M.K., Thomas, D.L., Joe-Wong, C.M., Bargar, J.R., Johnson, N., Brown, G.E., Maher, K., 2017. Element release and reaction-induced porosity alteration during shale-hydraulic fracturing fluid interactions. *Applied Geochemistry* 82, 47–62. doi:10.1016/j.apgeochem.2017.05.001
- Hayes, T., 2009. Sampling and Analysis of Water Streams Associated with the Development of Marcellus Shale Gas. Gas Technology Institute, Des Plaines, IL.
- Hermosin, M.C., Cornejo, J., White, J.L., Hess, F.D., 1982. Bioavailability of s-triazines adsorbed on montmorillonite. *Journal of Agricultural and Food Chemistry* 30, 728–733. doi:10.1021/jf00112a026
- Herwig, U., Klumpp, E., Narres, H.-D., Schwuger, M.J., 2001. Physicochemical interactions between atrazine and clay minerals. *Applied Clay Science* 18, 211–222. doi:10.1016/S0169-1317(01)00024-2
- Hinman, N.W., 2013. Water-Rock Interaction and Life. *Procedia Earth and Planetary Science* 7, 354–359. doi:10.1016/j.proeps.2013.03.228
- Hofstetter, T.B., Schwarzenbach, R.P., Haderlein, S.B., 2003. Reactivity of Fe(II) Species Associated with Clay Minerals. *Environmental Science & Technology* 37, 519–528. doi:10.1021/es025955r
- Hosterman, J.W., Whitlow, S.I., 1983. Clay mineralogy of Devonian shales in the Appalachian Basin (No. 1298), USGS Numbered Series. US Geological Survey, Washington, DC.

- Hu, Y., Liu, X., Xu, Z., 2003. Role of crystal structure in flotation separation of diasporite from kaolinite, pyrophyllite and illite. *Minerals Engineering* 16, 219–227. doi:10.1016/S0892-6875(02)00368-0
- Huang, W., Peng, P., 'an, Yu, Z., Fu, J., 2003. Effects of organic matter heterogeneity on sorption and desorption of organic contaminants by soils and sediments. *Applied Geochemistry* 18, 955–972. doi:10.1016/S0883-2927(02)00205-6
- Huang, Z., Zhong, H., Wang, S., Xia, L., Liu, G., 2013. Comparative studies on flotation of aluminosilicate minerals with Gemini cationic surfactants BDDA and EDDA. *Transactions of Nonferrous Metals Society of China* 23, 3055–3062. doi:10.1016/S1003-6326(13)62833-2
- Jada, A., Ait Akbour, R., 2014. Adsorption and Removal of Organic Dye at Quartz Sand-Water Interface. *Oil & Gas Science and Technology – Revue d'IFP Energies nouvelles* 69, 405–413. doi:10.2516/ogst/2013169
- Jaisi, D.P., Dong, H., Liu, C., 2007. Influence of biogenic Fe(II) on the extent of microbial reduction of Fe(III) in clay minerals nontronite, illite, and chlorite. *Geochimica et Cosmochimica Acta* 71, 1145–1158. doi:10.1016/j.gca.2006.11.027
- Javadi Nooshabadi, A., Hanumantha Rao, K., 2014. Formation of hydrogen peroxide by sulphide minerals. *Hydrometallurgy* 141, 82–88. doi:10.1016/j.hydromet.2013.10.011
- Jeong, by S., Wander, M.M., Kleineidam, S., Grathwohl, P., Ligouis, B., Werth, C.J., 2008. The Role of Condensed Carbonaceous Materials on the Sorption of Hydrophobic Organic Contaminants in Subsurface Sediments. *Environmental Science & Technology* 42, 1458–1464. doi:10.1021/es0719879
- Jew, A.D., Dustin, M.K., Harrison, A.L., Joe-Wong, C.M., Thomas, D.L., Maher, K., Brown, G.E., Bargar, J.R., 2017. Impact of Organics and Carbonates on the Oxidation and Precipitation of Iron during Hydraulic Fracturing of Shale. *Energy & Fuels* 31, 3643–3658. doi:10.1021/acs.energyfuels.6b03220
- Kahrilas, G.A., Blotvogel, J., Stewart, P.S., Borch, T., 2015. Biocides in hydraulic fracturing fluids: A critical review of their usage, mobility, degradation, and toxicity. *Environmental Science & Technology* 49, 16–32. doi:10.1021/es503724k
- Keiluweit, M., Kleber, M., 2009. Molecular-Level Interactions in Soils and Sediments: The Role of Aromatic  $\pi$ -Systems. *Environmental Science & Technology* 43, 3421–3429. doi:10.1021/es8033044
- Killops, S.D., Killops, V.J., 2005. *Introduction to organic geochemistry*, 2nd ed. ed. Blackwell Pub, Malden, MA.
- King, G.E., 2012. Hydraulic Fracturing 101: What Every Representative, Environmentalist, Regulator, Reporter, Investor, University Researcher, Neighbor and Engineer Should Know About Estimatin Frac Risk and Improving Performance in Unconventional Gas and Oil Wells. Presented at the SPE Hydraulic Fracturing Technology Conference, SPE International, The Woodlands, TX.
- Klimesch, D.S., Ray, A., Sloane, B., 1996. Autoclaved cement-quartz pastes: The effects on chemical and physical properties when using ground quartz with different surface areas Part I: Quartz of wide particle size distribution. *Cement and Concrete Research* 26, 1399–1408. doi:10.1016/0008-8846(96)00117-2
- Klumpp, E., Heitmann, H., Schwuger, M.J., 1993. Synergistic effects between cationic surfactants and organic pollutants on clay minerals. *Colloids and Surfaces A: Physicochemical and Engineering Aspects* 78, 93–98. doi:10.1016/0927-7757(93)80314-5
- Knauss, K.G., Wolery, T.J., 1988. The dissolution kinetics of quartz as a function of pH and time at 70°C. *Geochimica et Cosmochimica Acta* 52, 43–53. doi:10.1016/0016-7037(88)90055-5

- Koppelman, M.H., 1980. Adsorbed Cr(III) on Chlorite, Illite, and Kaolinite: An X-ray Photoelectron Spectroscopic Study. *Clays and Clay Minerals* 28, 119–124. doi:10.1346/CCMN.1980.0280207
- Kosmulski, M., 2014. The pH dependent surface charging and points of zero charge. VI. Update. *Journal of Colloid and Interface Science* 426, 209–212. doi:10.1016/j.jcis.2014.02.036
- Kosmulski, M., 2009a. pH-dependent surface charging and points of zero charge. IV. Update and new approach. *Journal of Colloid and Interface Science* 337, 439–448. doi:10.1016/j.jcis.2009.04.072
- Kosmulski, M., 2009b. pH-dependent surface charging and points of zero charge. IV. Update and new approach. *Journal of Colloid and Interface Science* 337, 439–448. doi:10.1016/j.jcis.2009.04.072
- Kovaios, I.D., Paraskeva, C.A., Koutsoukos, P.G., Payatakes, A.C., 2006. Adsorption of atrazine on soils: Model study. *Journal of Colloid and Interface Science* 299, 88–94. doi:10.1016/j.jcis.2006.01.057
- Kriegman-King, M.R., Reinhard, M., 1994. Transformation of Carbon Tetrachloride by Pyrite in Aqueous Solution. *Environmental Science & Technology* 28, 692–700. doi:10.1021/es00053a025
- Kubicki, J.D., Itoh, M.J., Schroeter, L.M., Apitz, S.E., 1997. Bonding mechanisms of salicylic acid adsorbed onto illite clay: an ATR-FTIR and molecular orbital study. *Environmental science & technology* 31, 1151–1156.
- Galaly, G., 2001. Pesticide–clay interactions and formulations. *Applied Clay Science* 18, 205–209. doi:10.1016/S0169-1317(01)00043-6
- Laha, S., Tansel, B., Ussawarujikulchai, A., 2009. Surfactant–soil interactions during surfactant-amended remediation of contaminated soils by hydrophobic organic compounds: A review. *Journal of Environmental Management* 90, 95–100. doi:10.1016/j.jenvman.2008.08.006
- Lahann, R.W., Campbell, R.C., 1980. Adsorption of palmitic acid on calcite. *Geochimica et Cosmochimica Acta* 44, 629–634. doi:10.1016/0016-7037(80)90152-0
- Laird, D.A., 1996. Interactions Between Atrazine and Smectite Surfaces, in: Meyer, M.T., Thurman, E.M. (Eds.), *Herbicide Metabolites in Surface Water and Groundwater*. American Chemical Society, Washington, DC, pp. 86–100.
- Lash, G.G., Blood, D.R., 2014. Organic matter accumulation, redox, and diagenetic history of the Marcellus Formation, southwestern Pennsylvania, Appalachian basin. *Marine and Petroleum Geology* 57, 244–263. doi:10.1016/j.marpetgeo.2014.06.001
- Lee, W., Batchelor, B., 2002. Abiotic reductive dechlorination of chlorinated ethylenes by iron-bearing soil minerals. 1. Pyrite and magnetite. *Environ. Sci. Technol.* 36, 5147–5154.
- Li, H.C., 1958. Adsorption of organic and inorganic ions on quartz. Massachusetts Institute of Technology, Boston, MA.
- Longbottom, T.L., Hockaday, W.C., Boling, K.S., Li, G., Letourmy, Y., Dong, H., Dworkin, S.I., 2016. Organic structural properties of kerogen as predictors of source rock type and hydrocarbon potential. *Fuel* 184, 792–798. doi:10.1016/j.fuel.2016.07.066
- Luther, G.W., 1987. Pyrite oxidation and reduction: Molecular orbital theory considerations. *Geochimica et Cosmochimica Acta* 51, 3193–3199. doi:10.1016/0016-7037(87)90127-X
- Ma, K., Cui, L., Dong, Y., Wang, T., Da, C., Hirasaki, G.J., Biswal, S.L., 2013. Adsorption of cationic and anionic surfactants on natural and synthetic carbonate materials. *Journal of Colloid and Interface Science* 408, 164–172. doi:10.1016/j.jcis.2013.07.006
- Marcon, V., Joseph, C., Carter, K.E., Hedges, S.W., Lopano, C.L., Guthrie, G.D., Hakala, J.A., 2017. Experimental insights into geochemical changes in hydraulically fractured Marcellus Shale. *Applied Geochemistry* 76, 36–50. doi:10.1016/j.apgeochem.2016.11.005

- Martin, S., Shchukarev, A., Hanna, K., Boily, J.-F., 2015. Kinetics and Mechanisms of Ciprofloxacin Oxidation on Hematite Surfaces. *Environmental Science & Technology* 49, 12197–12205. doi:10.1021/acs.est.5b02851
- Meloni, P., Carcangiu, G., Delogu, F., 2012. Specific surface area and chemical reactivity of quartz powders during mechanical processing. *Materials Research Bulletin* 47, 146–151. doi:10.1016/j.materresbull.2011.09.014
- Morey, G., Fournier, R., Rowe, J., 1962. The solubility of quartz in water in the temperature interval from 25° to 300° C. *Geochimica et Cosmochimica Acta* 26, 1029–1043. doi:10.1016/0016-7037(62)90027-3
- Morse, J.W., 1986. The surface chemistry of calcium carbonate minerals in natural waters: An overview. *Marine Chemistry* 20, 91–112. doi:10.1016/0304-4203(86)90068-X
- Morse, J.W., Arvidson, R.S., 2002. The dissolution kinetics of major sedimentary carbonate minerals. *Earth-Science Reviews* 58, 51–84. doi:10.1016/S0012-8252(01)00083-6
- Moslemi, H., Gharabaghi, M., 2017. A review on electrochemical behavior of pyrite in the froth flotation process. *Journal of Industrial and Engineering Chemistry* 47, 1–18. doi:10.1016/j.jiec.2016.12.012
- Moulin, P., Roques, H., 2003. Zeta potential measurement of calcium carbonate. *Journal of Colloid and Interface Science* 261, 115–126. doi:10.1016/S0021-9797(03)00057-2
- Mu, Y., Peng, Y., Lauten, R.A., 2016. The mechanism of pyrite depression at acidic pH by lignosulfonate-based biopolymers with different molecular compositions. *Minerals Engineering* 92, 37–46. doi:10.1016/j.mineng.2016.02.007
- Müller, S., Totsche, K.U., Kögel-Knabner, I., 2007. Sorption of polycyclic aromatic hydrocarbons to mineral surfaces. *European Journal of Soil Science* 58, 918–931. doi:10.1111/j.1365-2389.2007.00930.x
- Nagaraj, D.R., Ravishankar, S.A., 2007. Flotation reagents - A critical overview from an industry perspective, in: Fuerstenau, M.C., Jameson, G.J., Yoon, R.-H. (Eds.), *Froth Flotation: A Century of Innovation*. Society for Mining, Metallurgy, and Exploration, Littleton, Colo, p. 262.
- Narayanasamy, J., Kubicki, J.D., 2005. Mechanism of Hydroxyl Radical Generation from a Silica Surface: Molecular Orbital Calculations. *The Journal of Physical Chemistry B* 109, 21796–21807. doi:10.1021/jp0543025
- Nefso, E.K., Burns, S.E., McGrath, C.J., 2005. Degradation kinetics of TNT in the presence of six mineral surfaces and ferrous iron. *Journal of Hazardous Materials* 123, 79–88. doi:10.1016/j.jhazmat.2004.07.023
- Neumann, A., Hofstetter, T.B., Skarpele-Liati, M., Schwarzenbach, R.P., 2009. Reduction of Polychlorinated Ethanes and Carbon Tetrachloride by Structural Fe(II) in Smectites. *Environmental Science & Technology* 43, 4082–4089. doi:10.1021/es9001967
- Nijenhuis, I., Bosch, H.-J., Sinninghe Damsté, J., Brumsack, H.-J., De Lange, G., 1999. Organic matter and trace element rich sapropels and black shales: a geochemical comparison. *Earth and Planetary Science Letters* 169, 277–290. doi:10.1016/S0012-821X(99)00083-7
- Office of Pesticides and Toxic Substances, 1992. List of Pesticide Product Inert Ingredients. U.S. Environmental Protection Agency, Washington, DC.
- Orem, W., Tatu, C., Varonka, M., Lerch, H., Bates, A., Engle, M., Crosby, L., McIntosh, J., 2014. Organic substances in produced and formation water from unconventional natural gas extraction in coal and shale. *International Journal of Coal Geology* 126, 20–31. doi:10.1016/j.coal.2014.01.003
- Parthasarathy, H., Dzombak, D.A., Karamalidis, A.K., 2015. Alkali and alkaline earth metal chloride solutions influence sulfide mineral dissolution. *Chemical Geology* 412, 26–33. doi:10.1016/j.chemgeo.2015.07.017

- Paukert Vankeuren, A.N., Hakala, J.A., Jarvis, K., Moore, J.E., 2017. Mineral Reactions in Shale Gas Reservoirs: Barite Scale Formation from Reusing Produced Water As Hydraulic Fracturing Fluid. *Environmental Science & Technology* 51, 9391–9402. doi:10.1021/acs.est.7b01979
- Peng, Y., Grano, S., 2010. Inferring the distribution of iron oxidation species on mineral surfaces during grinding of base metal sulphides. *Electrochimica Acta* 55, 5470–5477. doi:10.1016/j.electacta.2010.04.097
- Philp, R.P., Calvin, M., 1976. Possible origin for insoluble organic (kerogen) debris in sediments from insoluble cell-wall materials of algae and bacteria. *Nature* 262, 134–136. doi:10.1038/262134a0
- Plummer, L.N., Parkhurst, D.L., Wigley, T.M.L., 1979. Critical Review of the Kinetics of Calcite Dissolution and Precipitation, in: Jenne, E.A. (Ed.), *Chemical Modeling in Aqueous Systems*. AMERICAN CHEMICAL SOCIETY, WASHINGTON, D. C., pp. 537–573.
- Pokrovsky, O.S., Schott, J., Thomas, F., 1999. Dolomite surface speciation and reactivity in aquatic systems. *Geochimica et Cosmochimica Acta* 63, 3133–3143. doi:10.1016/S0016-7037(99)00240-9
- Ran, Y., Xing, B., Suresh, P., Rao, C., Fu, J., 2004. Importance of adsorption (hole-filling) mechanism for hydrophobic organic contaminants on an aquifer kerogen isolate. *Environ. Sci. Technol.* 38, 4340–4348.
- Roen, J.B., 1984. Geology of the Devonian black shales of the Appalachian Basin. *Organic Geochemistry* 5, 241–254. doi:10.1016/0146-6380(84)90011-1
- Rogers, J.D., Burke, T.L., Osborn, S.G., Ryan, J.N., 2015. A Framework for Identifying Organic Compounds of Concern in Hydraulic Fracturing Fluids Based on Their Mobility and Persistence in Groundwater. *Environmental Science & Technology Letters* 2, 158–164. doi:10.1021/acs.estlett.5b00090
- Rowan, E.L., Engle, M.A., Kirby, C.S., Kraemer, T.F., 2011. Radium Content of Oil- and Gas-Field Produced Waters in the Northern Appalachian Basin (USA): Summary and Discussion of Data (No. 5135), Scientific Investigations Report 2011. US Geological Survey, Reston, VA.
- Sánchez-Martín, M.J., Dorado, M.C., del Hoyo, C., Rodríguez-Cruz, M.S., 2008. Influence of clay mineral structure and surfactant nature on the adsorption capacity of surfactants by clays. *Journal of Hazardous Materials* 150, 115–123. doi:10.1016/j.jhazmat.2007.04.093
- Sánchez-Martín, M.J., Rodríguez-Cruz, M.S., Andrades, M.S., Sanchez-Camazano, M., 2006. Efficiency of different clay minerals modified with a cationic surfactant in the adsorption of pesticides: Influence of clay type and pesticide hydrophobicity. *Applied Clay Science* 31, 216–228. doi:10.1016/j.clay.2005.07.008
- Saxby, J.D., 1976. Chemical separation and characterization of kerogen from oil shale, in: Yen, T.F., Chilingar, G.V. (Eds.), *Oil Shale*. Elsevier Scientific Pub. Co., Amsterdam; New York, p. 20.
- Schieder, D., Dobias, B., Klumpp, E., Schwuger, M.J., 1994. Adsorption and solubilisation of phenols in the hexadecyltrimethylammonium chloride adsorbed layer on quartz and corundum. *Colloids and Surfaces A: Physicochemical and Engineering Aspects* 88, 103–111. doi:10.1016/0927-7757(94)80090-1
- Schwarzenbach, R.P., Gschwend, P.M., Imboden, D.M., 2003. *Environmental organic chemistry*, 2. ed. ed. Wiley, New York.
- Seabaugh, J.L., Dong, H., Kukkadapu, R.K., Eberl, D.D., Morton, J.P., Kim, J., 2006. Microbial reduction of Fe(III) in the Fithian and Muloorina illites: contrasting extents and rates of bioreduction. *Clays and Clay Minerals* 54, 67–79. doi:10.1346/CCMN.2006.0540109

- Shi, X., Ji, L., Zhu, D., 2010. Investigating roles of organic and inorganic soil components in sorption of polar and nonpolar aromatic compounds. *Environmental Pollution* 158, 319–324. doi:10.1016/j.envpol.2009.06.036
- Siobhán, S., Roubaud, M., 1997. Adsorption of <sup>137</sup>Cs on Montmorillonite and Illite: Effect of Charge Compensating Cation, Ionic Strength, Concentration of Cs, K and Fulvic Acid. *Clays and Clay Minerals* 45, 251–260.
- Soeder, D.J., 2010. The Marcellus Shale: Resources and Reservations. *Eos, Transactions American Geophysical Union* 91, 277–278. doi:10.1029/2010EO320001
- Somasundaran, P., Zhang, L., 2006. Adsorption of surfactants on minerals for wettability control in improved oil recovery processes. *Journal of Petroleum Science and Engineering* 52, 198–212. doi:10.1016/j.petrol.2006.03.022
- Sposito, G., Grasso, D., 1999. Electrical double layer structure, forces, and fields at the clay-water interface, in: Hsu, J.-P. (Ed.), *Interfacial Forces and Fields: Theory and Applications*, Surfactant Science Series. M. Dekker, New York, p. 45.
- Stevens, C., 1998. Environmental degradation pathways for the breakdown of polydimethylsiloxanes. *Journal of Inorganic Biochemistry* 69, 203–207. doi:10.1016/S0162-0134(97)10019-8
- Stringfellow, W.T., Domen, J.K., Camarillo, M.K., Sandelin, W.L., Borglin, S., 2014. Physical, chemical, and biological characteristics of compounds used in hydraulic fracturing. *Journal of Hazardous Materials* 275, 37–54. doi:10.1016/j.jhazmat.2014.04.040
- Tan, H., Skinner, W., Addai-Mensah, J., 2013. pH-mediated interfacial chemistry and particle interactions in aqueous chlorite dispersions. *Chemical Engineering Research and Design* 91, 448–456. doi:10.1016/j.cherd.2012.08.011
- Tao, Q.H., Wang, D.S., Tang, H.X., 2006. Effect of surfactants at low concentrations on the sorption of atrazine by natural sediment. *Water Environ. Res.* 78, 653–660.
- Teng, H., 2005. Water/Rocks Interaction, in: Lehr, J.H., Keeley, J. (Eds.), *Water Encyclopedia*. John Wiley & Sons, Inc., Hoboken, NJ, USA. doi:10.1002/047147844X.gw1520
- Tiab, D., Donaldson, E.C., 2004. Introduction to Mineralogy, in: *Petrophysics: Theory and Practice of Measuring Reservoir Rock and Fluid Transport Properties*. Gulf Professional Pub, Boston, pp. 1–28.
- Todd, E., Sherman, D., Purton, J., 2003. Surface oxidation of pyrite under ambient atmospheric and aqueous (pH = 2 to 10) conditions: electronic structure and mineralogy from X-ray absorption spectroscopy. *Geochimica et Cosmochimica Acta* 67, 881–893. doi:10.1016/S0016-7037(02)00957-2
- U.S. Crude Oil and Natural Gas Proved Reserves, Year-end 2015, 2016. . U.S. Energy Information Administration (EIA), Washington, DC.
- Vandenbroucke, M., Largeau, C., 2007. Kerogen origin, evolution and structure. *Organic Geochemistry* 38, 719–833. doi:10.1016/j.orggeochem.2007.01.001
- Vdović, N., 2001. Electrokinetic behaviour of calcite—the relationship with other calcite properties. *Chemical Geology* 177, 241–248. doi:10.1016/S0009-2541(00)00397-1
- Vlachy, N., Jagoda-Cwiklik, B., Vácha, R., Touraud, D., Jungwirth, P., Kunz, W., 2009. Hofmeister series and specific interactions of charged headgroups with aqueous ions. *Advances in Colloid and Interface Science* 146, 42–47. doi:10.1016/j.cis.2008.09.010
- Wainipiee, W., Cuadros, J., Sephton, M.A., Unsworth, C., Gill, M.G., Strekopytov, S., Weiss, D.J., 2013. The effects of oil on As(V) adsorption on illite, kaolinite, montmorillonite and chlorite. *Geochimica et Cosmochimica Acta* 121, 487–502. doi:10.1016/j.gca.2013.07.018
- Walton, J., Woocay, A., 2013. Environmental Issues Related to Enhanced Production of Natural Gas by Hydraulic Fracturing. *Journal of Green Building* 8, 62–71. doi:10.3992/jgb.8.1.62

- Wang, G., Carr, T.R., 2012. Methodology of organic-rich shale lithofacies identification and prediction: A case study from Marcellus Shale in the Appalachian basin. *Computers & Geosciences* 49, 151–163. doi:10.1016/j.cageo.2012.07.011
- Wang, X.-H., 1995. Interfacial Electrochemistry of Pyrite Oxidation and Flotation. *Journal of Colloid and Interface Science* 171, 413–428. doi:10.1006/jcis.1995.1198
- Weber, J.B., 1970. Mechanisms of adsorption of s-triazines by clay colloids and factors affecting plant availability, in: Gunther, F.A., Gunther, J.D. (Eds.), *Single Pesticide Volume: The Triazine Herbicides*. Springer New York, New York, NY, pp. 93–130.
- Weerasooriya, R., Dharmasena, B., 2001. Pyrite-assisted degradation of trichloroethene (TCE). *Chemosphere* 42, 389–396. doi:10.1016/S0045-6535(00)00160-0
- Weerasooriya, R., Tobschall, H.J., 2005. Pyrite–water interactions: Effects of pH and pFe on surface charge. *Colloids and Surfaces A: Physicochemical and Engineering Aspects* 264, 68–74. doi:10.1016/j.colsurfa.2005.05.012
- Wei, J., Furrer, G., Kaufmann, S., Schulin, R., 2001. Influence of clay minerals on the hydrolysis of carbamate pesticides. *Environmental science & technology* 35, 2226–2232.
- Werne, J.P., Sagemand, B.B., Lyons, T.W., Hollander, D.J., 2002. An integrated assessment of a “type euxinic” deposit: Evidence for multiple controls on black shale deposition in the middle Devonian Oatka Creek formation. *American Journal of Science* 302, 110–143. doi:10.2475/ajs.302.2.110
- Xia, L., Zhong, H., Liu, G., Huang, Z., Chang, Q., Li, X., 2009. Comparative studies on flotation of illite, pyrophyllite and kaolinite with Gemini and conventional cationic surfactants. *Transactions of Nonferrous Metals Society of China* 19, 446–453. doi:10.1016/S1003-6326(08)60293-9
- Yang, C., Huang, W., Xiao, B., Yu, Z., Peng, P., 'an, Fu, J., Sheng, G., 2004. Intercorrelations among Degree of Geochemical Alterations, Physicochemical Properties, and Organic Sorption Equilibria of Kerogen. *Environmental Science & Technology* 38, 4396–4408. doi:10.1021/es0350381
- Zelenev, A.S., Champagne, L.M., Hamilton, M., 2011. Investigation of interactions of diluted microemulsions with shale rock and sand by adsorption and wettability measurements. *Colloids and Surfaces A: Physicochemical and Engineering Aspects* 391, 201–207. doi:10.1016/j.colsurfa.2011.07.007
- Zhang, J., He, M., 2011. Effect of Surfactants on Sorption and Desorption of Phenanthrene onto Black Carbon. *Water Environment Research* 83, 15–22. doi:10.2175/106143010X12681059116536
- Zhang, J., Zeng, J., He, M., 2009. Effects of temperature and surfactants on naphthalene and phenanthrene sorption by soil. *Journal of Environmental Sciences* 21, 667–674. doi:10.1016/S1001-0742(08)62297-4
- Zhang, Y., Tran, H.P., Hussain, I., Zhong, Y., Huang, S., 2015. Degradation of p-chloroaniline by pyrite in aqueous solutions. *Chemical Engineering Journal* 279, 396–401. doi:10.1016/j.cej.2015.03.016
- Zhou, L., Das, S., Ellis, B.R., 2016. Effect of Surfactant Adsorption on the Wettability Alteration of Gas-Bearing Shales. *Environmental Engineering Science* 33, 766–777. doi:10.1089/ees.2016.0003
- Zullig, J.J., Morse, J.W., 1988. Interaction of organic acids with carbonate mineral surfaces in seawater and related solutions: I. Fatty acid adsorption. *Geochimica et Cosmochimica Acta* 52, 1667–1678. doi:10.1016/0016-7037(88)90235-9

**Chapter 3      Pyrite-induced reduction of organobromide  
biocides: Case study of DBNPA**

The information presented in this chapter will appear as a publication in a peer-reviewed journal with the tentative title "Pyrite-induced reduction of organobromide biocides: Case study of DBNPA " by Nizette Consolazio, Gregory V. Lowry and Athanasios K. Karamalidis.

### 3.1 Abstract

Bromine-containing biocides such as 2,2-dibromo-3-nitrilopropionamide or DBNPA are needed to decontaminate and protect hydraulically fractured wells from microbial degradation over their lifetime. Like their chlorinated counterparts, organobromides such as DBNPA are likely to be degraded under reducing conditions. This study investigates the role of pyrite, an abundant shale mineral with reduced iron, on the degradation of DBNPA. The results show that pyrite reductively debrominates DBNPA to form 2-monobromo-3-nitrilopropionamide, MBNPA. The hydrolysis product dibromoacetonitrile or DBAN was not detected over the time frame of this experiment. The surface area normalized first-order initial degradation rate constant was found to be  $5.1 \text{ Lm}^{-2}\text{day}^{-1}$ . In aqueous solutions, pyrite dissolves to form  $\text{Fe}^{\text{II}}$  ions and is oxidized to release  $\text{SO}_4^{2-}$  ions. These products of pyrite are known reducing agents, but their reaction rates with DBNPA suggest that these species do little to contribute to DBNPA reduction. Instead, a likely mechanism is a two-electron transfer from the disulfide groups on the pyrite surface, resulting in reduction of DBNPA via an anionic intermediate. This study confirms that pyrite can affect the persistence of DBNPA and change the distribution of reaction products. As a result, pyrite can change the efficacy and risk of DBNPA use in hydraulic fracturing.

### **3.2 Introduction**

There is abundant concern for the fate of anthropogenic bromine-containing compounds in the environment. One such chemical is methyl bromide, which was used in the US as an agricultural fumigant to limit the spread of pests and diseases before being phased out in 2001 (Noling and Becker, 1994). As a result of its widespread use, biocide residues in food was one of the largest pathways for exposure to toxic brominated organics, and remains a cause for concern in other countries where methyl bromide is still used (Vainikka and Hupa, 2012; Greve, 1983; Wittayanan et al., 2017). Flame retardants such as polybrominated diphenyl ethers (PBDEs) comprise another major group of organobromides that are widely distributed in the environment: in 2008, flame retardants accounted for 50% of the anthropogenic organobromine market (Vainikka and Hupa, 2012). The persistence and ubiquity of these anthropogenic compounds in nature have sparked numerous studies investigating their effect on human health and the environment, and has resulted in the phase out of certain PBDEs (Renner, 2000; Dodson et al., 2012).

Some organobromides have proven to be an effective class of disinfecting alternatives to chlorine for water treatment, but improper disposal may have deleterious environmental consequences. Although more expensive than chlorine, organobromides can be used at wider pH ranges and leave fewer residuals. Therefore they can be more effective and safer than chlorine (Nalepa, 2004). Because of the efficacy of these compounds in industrial applications, they have been successfully applied to hydraulic fracturing as well. These biocides include dibromodicyanobutane, bronopol, bromohlorodimethylhydantoin and 2,2-dibromo-3-nitrilopropionamide (DBNPA) (Stringfellow et al., 2014; Elsner and Hoelzer, 2016; Kahrilas et al., 2015). Biocides such bronopol readily decompose into smaller, more toxic chemicals such as formaldehyde (Vainikka and Hupa, 2012). Others take advantage of hydrophobic bromine group

to partition into bacterial cell membranes and disrupt normal cellular function (Bazzini and Wermuth, 2015; Williams et al., 1988; Schwarzenbach et al., 2003). Although intended for the control of bacteria, these biocides and many of their by-products are also toxic to aquatic and terrestrial organisms if inadvertently released into the environment (US EPA, 1994; US EPA, 1995; US EPA, 1996; US EPA, 2004).

Like their chlorinated counterparts, organobromides are likely to be degraded by reducing minerals such as pyrite. Pyrite is known to reduce recalcitrant organohalogenes such as trichloroethylene (TCE) and carbon tetrachloride (Lee and Batchelor, 2002; Weerasooriya and Dharmasena, 2001; Kriegman-King and Reinhard, 1994). Organohalides are oxidizing agents and are many can be reduced in certain environmental conditions. Studies have shown that the dehalogenation of organobromides such as bromoxynil, bromacil, 1,2-dibromo-3-chloropropane, and 2,3-dibromobutane can be catalyzed by bacterial electron mediators (Castro and Belser, 1968; Adrian and Suflita, 1990; Cupples et al., 2005). In addition, synthesized nanoscale zerovalent iron (nZVI) has been shown to degrade persistent polybrominated diphenyl ethers in flame retardants (Zhuang et al., 2012; Shih and Tai, 2010). These reactions suggest that pyrite in shale formations may also reduce brominated biocides such as DBNPA. However, the reactivity of brominated compounds with pyrite has yet to be explored, and in particular, the specific biocides used for hydraulic fracturing.

The overall goal of this study is to gain insight into the role that pyrite in reservoir systems may have on the fate of DBNPA and, as a consequence, related organobromide disinfectants. In this chapter, DBNPA is used as a model biocide to explore the effect of pyrite on the persistence of brominated biocides. The reactivity of DBNPA with pyrite and pyrite's reaction products was assessed by measuring (i) the rates and products of DBNPA degradation with pyrite and (ii) the rates and products of DBNPA degradation with  $\text{Fe}^{\text{II}}$ ,  $\text{S}_2\text{O}_3^{2-}$ , and  $\text{SO}_4^{2-}$ .

This work will provide insight in the role that pyrite in the subsurface may have on the efficacy and environmental risk associated with organobromide biocides.

### **3.3 Background on DBNPA**

DBNPA is commonly used to control microbes in processes involving continuously recycled water such as in paper making and in recirculating cooling towers. DBNPA is also an attractive biocide for oil and gas operations because it is very soluble in glycols (which are often used as a corrosion inhibitor in hydraulic fracturing fluids) and is effective at inhibiting sulfate-reducing bacteria (Wolf and Sterner, 1972). Estimates suggest that it is used in 18 to 24% of fracking operations making it one of the most commonly used hydraulic fracturing biocides (Kahrilas et al., 2015; Elsner and Hoelzer, 2016).

Current risk assessments of DBNPA illustrate that the risk to human and environmental health depends heavily on the process to which the biocide is applied. In recirculating processes, the concentrations of DBNPA and its reaction products are low enough to be mitigated with the use of a secondary biological treatment before disposal to surface water. However in single flow-through cooling tower systems and secondary oil recovery systems, a secondary biological treatment was deemed inadequate at reducing concentrations of the biocide below the level of concern (LOC) for several fish species (US EPA, 1994; Klaine et al., 1996). These risk assessment make clear the need for well-informed decisions before disposing used fluids containing biocide formulations. While these models attempt to determine the concentration of DBNPA and its reaction products over time, they assume that the reactivity of DBNPA, when pumped underground, is identical to that measured in deionized water at ambient conditions. A fundamental understanding of the surface-catalyzed reactions that take place in the subsurface is essential to further improve exposure models and our understanding of the toxicity of these compounds.

Previous studies (Exner et al., 1973; Blanchard et al., 1987) have elucidated the degradation of DBNPA's distinct functional groups in aqueous solutions. The amide group hydrolyzes due to hydroxide ( $\text{OH}^-$ ) attack to form 2,2-dibromoacetonitrile (DBAN) and dibromoacetamide via an abnormal Hoffman rearrangement (Figure 3-1, pathway 1). Alternatively, the bromide group can be lost due to nucleophilic attack, forming 2-monobromo-3-nitrilopropionamide (MBNPA) and cyanoacetamide (Figure 3-1, pathway 2). Hydroxide ions,  $\text{OH}^-$ , are weak nucleophiles and as a result, debromination can occur in distilled water. However, this degradation pathway will occur much faster in the presence of a stronger nucleophile or reducing agent. The general result is that the degradation of DBNPA increases as pH increases, due to higher concentrations of  $\text{OH}^-$  ions. On the other hand, an increase in reducing or nucleophilic groups causes debromination. Over time (on the order of several months) both pathways leads to the formation of organic acids. Mayes et al. (1985) compared the acute toxicity of DBAN, DBNPA and MBNPA and found the first to be the most hazardous of the three. They reported the 50% lethal concentration ( $\text{LC}_{50}$ ) of DBAN to be 0.55 mg/L, much lower, and therefore more toxic than an  $\text{LC}_{50}$  of 1.8 mg/L for DBNPA and 3.4 mg/L for MBNPA. This well-established understanding of the degradation of DBNPA in aqueous systems presents a unique opportunity to study the consequences of the interactions of a brominated compound with pyrite on the persistence and toxicity of DBNPA.

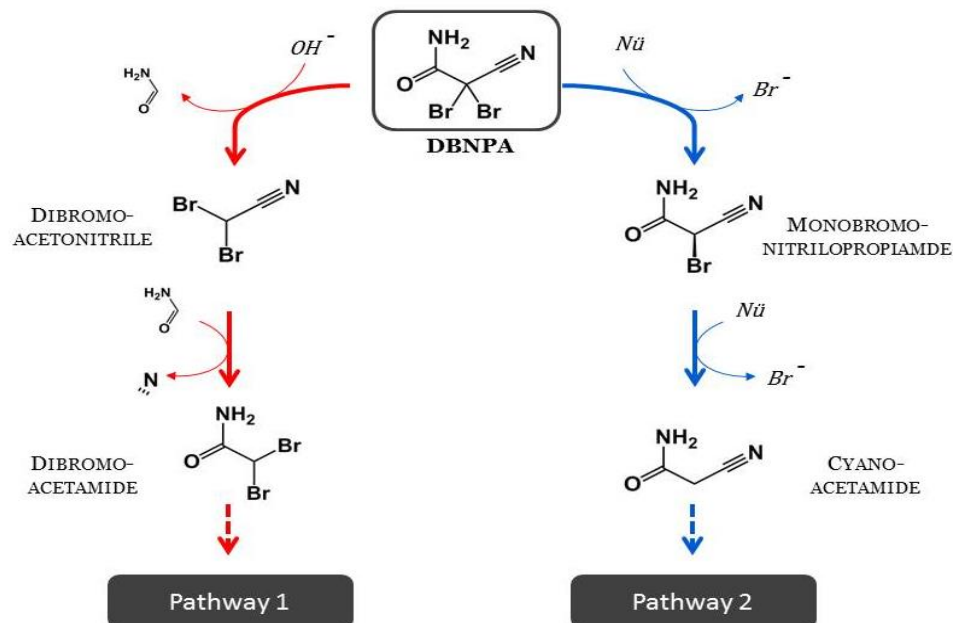


**Figure 3-1.** Reaction scheme illustrating two proposed degradation pathways for the biocide DBNPA. Base-catalyzed hydrolysis (Pathway 1) leads to dibromoacetone nitrile (DBAN). Reduction by nucleophilic elimination (Pathway 2) leads to monobromonitrilopropamide (MBNPA). Source: Exner et al., 1973; Blanchard et al., 1987.

### 3.4 Methods

#### 3.4.1 Materials

The chemicals used in this study were DBNPA (96%, Aldrich), dibromoacetone nitrile (90%, Supelco), dibromoacetamide (98%, Alfa Chemistry), monobromonitrilopropamide (95%, Enamine), cyanoacetamide (99%, Aldrich), methanol (98%, BDH Chemicals), ethanol (200 proof ACS/USP grade, Pharmco-Aaper), acetonitrile (99.8% EMD), sodium sulfate (ACS anhydrous, Fisher Scientific), sodium thiosulfate (99.5%, Fisher Scientific), sodium chloride (99%, Sigma Aldrich), iron (ii) chloride (ACS grade, Fisher Scientific), hydrochloric acid (36.5 - 38%, BDH), formic acid (96+%, Alfa Aesar), and acetone (99.5%, EM Science). All chemicals were used as received. Research grade pyrite (Zacatecas, Mexico) was obtained from Wards chemical. Methanol stock solutions of DBNPA and its reaction products were prepared and used

within a day. Water was obtained from a Barnstead 18.1 M $\Omega$  water system and oxygen was removed for anoxic experiments by purging with N<sub>2</sub> (99%, Butler Gas supply).

### *3.4.2 Pyrite preparation*

Large pyrite aggregates greater than 10 mm in diameter were first crushed by using a ceramic mortar and pestle, then further size-reduced with an 8530 Shatterbox. The fraction between 38 and 75  $\mu$ m was retained by wet-sieving in 70% ethanol (Wolfe et al., 2007). The surface was then cleaned to dissolve the iron oxide layer that forms on the surface of pyrite due to prolonged exposure to air. This was done by rinsing the pyrite in boiling acid, followed by deionized water and then acetone (Paschka and Dzombak, 2004). The acetone was removed by placing the pyrite in 105°C oven for 5 mins. The pyrite was cooled and stored under vacuum. Sedimentary pyrite was not available during the period of this study. Hydrothermal pyrite is a suitable proxy for probing the fundamental degradation mechanisms as in this study (Liu et al., 2008a) However, as sedimentary pyrite is often more varied in chemistry than the hydrothermal variety, additional experiments may be needed to accurately translate these results to shale formations (Liu et al., 2008b).

### *3.4.3 Batch experiments*

Batch experiments were performed in amber vials (60 mL) sealed with polypropylene screw caps fitted with polytetrafluoroethylene (PTFE) and silicone septa. In solutions in which pH is controlled, a 100 mM formate buffer is used. Anoxic experiments were set up and sampled in a glove box under nitrogen atmosphere with 2% hydrogen. Between 0.275 to 1.1 g of acid-washed pyrite were added to each vial investigating the effect of pyrite. In experiments testing the effect of a cation or anion, solutions of between 1 mM and 2 mM of the salt were prepared. Each experiment was initiated by adding a known amount of DBNPA stock solution to each vial.

Solutions involving pyrite were then placed on an end-over-end tumbler to ensure adequate mixing. Samples were taken from each batch reactor, filtered into autosampler vials and immediately analyzed over the course of 10 to 50 hours, until solution concentrations in one of the vials dropped below zero. The pH of each of these solutions was taken at the end of each experiment.

#### *3.4.4 Analytical Methods*

The analytical separation of DBNPA and degradation products was performed by high performance liquid chromatography, HPLC (Agilent 1100) equipped with a ZORBAX Eclipse C18 column (4.6 x 150 mm, 5  $\mu$ m) at 30°C. Ten microliters of each sample was isocratically eluted with 30% acetonitrile and 70% water, both acidified with 0.1% formic acid at a flowrate of 1 mL/min for 8 minutes. Detection was done with UV-visible detection at 214 nm. A triple quadrupole mass spectrometer, QQQ (Agilent 6430) in selected ion monitoring (SIM) mode was used to confirm the identity of the products. The mass spectrometer source parameters were the following: 300°C gas temperature; 10 L/min N<sub>2</sub> gas flow at 60 psi; capillary voltage at 400 V. The detection limits were about 0.3 mM for the compounds investigated.

### **3.5 Results**

#### *3.5.1 Effect of pyrite loading on the rate of degradation*

Pyrite concentrations of 5, 10 and 15 g/L pyrite result in accelerated degradation of DBNPA under anoxic aqueous conditions (Figure 3-2). In the control (pH 3.1, formate buffer), DBNPA undergoes negligible hydrolysis over 10 hours. In comparison, the addition of pyrite leads to rapid degradation of DBNPA over the course of the experiment. Although the final pH of solutions containing pyrite measure between 2.5 and 2.9, Exner et al. (1973) show that

hydrolysis rates are expected to be similar over the pH range from 2.5 to 3.1 so the observed increase in degradation of DBNPA is attributed to the pyrite. DBNPA concentrations in solutions with pyrite gradually decrease monotonically with time until concentrations fall below the limit of detection. The rate of degradation increases with increasing pyrite mass (and therefore surface area).

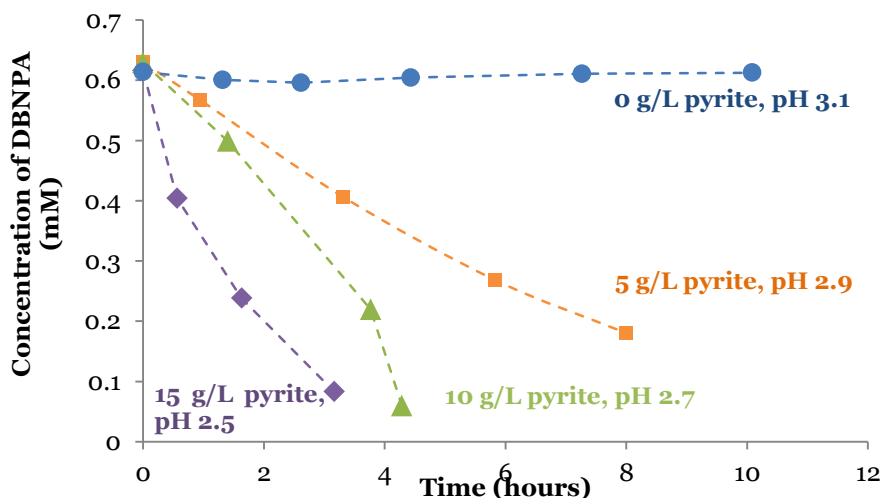


**Figure 3-2. Fraction of DBNPA remaining as a function of time (h), in aqueous suspensions of 0 g/L, 5 g/L, 10 g/L and 15 g/L of pyrite (FeS<sub>2</sub>). The experiment was performed in nitrogen-sparged water, with an initial DBNPA concentration of 0.62 mM. The final pH was measured between 2.5 and 2.9 for pyrite solutions and 3.1 for the solution without pyrite.**

The degradation kinetics of DBNPA suggests that the reaction is surface-controlled. Because of the limited data points for each experiment, the difference between the goodness of fit of zero- and first-order degradation models (with respect to DBNPA) is statistically insignificant: the values of R<sup>2</sup> are all very similar. However, the exercise does offer some insight into the reactivity of pyrite sites. Over the first 6 hours, in low concentrations of pyrite (5 g/L), the degradation of DBNPA very closely approximates zero-order reaction kinetics (R<sup>2</sup> = 0.997), likely due to saturation of the pyrite reactive sites. In the sample with the least pyrite, the reaction is independent of the concentration of DBNPA, but depends instead on the limited number of reactive DBNPA sites. However, DBNPA solutions with higher concentrations of pyrite (15 g/L) instead display first-order kinetics (R<sup>2</sup> = 0.995). In this case, the pyrite sites are

no longer the rate limiting factor and the degradation rate depends on the concentration of DBNPA. Table 3-1 summarizes the zero- and first-order degradation rates for each solution with pyrite. First- and zero-order degradation rates were also reported for the degradation of carbon tetrachloride (Kriegman-King and Reinhard, 1994) and trichloroethylene (Weerasooriya and Dharmasena, 2001). A few studies have instead demonstrated continuously declining reaction rates with pyrite over time (Lee and Batchelor, 2002; Oh et al., 2008). However, this is likely due to the deactivation of pyrite active sites over long time periods, and is not apparent in this study.

**Table 3-1. Zero- and first-order degradation rates for experiments containing 5, 10 and 15 g/L of pyrite.**

Concentration of pyrite (g/L)	Zero Order		First Order	
	Degradation rate (mM/h)	R <sup>2</sup>	Degradation Rate (hr <sup>-1</sup> )	R <sup>2</sup>
5	0.062	0.997	0.157	0.995
10	0.110	0.996	0.287	0.973
15	0.222	0.941	0.621	0.996

The pseudo-first order degradation rates of DBNPA increase linearly with pyrite amount, at constant initial DBNPA concentrations (Figure 3-3). The slope allows the calculation of a mass-normalized first order rate constant, estimated at 0.046 Lg<sup>-1</sup>hr<sup>-1</sup> for pyrite concentrations up to 15 g/L. Assuming a surface area of 0.22 m<sup>2</sup>/g (Wolfe et al., 2007), this translates to a surface area-normalized rate constant of 5.1 Lm<sup>-2</sup>day<sup>-1</sup>. The results indicate a strong dependence of reaction rates on pyrite surface area. It must be noted that this rate is specific to the pyrite density of sites, size fraction and pre-treatment. This rate is several orders of magnitude greater than that calculated for recalcitrant chlorinated ethenes (Lee and Batchelor, 2002).

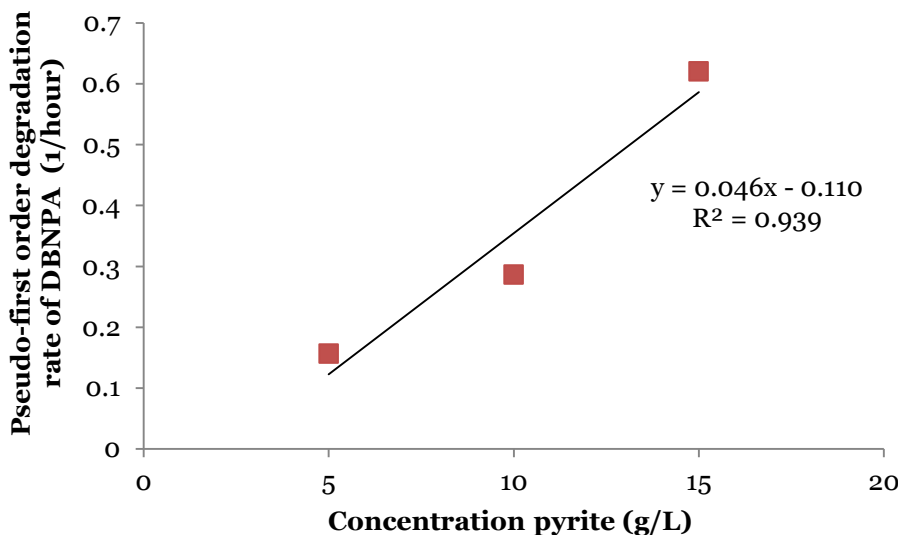


**Figure 3-3. The effect of pyrite concentration on the pseudo-first order degradation rate of DBNPA. The experiment was performed in nitrogen-sparged water, with an initial DBNPA concentration of 0.6 mM. The final pH measured between 2.5 and 2.9 for pyrite solutions.**

### 3.5.2 Change in DBNPA reaction products due to pyrite

The addition of pyrite leads to the debromination of DBNPA, as illustrated by measured concentrations of MBNPA. Here, we look at the yield of MBNPA, which refers to the amount of a specific product formed per mole of reactant consumed, Equation 3-1.

$$Yield_{MBNPA} = \frac{\text{Moles MBNPA formed}}{\text{Moles of DBNPA converted}} \quad 3-1$$

Figure 3-4 shows that initially, for each molecule of DBNPA that is lost, one molecule of MBNPA is measured in solution. Despite differing concentrations of pyrite, the initial degradation rates of DBNPA are equal to initial production rates of MBNPA. This suggests that only the debromination pathway (Figure 3-1, pathway 2) is significant in removing DBNPA from solution. At later times, in solutions with 10 and 15 g/L of pyrite, measured concentrations of MBNPA diverge from the line indicating an MBNPA yield of less than 100%. It is possible that in the solutions with higher concentrations of pyrite, MBNPA is further debrominated to form cyanoacetamide, resulting in the decreased yield of MBNPA. However, because cyanoacetamide

could not be measured using LC-MS, this could not be verified. The hydrolysis product DBAN was not detected in any of the samples, indicating that the hydrolysis pathway is not significant in the presence of pyrite.

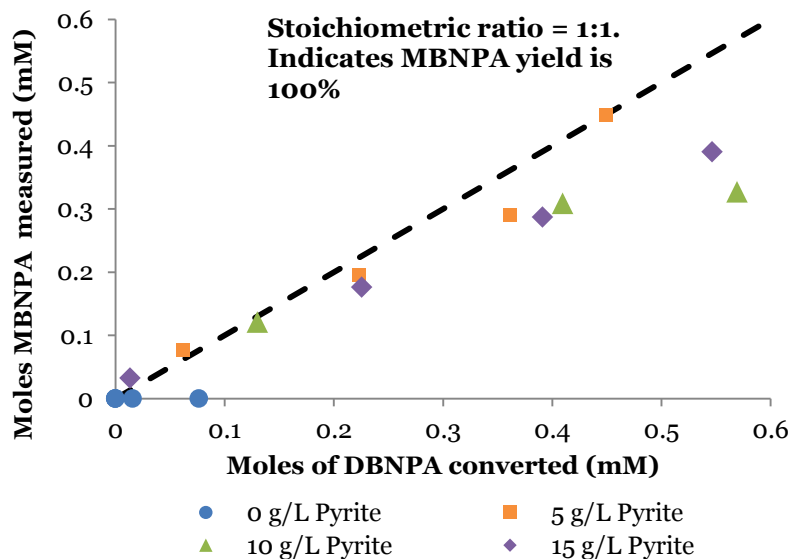


Figure 3-4. Measured monobromonitrilopropamide (MBNPA) concentrations as a function of DBNPA converted in 0 g/L, 5 g/L, 10 g/L and 15 g/L of pyrite. The dotted line represents a yield of 100% for MBNPA production.

### 3.5.3 Effect of $Fe^{II}$

Experiments were performed to determine the rate of DBNPA degradation with free  $Fe^{II}$ . As pyrite dissolves,  $Fe^{II}$  is produced, which is itself a reducing agent (standard redox potential for the  $Fe^{III}$ - $Fe^{II}$  couple,  $E^{\circ}H = 0.77$  V). Under anoxic conditions,  $Fe^{II}$  has been shown to reduce carbamate pesticides (Strathmann and Stone, 2001). Approximately 1 mM of  $FeCl_2$  solution was added to an equal concentration of DBNPA and the latter monitored over time. The pH was buffered at 3.1 to simulate the conditions with pyrite.

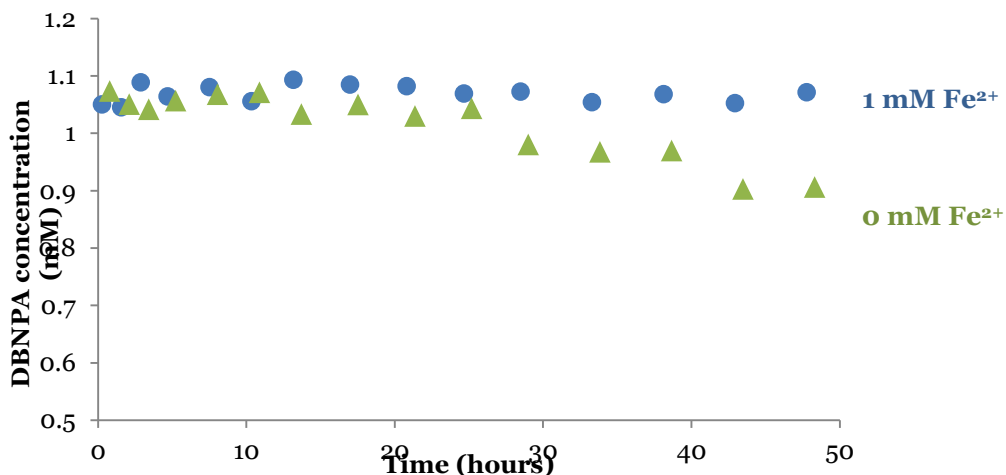


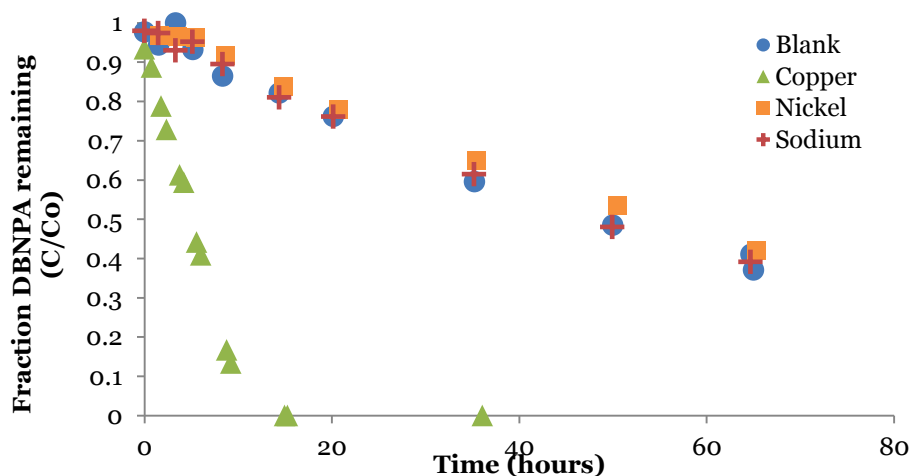
Figure 3-5. The concentration of DBNPA as a function of time (h) in the presence and absence of equal moles of FeCl<sub>2</sub>. The initial concentration of DBNPA was 1.06 mM. The experiment was performed in nitrogen-sparged water. Both experiments were performed in a formate buffer at pH 3.1.

Figure 3-5 illustrates that over 50 hours, Fe<sup>II</sup> alone in solution (in the absence of pyrite) had a limited effect on the persistence of DBNPA when compared to the control. DBNPA shows negligible degradation over time in the presence of FeCl<sub>2</sub>. Consistent with these results, previous research investigating the dehalogenation of organic compounds underscore that reduction by the Fe<sup>III</sup>–Fe<sup>II</sup> couple only occurs in the presence of a bulk reductant or electron transfer mediator. For example, previous studies show that polychlorinated and polybrominated methanes are only reduced by Fe<sup>II</sup> bound to the surface of iron oxide surfaces (Pecher et al., 2002; Amonette et al., 2000). In fact in our studies, Fe<sup>II</sup> appears to stabilize against DBNPA degradation, an observation noted with other amides with divalent metals (Huang and Stone, 1999; Sayre et al., 1992).

#### 3.5.4 Effect of other salts

To investigate the effect of various chloride salts (CuCl<sub>2</sub>, NiCl<sub>2</sub>, NaCl) were added to DBNPA to determine the effect of chloride and divalent cations on the stability of DBNPA (pH = 4.8) without pyrite. Because these experiments were run at a higher pH than those in previous

experiments, a control at the same pH was added to easily compare the contribution of the added salts. Figure 3-6 shows that the chloride ion, and the nickel and sodium cations had no perceptible effect on DBNPA degradation over 60 hours. In contrast, Cu<sup>II</sup> results in accelerated degradation of DBNPA, yielding an order of magnitude increase in the degradation rate. These results differ from those of Exner et al. (1973) who reported no effect of Cu<sup>II</sup> under air-saturated conditions. These results also confirm increased degradation (presumably hydrolysis) rates at pH=4.8 compared to pH=3.1.



**Figure 3-6. Fraction of DBNPA remaining as a function of time (h), in the presence of 1 mM CuCl<sub>2</sub>, 1 mM NiCl<sub>2</sub>, 2 mM NaCl and control (containing no chloride salt). The experiments were performed in nitrogen-sparged water, with an initial DBNPA concentration of 1.7 mM. All chloride experiments were performed in a formate buffer at pH 4.8.**

Analysis of the reaction products illustrates that Cu<sup>II</sup> catalyzes the base-catalyzed hydrolysis reaction. Figure 3-7 shows that the addition of Cu<sup>II</sup> leads to the instant formation of DBAN (Figure 3-1, pathway 1), while the debromination reaction that leads to MBNPA (Figure 3-1, pathway 2) is unaffected. Divalent metal ions such as Co<sup>II</sup> and Ni<sup>II</sup> are known to catalyze the degradation of some labile organic compounds. Dissolved metals can promote base-catalyzed hydrolysis due to their ability to complex with either incoming hydroxide ions (OH<sup>-</sup>), amide groups or both. Smolen and Stone (1997) compiled the complex formation constants for Cu<sup>II</sup>, Ni<sup>II</sup>, and Fe<sup>II</sup> with (i) OH<sup>-</sup> the first hydroxo species (K<sub>1</sub>); and (ii) NH<sub>3</sub>, which may be considered a

proxy for complexation with amides ( $K_{\text{NH}_3}$ ). The values in Table 3-2 illustrate that  $\text{Cu}^{\text{II}}$  complexes are expected to be several order of magnitude stronger than the other metal ions tested in this experiment. This may explain why only  $\text{Cu}^{\text{II}}$  catalyzed the degradation of DBNPA. This study and other empirical evidence in Sayre et al. (1992) and Fife and Bembi (1993) underscore the ability of  $\text{Cu}^{\text{II}}$  to enhance the hydrolysis of amides. On the other hand, because the bromide group is not expected to form strong complexes with  $\text{Cu}^{\text{II}}$ , the debromination pathway is unaffected.

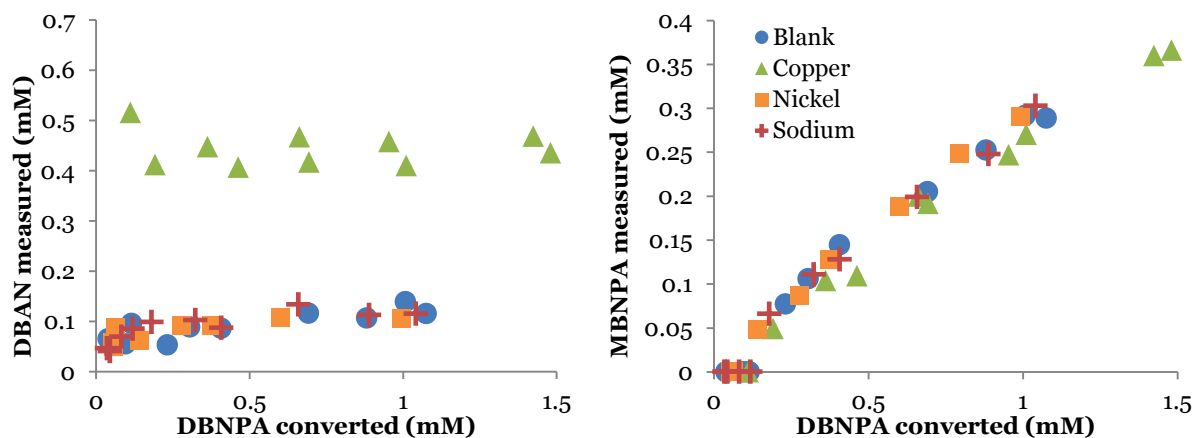


**Figure 3-7. Measured monobromonitrilopropamide (MBNPA) and dibromoacetonitrile (DBAN) concentrations in the presence of 1 mM  $\text{CuCl}_2$ , 1 mM  $\text{NiCl}_2$ , 2 mM  $\text{NaCl}$  and control (containing no chloride salt). The experiments were performed in nitrogen-sparged water, with an initial DBNPA concentration of 1.7 mM. All chloride experiments were performed in a formate buffer at pH 4.8.**

**Table 3-2. Constants for complexation with OH<sup>-</sup> (log \*K<sub>1</sub>) and NH<sub>3</sub> (log K<sub>NH3</sub>) for divalent metal ions considered in this study from Smolen and Stone (1997), data originally retrieved from the NIST database by Smith et al. (1995).**

	$Me^{2+} + H_2O \rightarrow MeOH^+ + H^+$	$Me^{2+} + NH_3 \rightarrow MeNH_3^{2+}$
	log *K <sub>1</sub>	log K <sub>NH3</sub>
Cu <sup>II</sup>	-7.5	4.2
Ni <sup>II</sup>	-9.9	2.9
Fe <sup>II</sup>	-9.4	1.5

### 3.5.5 Effect of sulfur oxyanions

The oxidation of pyrite, either by molecular oxygen or oxidizing organic compounds leads to the formation of sulfur oxyanions. When this occurs, the sulfide dimers first form a thiosulfate intermediate, S<sub>2</sub>O<sub>3</sub>, which is then rapidly oxidized to sulfate, SO<sub>4</sub><sup>2-</sup> (Descostes et al., 2004; Luther, 1987; Kriegman-King and Reinhard, 1994). Both of these products are important environmental nucleophiles, with thiosulfate being recognized as the much stronger of the two (Schwarzenbach et al., 2003). Thus, the sulfur oxyanions formed due to the oxidation of pyrite by DBNPA (or by O<sub>2</sub> under aerobic conditions) may also react with residual DBNPA molecules.

To determine the effect of these oxidation products, 1 mM of Na<sub>2</sub>S<sub>2</sub>O<sub>3</sub> and Na<sub>2</sub>SO<sub>4</sub> were each added to DBNPA solutions and compared to 2 mM NaCl and blank solution controls (pH = 4.8). Again, this experiment was buffered at pH 4.8. Sulfate had no effect on the degradation of DBNPA. Thiosulfate, a strong reducing agent (standard redox potential, E<sup>o</sup><sub>H</sub> = -0.93 V for the Na<sub>2</sub>SO<sub>4</sub>- Na<sub>2</sub>S<sub>2</sub>O<sub>3</sub> couple) had an immediate and significant impact on the persistence of DBNPA as previously noted by Exner et al. (1973). The data in Figure 3-8 and analyses of the reaction products suggest there was immediate reduction of DBNPA to form MBNPA (pathway 2) until the thiosulfate is depleted. This is followed by a slow hydrolysis that is similar to, but slightly less than the rate seen in the controls.

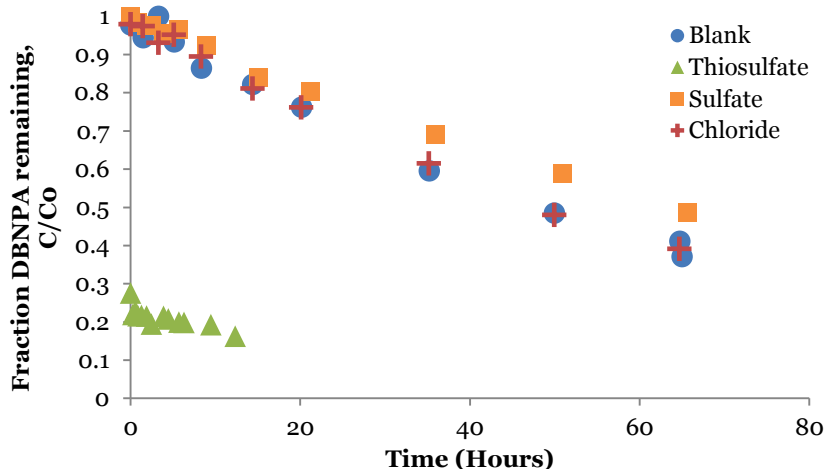


Figure 3-8. Fraction of DBNPA remaining as a function of time (h), in the presence of 1 mM  $\text{Na}_2\text{S}_2\text{O}_3$ , 1 mM  $\text{Na}_2\text{SO}_4$ , 2 mM  $\text{NaCl}$  and control (containing no sodium salt). The experiment was performed in nitrogen-sparged water, with an initial DBNPA concentration of 1.7 mM. All chloride experiments were performed in a formate buffer at pH 4.8.

### 3.6 Discussion

As DBNPA hydrolysis rates and pathways change with  $\text{OH}^-$  concentration, the persistence of this compound during the shut-in phase of hydraulic fracturing depends upon the pH of the fluid. At higher pH, DBNPA will degrade faster, producing more DBAN and dibromoacetamide. Measured pH values of produced water range from 5.1 to 8.4 (Barbot et al., 2013). Interestingly, Harrison et al. (2017) postulate that the pH of the produced water is a function of pyrite and calcium carbonate amounts: shale formations with lower abundances of pyrite and higher amounts of carbonate generate produced water with higher pH. In this way, the pyrite to calcium carbonate ratio indirectly controls the importance of amide hydrolysis of DBNPA.

The experimental data point to a heterogeneous reduction of DBNPA due to the presence of pyrite under anoxic conditions. The reaction is controlled by the pyrite-fluid interface and not by the concentration of hydrolysis ( $\text{Fe}^{\text{II}}$ ) and oxidation products ( $\text{S}_2\text{O}_3^{2-}$  and  $\text{SO}_4^{2-}$ ). Molecular orbital theory posits that the disulfide ( $\text{S}_2^{2-}$ ) group on pyrite can act as an electron source:  $\text{S}_2^{2-}$

can transfer electrons from the two pi antibonding ( $\pi^*$ ) highest occupied molecular orbitals (HOMO) to the lowest unoccupied molecular orbitals (LUMO) of halogenated compounds (Luther, 1987). It is not unlikely that thiosulfate contributes to DBNPA reduction. However, concentrations of  $S_2O_3^{2-}$  are expected to be low as this strong reducing agent will be quickly depleted by any oxidizing agents. As such, the contribution from  $S_2O_3^{2-}$  is expected to be quite small.

The product distribution observed with on the addition of pyrite can be used to propose a reduction mechanism. To obtain almost 100% initial selectivity for MBNPA, the intermediate must be an anion which can then react with  $H^+$  ions in solution. According to this mechanism, the bromide,  $-Br$  group is always replaced with a hydrogen,  $-H$  to form MBNPA (as illustrated in Figure 3-9). A one-electron reduction would generate a radical intermediate which further react to yield a mixture of additional products. Therefore, a two-electron reduction appears to be the primary mechanism at play.

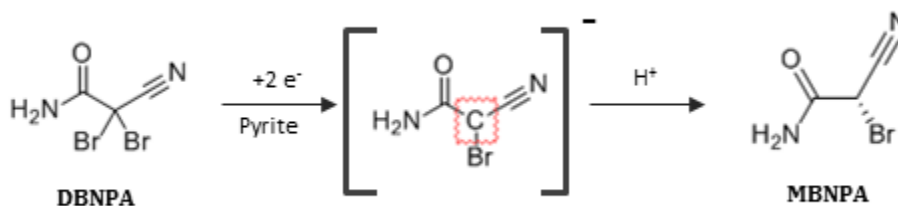


**Figure 3-9. Proposed two-electron pathway for the reduction of DBNPA to MBNPA, highlighting the anionic intermediate.**

While the results in these studies are not predictive of the actual behavior in shale formations, they illustrate that pyrite can change the expected lifetime and products of DBNPA reactions. This may have a pronounced result on the assessment of the risk of this biocide in hydraulic fracturing. Pyrite, due to lower pH and redox reactions, results in a greater selectivity towards MBNPA over the alternative daughter product, DBAN. MBNPA is the least toxic of the

three measured compounds with an LC<sub>50</sub> of 3.4 mg/L (compared to 1.8 mg/L for DBNPA and 0.55 mg/L for DBAN) (Mayes et al., 1985).

Overall, this study opens the door to the possibility of reduction of other brominated biocides with pyrite, even biocides that are more stable to hydrolysis such as dibromodicyanobutane. From a thermodynamic point of view, halogenated compounds are often good oxidizing agents: halogens have a strong tendency to accept electrons due to their high electronegativity and stability as anions (Schwarzenbach et al., 2003). These results have highlighted that halogens are susceptible to reduction by pyrite, while the other functional groups (amide,  $-C(=O)NH_2$  and nitrile,  $-C\equiv N$ ) are stable to reduction by pyrite (at times less than 10 hours). This work is the first to report the reduction of organobromides by pyrite, and suggests that pyrite can have pronounced effects on the persistence of other brominated biocides used in hydraulic fracturing such as dibromodicyanobutane.

### 3.7 References

- Adrian, N.R., Suflita, J.M., 1990. Reductive dehalogenation of a nitrogen heterocyclic herbicide in anoxic aquifer slurries. *Appl. Environ. Microbiol.* 56, 292–294.
- Amonette, J.E., Workman, D.J., Kennedy, D.W., Fruchter, J.S., Gorby, Y.A., 2000. Dechlorination of Carbon Tetrachloride by Fe(II) Associated with Goethite. *Environmental Science & Technology* 34, 4606–4613. doi:10.1021/es9913582
- Barbot, E., Vidic, N.S., Gregory, K.B., Vidic, R.D., 2013. Spatial and Temporal Correlation of Water Quality Parameters of Produced Waters from Devonian-Age Shale following Hydraulic Fracturing. *Environmental Science & Technology* 47, 2562–2569. doi:10.1021/es304638h
- Bazzini, P., Wermuth, C.G., 2015. Substituent groups, in: *The Practice of Medicinal Chemistry*. Elsevier.
- Blanchard, F.A., Gonsior, S.J., Hopkins, D.L., 1987. 2,2-Dibromo-3-nitrilopropionamide (DBNPA) chemical degradation in natural waters: Experimental evaluation and modeling of competitive pathways. *Water Research* 21, 801–807. doi:10.1016/0043-1354(87)90155-2
- Castro, C.E., Belser, N.O., 1968. Biodehalogenation. Reductive Dehalogenation of the Biocides Ethylene Dibromide, 1,2-Dibromo-3-chloropropane, and 2,3-Dibromobutane in Soil. *Environmental Science & Technology* 2, 779–783. doi:10.1021/es60173a019
- Cupples, A.M., Sanford, R.A., Sims, G.K., 2005. Dehalogenation of the Herbicides Bromoxynil (3,5-Dibromo-4-Hydroxybenzoxynitrile) and Ioxynil (3,5-Diiodo-4-Hydroxybenzoxynitrile) by *Desulfotobacterium chlororespirans*. *Applied and Environmental Microbiology* 71, 3741–3746. doi:10.1128/AEM.71.7.3741-3746.2005
- Descostes, M., Vitorge, P., Beaucaire, C., 2004. Pyrite dissolution in acidic media. *Geochimica et Cosmochimica Acta* 68, 4559–4569. doi:10.1016/j.gca.2004.04.012
- Dodson, R.E., Perovich, L.J., Covaci, A., Van den Eede, N., Ionas, A.C., Dirtu, A.C., Brody, J.G., Rudel, R.A., 2012. After the PBDE Phase-Out: A Broad Suite of Flame Retardants in Repeat House Dust Samples from California. *Environmental Science & Technology* 46, 13056–13066. doi:10.1021/es303879n
- Elsner, M., Hoelzer, K., 2016. Quantitative survey and structural classification of hydraulic fracturing chemicals reported in unconventional gas production. *Environmental Science & Technology* 50, 3290–3314. doi:10.1021/acs.est.5b02818
- Exner, J.H., Burk, G.A., Kyriacou, D., 1973. Rates and products of decomposition of 2,2-dibromo-3-nitrilopropionamide. *Journal of Agricultural and Food Chemistry* 21, 838–842. doi:10.1021/jf60189a012
- Greve, P.A., 1983. Bromide-ion residues in food and feedstuffs. *Food and Chemical Toxicology* 21, 357–359. doi:10.1016/0278-6915(83)90088-1
- Harrison, A.L., Jew, A.D., Dustin, M.K., Thomas, D.L., Joe-Wong, C.M., Bargar, J.R., Johnson, N., Brown, G.E., Maher, K., 2017. Element release and reaction-induced porosity alteration during shale-hydraulic fracturing fluid interactions. *Applied Geochemistry* 82, 47–62. doi:10.1016/j.apgeochem.2017.05.001
- Huang, C.-H., Stone, A.T., 1999. Hydrolysis of Naptalam and Structurally Related Amides: Inhibition by Dissolved Metal Ions and Metal (Hydr)Oxide Surfaces. *Journal of Agricultural and Food Chemistry* 47, 4425–4434. doi:10.1021/jf990423o
- Kahrilas, G.A., Blotvogel, J., Stewart, P.S., Borch, T., 2015. Biocides in hydraulic fracturing fluids: A critical review of their usage, mobility, degradation, and toxicity. *Environmental Science & Technology* 49, 16–32. doi:10.1021/es503724k

- Klaine, S.J., Cobb, G.P., Dickerson, R.L., Dixon, K.R., Kendall, R.J., Smith, E.E., Solomon, K.R., 1996. An ecological risk assessment for the use of the biocide, dibromonitripropionamide (DBNPA), in industrial cooling systems. *Environmental Toxicology and Chemistry* 15, 21–30. doi:10.1002/etc.5620150104
- Kriegman-King, M.R., Reinhard, M., 1994. Transformation of Carbon Tetrachloride by Pyrite in Aqueous Solution. *Environmental Science & Technology* 28, 692–700. doi:10.1021/es00053a025
- Lee, W., Batchelor, B., 2002. Abiotic reductive dechlorination of chlorinated ethylenes by iron-bearing soil minerals. 1. Pyrite and magnetite. *Environ. Sci. Technol.* 36, 5147–5154.
- Liu, R., Wolfe, A.L., Dzombak, D.A., Horwitz, C.P., Stewart, B.W., Capo, R.C., 2008a. Electrochemical study of hydrothermal and sedimentary pyrite dissolution. *Applied Geochemistry* 23, 2724–2734. doi:10.1016/j.apgeochem.2008.06.005
- Liu, R., Wolfe, A.L., Dzombak, D.A., Stewart, B.W., Capo, R.C., 2008b. Comparison of dissolution under oxic acid drainage conditions for eight sedimentary and hydrothermal pyrite samples. *Environmental Geology* 56, 171–182. doi:10.1007/s00254-007-1149-0
- Luther, G.W., 1987. Pyrite oxidation and reduction: Molecular orbital theory considerations. *Geochimica et Cosmochimica Acta* 51, 3193–3199. doi:10.1016/0016-7037(87)90127-X
- Mayes, M.A., Blanchard, F.A., Hopkins, D.L., Takahashi, I.T., 1985. Static acute toxicity of dibromonitripropionamide and selected degradation products to the fathead minnow (*Pimephales Promelas rafinesque*). *Environmental Toxicology and Chemistry* 4, 823–830. doi:10.1002/etc.5620040613
- Nalepa, C., 2004. 25 Years of bromine chemistry in industrial water systems: a review (No. 04087), Corrosion. NACE International, Houston, TX.
- Noling, J.W., Becker, J.O., 1994. The Challenge of Research and Extension to Define and Implement Alternatives to Methyl Bromide. *Journal of Nematology* 26, 573–586.
- Paschka, M.G., Dzombak, D.A., 2004. Use of Dissolved Sulfur Species to Measure Pyrite Dissolution in Water at pH 3 and 6. *Environmental Engineering Science* 21, 411–420. doi:10.1089/1092875041358502
- Pecher, K., Haderlein, S.B., Schwarzenbach, R.P., 2002. Reduction of Polyhalogenated Methanes by Surface-Bound Fe(II) in Aqueous Suspensions of Iron Oxides. *Environmental Science & Technology* 36, 1734–1741. doi:10.1021/es0111910
- Renner, R., 2000. What Fate for Brominated Fire Retardants? *Environmental Science & Technology* 34, 222A–226A. doi:10.1021/es003269r
- Reregistration eligibility decision for 2,2-dibromo-3-nitripropionamide (DBNPA) (Case 3056), 1994. . U.S. Environmental Protection Agency (EPA).
- Reregistration eligibility decision for bronopol (Case 2770), 1995. . U.S. Environmental Protection Agency (EPA).
- Reregistration eligibility decision for dibromodicyanobutane (Case 2780), 1996. . U.S. Environmental Protection Agency (EPA).
- Reregistration eligibility decision for halohydantoin (Case 3055), 2004. . U.S. Environmental Protection Agency (EPA).
- Sayre, L.M., Reddy, K.V., Jacobson, A.R., Tang, W., 1992. Metal ion catalysis of amide hydrolysis. Very large rate enhancements by copper(II) in the hydrolysis of simple ligand-functionalized tertiary amides. *Inorganic Chemistry* 31, 935–937. doi:10.1021/ic00032a001
- Schwarzenbach, R.P., Gschwend, P.M., Imboden, D.M., 2003. *Environmental organic chemistry*, 2. ed. ed. Wiley, New York.
- Shih, Y., Tai, Y., 2010. Reaction of decabrominated diphenyl ether by zerovalent iron nanoparticles. *Chemosphere* 78, 1200–1206. doi:10.1016/j.chemosphere.2009.12.061

- Smith, R.M., Martell, A.E., Motekaitis, R.J., 1995. NIST Critically Selected Stability Constants of Metal Complexes Database. National Institute of Standards and Technology (NIST), Gaithersburg, MD.
- Smolen, J.M., Stone, A.T., 1997. Divalent Metal Ion-Catalyzed Hydrolysis of Phosphorothionate Ester Pesticides and Their Corresponding Oxonates. *Environmental Science & Technology* 31, 1664–1673. doi:10.1021/es960499q
- Strathmann, T.J., Stone, A.T., 2001. Reduction of the Carbamate Pesticides Oxamyl and Methomyl by Dissolved Fe II and Cu I. *Environmental Science & Technology* 35, 2461–2469. doi:10.1021/es001824j
- Stringfellow, W.T., Domen, J.K., Camarillo, M.K., Sandelin, W.L., Borglin, S., 2014. Physical, chemical, and biological characteristics of compounds used in hydraulic fracturing. *Journal of Hazardous Materials* 275, 37–54. doi:10.1016/j.jhazmat.2014.04.040
- Vainikka, P., Hupa, M., 2012. Review on bromine in solid fuels – Part 2: Anthropogenic occurrence. *Fuel* 94, 34–51. doi:10.1016/j.fuel.2011.11.021
- Weerasooriya, R., Dharmasena, B., 2001. Pyrite-assisted degradation of trichloroethene (TCE). *Chemosphere* 42, 389–396.
- Williams, D.E., Elder, E.D., Worley, S.D., 1988. Is free halogen necessary for disinfection? *Appl. Environ. Microbiol.* 54, 2583–2585.
- Wittayanan, W., Jongmevasna, W., Kaewklapanacharoen, L., Atisook, K., 2017. Method development and validation of hydrogen phosphide and inorganic bromide determined as fumigant residues in commercialized rice grains in Thailand. *International Food Research Journal* 24.
- Wolf, P.A., Sterner, P.W., 1972. 2,2-Dibromo-3-Nitrilopropionamide, a Compound with Slicicidal Activity. *Applied Microbiology* 24, 581–584.
- Wolfe, A.L., Liu, R., Stewart, B.W., Capo, R.C., Dzombak, D.A., 2007. A method for generating uniform size-segregated pyrite particle fractions. *Geochemical Transactions* 8, 9. doi:10.1186/1467-4866-8-9
- Zhuang, Y., Jin, L., Luthy, R.G., 2012. Kinetics and pathways for the debromination of polybrominated diphenyl ethers by bimetallic and nanoscale zerovalent iron: Effects of particle properties and catalyst. *Chemosphere* 89, 426–432. doi:10.1016/j.chemosphere.2012.05.078

## **Chapter 4      Abiotic degradation of dazomet: hydrolysis and degradation with pyrite**

The information presented in this chapter will appear as a publication in a peer-reviewed journal with the tentative title "Abiotic degradation of dazomet: implications for persistence under Marcellus Shale conditions" by Nizette Consolazio, Gregory V. Lowry and Athanasios K. Karamalidis.

#### 4.1 Abstract

Hydraulic fracturing and horizontal drilling in the Marcellus Shale present a novel use of chemical additives at unprecedented volumes. This study investigates the effect of pH, temperature, ionic strength and the presence of pyrite on the kinetics of dazomet degradation, a commonly-used biocide, under a range of conditions expected during hydraulic fracturing. The results show that the degradation rate of dazomet is highly dependent on many of the variables tested. The hydrolysis is base-catalyzed over the pH range of interest which results in half-lives decreasing from 8.5 hours to 3.4 hours as the pH is increased from 4.1 and 8.2. Dissolved Fe<sup>II</sup> ions catalyze dazomet degradation kinetics with solutions of 0.8 mM Fe<sup>II</sup> causing degradation rates to increase by 190% over iron-free water. Increasing temperatures from 34°C to 57°C quadrupled hydrolysis rates (estimated activation energy of 60 kJ/mol). Reaction with the oxygen-exposed pyrite surface led to accelerated degradation of dazomet, but unoxidized pyrite had no effect on measurable effect on the degradation rate of dazomet. The key hydrolysis products of dazomet degradation are formaldehyde and methyl isothiocyanate which are shown to be significantly more toxic than the parent compound. The study points to the need to assess the specific environmental conditions and any toxic by-products in conducting risk assessments for geological applications.

## 4.2 Introduction

The success of hydraulic fracturing has been a pivotal advancement for the natural gas industry in the US. To extract the natural gas, an average of 1.5 million gallons of fluid are pumped into the formation to fracture it, allowing the trapped natural gas to flow (U.S. EPA, 2015). With it comes waste or produced water that is collected for disposal (King, 2012; Carter et al., 2011). In addition to chemical residues, the produced water contains high levels of total dissolved solids, organics, radionuclides and pH ranging from 5.1 to 8.4 (Barbot et al., 2013; Orem et al, 2014; Rowan et al., 2011). This fracking fluid or produced water may contaminate surface waters and soils due to unintended spills or leaks (Zhang et al., 2017; Vengosh et al., 2014; Elliott et al., 2016; Rogers et al. 2015; Jain et al., 2017).

Various chemicals are mixed into the fracking fluid to improve the efficiency of the process. One additive of interest is dazomet, frequently used in the Marcellus Shale as a biocide to limit microbial growth (US EPA, 2008; Carter et al., 2013; Gaspar et al., 2014; Kahrilas et al., 2015). Chemically, it falls under the group of dithiocarbamates, a sulfur analog to carbamates or urethanes. It is a cyclic propesticide, which rapidly hydrolyzes in water to form methyl isothiocyanate (MITC), formaldehyde and other compounds (Figure 4-1). MITC, the primary product on addition to soils is responsible for its ability to limit the growth of weeds and soil-borne pathogens in agriculture (US EPA, 2008). The non-specific toxicity of MITC is due to its ability to cause perturbation of metal-enzymes or thiol-containing proteins, its formation of reactive oxygen species or metal toxicity due to the chelation of heavy metals (Tilton et al., 2006). Manufacturers recommend using dazomet at concentrations between 200 and 1000 mg/L in fracking fluids and 150 and 200 mg/L in produced water that will be reused (BASF, 2000). Its degradation product hexahydro-1,3,5-trimethyl-1,3,5-triazine-2-thione has been measured in produced water at concentrations between 0.01 and 1.6 mg/L (Orem et al., 2014).

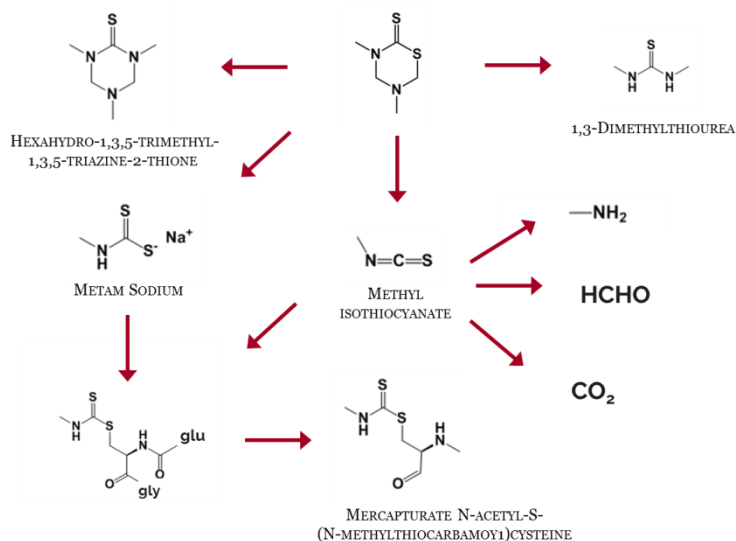


**Figure 4-1. Structures of the key hydrolysis and metabolized products of dazomet as reported by Roberts and Hudson (1999).**

Of the many minerals present in shale, we focus on possible reactions with pyrite,  $\text{FeS}_2$ , which may significantly influence the degradation of dazomet in the Marcellus Shale. The overall objective of this chapter is to quantify the influence of water chemistry and interactions with pyrite on the degradation of the sulfur-containing biocide, dazomet. To investigate the kinetics of dazomet degradation, single-parameter experiments were performed to investigate the rate of dazomet degradation at differing pH, temperature, ionic composition and pyrite solids content. The observed reaction products were also measured.

### 4.3 Methods and Materials

#### 4.3.1 Chemicals

Dazomet (3,5-dimethyltetrahydro-1,3,5-thiadiazine-2-thione), methyl isothiocyanate (97%), N,N dimethylthiourea (99%), and nitrobenzene (> 99.5%) were purchased from Sigma-Aldrich. Methanol (99.8% minimum), HCl (35.5 – 38%), and acetone (99.0% minimum) were from BDH Chemicals. Ammonium formate (97%) and formic acid (96+%) were from Alfa Aesar.

HPLC grade acetonitrile (99.9%), dichloromethane (99.9%), 200 proof ethanol, zinc acetate, iodine, potassium iodine, anhydrous sodium thiosulfate, soluble starch, iron (II) chloride were obtained from Fisher Scientific. TCI America supplied 2,4 dinitrophenylhydrazine hydrochloride (DNPH·HCl) (>98%) and formalin solution (37%) and n-hexane (99+%) were from Acros Organics. High purity pyrite (FeS<sub>2</sub>) was obtained from Ward's Science, from Zacatecas, Mexico. For all experiments, ultrapure water (18.1 MΩ) purified with the Barnstead water system was used.

Dazomet was analyzed using a liquid chromatograph (HPLC, Agilent 1100), equipped with variable wavelength detector (VWD) coupled to a triple quadrupole mass spectrometer (QQQ, Agilent 6430). The organics were analyzed with gas chromatography-mass spectrometer (GC-MS, Agilent 7890B; Agilent 5977A). The reaction products were identified with the NIST 11 MS library. The pH of the solutions was measured using model Accumet XL60 pH meter with Accumet 13-620-299 pH electrode.

#### 4.3.2 *Batch reactors*

Because of dazomet's rapid hydrolysis in water, stock solutions of 1000 mg/L (~8 mM) were prepared in methanol. Experiments were conducted in 60 mL amber vials and sealed with mini PTFE mininert caps. Water was added to the vials and then spiked with the appropriate mass of dazomet stock. The volume of the methanolic spike was kept below 5 vol% to limit any effect of co-solvency on the activity of dazomet. The pH was measured approximately 6.3 immediately after dazomet addition to solution for experiments not controlling the pH. In experiments under controlled pH conditions, a 100 mM formate-formic acid buffer was used. To investigate the effect of temperature, the vials were placed in a water bath. For anoxic experiments, the reactors were set in up a glove box (2.5% hydrogen), and nitrogen-sparged 18.1 MΩ water was used. Where possible, the samples were placed into a 2 mL amber LC screw top

vials topped with PTFE/silicone caps. These were then repeatedly sampled using the programmable auto sampler. One replicate was performed for each condition. Experiments with iron were performed by adding  $\text{FeCl}_2 \cdot 4\text{H}_2\text{O}$  to a pH 2.7 formate buffer under anoxic conditions. Iron concentrations were measured using the ferrozine method outlined by Viollier et al. (2000).

#### 4.3.3 *Pyrite preparation*

Pyrite was crushed using a mortar and pestle and wet-sieved with 70% ethanol and water as outlined in Wolfe et al. (2007). For this study, particles with particle size ranging between 37 – 250  $\mu\text{m}$  were used. To remove any oxidation products, about 7 g of pyrite was added to 50 mL boiling HCl and stirred for 10 minutes as in Paschka and Dzombak (2004). The pyrite was then rinsed in 25 mL boiling HCl twice, water once, and then boiling acetone thrice. The resulting pyrite samples were oven-dried at 105°C for 30 mins and then cooled under vacuum. 2-propanol was used as hydroxyl radical ( $\bullet\text{OH}$ ) scavenger to determine whether these species may be responsible for biocide degradation. Sedimentary pyrite was not available during the period of this study. Hydrothermal pyrite is a suitable proxy for probing the fundamental degradation mechanisms as in this study (Liu et al., 2008a) However, as sedimentary pyrite is often more varied in chemistry than the hydrothermal variety, additional experiments may be needed to accurately translate these results to shale formations (Liu et al., 2008b).

#### 4.3.4 *Dazomet reaction rate analysis*

Quantification of dazomet was done using liquid chromatography coupled with tandem mass spectroscopy (LC-QQQ). Five microliters of the aqueous solutions of dazomet (concentrations up to 200 ppm) were injected onto a ZORBAX Eclipse C18 column (4.6 x 150 mm, 5  $\mu\text{m}$ ) at 30°C. The solutions were separated using an isocratic run of 25% acetonitrile and

75% water, acidified with 0.1% formic acid at a flowrate of 1 mL/min. The mass spectrometer source parameters were the following: 300°C gas temperature; 11 L/min N<sub>2</sub> gas flow at 14 psi; capillary voltage at 4000 V.

#### 4.3.5 *Dazomet reaction products*

Gas chromatography (GC) analysis of the dazomet reaction products was analyzed by first performing liquid-liquid extraction. Five milliliters of the aqueous reaction solution was spiked with 20 µL of 2 mg/mL nitrobenzene in dichloromethane, added to 2 mL of dichloromethane, shaken and left to separate. The organic phase was removed and 1 µL of the solution was injected splitless mode at 240°C onto an Agilent J&W HP-5MS column (30m x 0.25 mm x 0.25 µm). The carrier gas was ultra-high purity helium at a constant velocity of 30 cm/sec. The oven was held at 40°C for 1 minute; ramped up to 50°C at 5°C/min; 100°C at 15°C/min; 210°C at 20°C/min and then held for 5 mins. The MS transfer line, quadrupole and source temperatures were set to 280°C, 150°C and 230°C, respectively. MS was done in scan mode (m/z 40 – 350).

The detection of formaldehyde was adapted from Facchini et al. (1989). The aqueous samples were first filtered with a SPE cartridge to remove other sulfide-containing organic compounds. One milliliter of acidic DNPH solution ( $5 \times 10^{-3}$  M in 2N HCl), 1 mL of the aqueous sample, and 2 mL of hexane were added to a glass reaction vial. The mixture was shaken and left to react for 45 minutes. After this, the organic layer was extracted and 20 µL was injected onto the ZORBAX Eclipse C18 column (4.6 x 150 mm, 5 µm) at 30°C. The mobile phase was 70% acetonitrile, 30% water mixture with 0.1% formic acid and operated at a flowrate of 1 mL/min. The absorbance of aldehyde-DNPH was measured at 360 nm, and formaldehyde identified by its peak retention time. The sample concentration was calculated using a calibration done with formalin standards.

Sulfide, S<sup>2-</sup>, was quantified using an iodometric titration based on the U.S. Geological Survey method I 3840-85 (Fishman and Friedman, 1989). Exactly 10 mL of the aqueous solution was pipetted into an Erlenmeyer flask and 2 g of zinc acetate per liter of sample added to fix the sulfide in the sample. One milliliter of 0.01 N I<sub>2</sub> solution was added to the sample and mixed well, followed by 1 mL of concentrated HCl. The solution was then titrated using 0.01 N Na<sub>2</sub>S<sub>2</sub>O<sub>3</sub> with 1-2 drops of starch solution as the indicator. The procedure was repeated using a blank of 10 mL water. The concentration of sulfide was then calculated using equation 1.

$$S^{2-} (M) = 500 \times (mL Na_2S_2O_3_{blank} - mL Na_2S_2O_3_{sample}) \quad \text{Eq. 2}$$

## 4.4 Results

### 4.4.1 Effect of pH on the removal of dazomet

Solution pH is often a controlling variable for the abiotic degradation of organic compounds. Experiments investigating the effect of pH were performed at four values that span in the range of pH expected in produced waters: 3.4, 4.1, 8.2 and 9.5. Other variables were kept constant among vials (initial concentration of 60 μM, 20°C, oxygen-saturated water). Figure 4-2a follows the natural logarithm of the fraction of dazomet remaining with time. The degradation rates were calculated assuming pseudo-first order reactions with respect to dazomet, and the half-lives plotted against pH in Figure 4-2b. Least-squared regressions supported this assumption (R<sup>2</sup> > 0.99). This was further confirmed as experiments varying initial dazomet concentrations (12 μM, 49 μM and 490 μM) resulted in similar degradation rates (Table 4-1).

Base-catalysis dominates in the pH range studied. Between pH 3 and 4, the degradation rate of dazomet is almost unchanged with pH, with half-lives at around 8.5 hours. This implies that acid catalysis is insignificant (k<sub>A</sub> ≈ 0), as an order of magnitude increase in H<sup>+</sup> ions had little

effect on dazomet's susceptibility to hydrolysis. As the pH increases above 4, dazomet hydrolysis also increases, with half-lives of 3.4 and 1.3 hours at pH 8.2 and 9.5, respectively. In this region, the apparent half-life of dazomet correlate closely with the logarithm of the concentration of hydroxide ions ( $\text{OH}^-$ ) ( $R^2 = 0.998$ ).

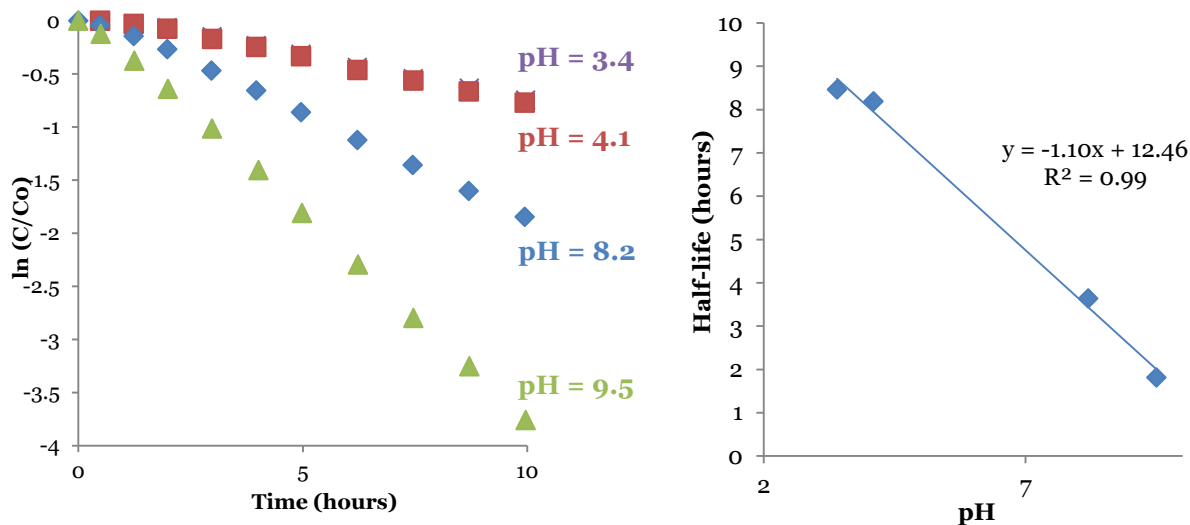


**Figure 4-2. (a) The hydrolytic degradation of dazomet as a function of time (h), at pH 3.4, 4.1, 8.2 and 9.5 according to pseudo-first order kinetics (b) Dazomet half-life as a function of pH, calculated from the data in (a). The initial concentration of these experiments was 80  $\mu\text{M}$ , performed at 20°C and run under oxic conditions**

#### 4.4.2 Effect of dissolved species on the removal of dazomet

Of the metals most frequently present in produced water, iron species are known to influence the degradation of organic compounds. While this effect is often negligible in surface waters, concentrations in produced water are many order of magnitude higher, with median values about 0.8 mM (Abualfara et al., 2014; Barbot et al., 2013). We investigated the reaction between dazomet and dissolved  $\text{Fe}^{\text{II}}$  by monitoring the disappearance of 80  $\mu\text{M}$  of dazomet in

excess Fe<sup>II</sup>, 0.4 mM and 0.8 mM as measured by the ferrozine method. The experiment was buffered at pH 3 under anoxic conditions to avoid the precipitation of iron hydroxo complexes.

Figure 4-3 shows that Fe<sup>II</sup> accelerates the degradation of dazomet. Solutions of 0.4 and 0.8mM Fe<sup>II</sup> caused an increase of 71% and 190% in degradation rates over iron-free water. Chemical equilibrium modeling using Visual MINTEQ version 3.1 was performed to confirm that Fe<sup>II</sup> was the most dominant species present. Controls were also performed with nitrogen-purged water under an oxygen atmosphere. This confirmed that oxidative degradation does not affect the persistence of dazomet.

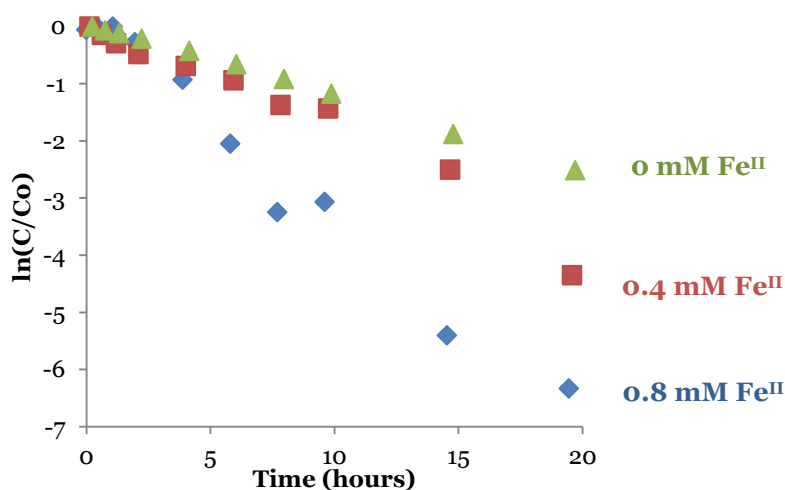


**Figure 4-3.** The degradation of dazomet as a function of time (h) in the presence of 0 mM, 0.4 mM and 0.8 mM dissolved Fe<sup>II</sup> according to pseudo-first order kinetics. The reactions were conducted at pH 3, 20°C under anoxic conditions. Initial dazomet concentration was 80 μM.

#### 4.4.3 Effect of dissolved species on the removal of dazomet

Of the metals most frequently present in produced water, iron species are known to influence the degradation of organic compounds. While this effect is often negligible in surface waters, concentrations in produced water are many order of magnitude higher, with median values about 0.8 mM (Abualfara et al., 2014; Barbot et al., 2013). We investigated the reaction between dazomet and dissolved Fe<sup>II</sup> by monitoring the disappearance of 80 μM of dazomet in

excess Fe<sup>II</sup>, 0.4 mM and 0.8 mM as measured by the ferrozine method. The experiment was buffered at pH 3 under anoxic conditions to avoid the precipitation of iron hydroxo complexes.

Figure 4-3 shows that Fe<sup>II</sup> accelerates the degradation of dazomet. Solutions of 0.4 and 0.8mM Fe<sup>II</sup> caused an increase of 71% and 190% in degradation rates over iron-free water. Chemical equilibrium modeling using Visual MINTEQ version 3.1 was performed to confirm that Fe<sup>II</sup> was the most dominant species present. Controls were also performed with nitrogen-purged water under an oxygen atmosphere. This confirmed that oxidative degradation does not affect the persistence of dazomet.

As the effect of ionic strength on dazomet has not been reported in literature, experiments with NaCl were performed as a control in order to disentangle the effect of ionic strength and catalysis by specific metal ions. Sodium is by far the largest metal ion in produced water, measuring on the order of 5 M (Barbot et al., 2013). In experiments varying ionic strength up to 100 mM NaCl, no detectable change was found in the rates of degradation of dazomet (Table 4-1). This result may be extended to even higher concentrations as salinity typically only has a measureable effect on hydrolysis when multiple charged species are involved in the formation of the transition state (Atkins and de Paula, 2006).

#### *4.4.4 Effect of temperature on the removal of dazomet*

Activation parameters were estimated by determining rate constants at various temperatures. This allows the interpolation of dazomet hydrolysis at elevated temperatures (keeping all other factors constant). The natural logarithm of the fraction of dazomet remaining over time at 34°C, 49°C and 57°C are shown in Figure 4-4. Here, pH was not controlled but remained constant at 6.3 throughout the experiments. These experiments were conducted above room temperature to avoid fluctuations in ambient air temperature. The observed hydrolysis

rate constant,  $k_{obs}$ , again fit pseudo-first order kinetics with respect to dazomet at all temperatures tested ( $R^2 = 0.99$ ).

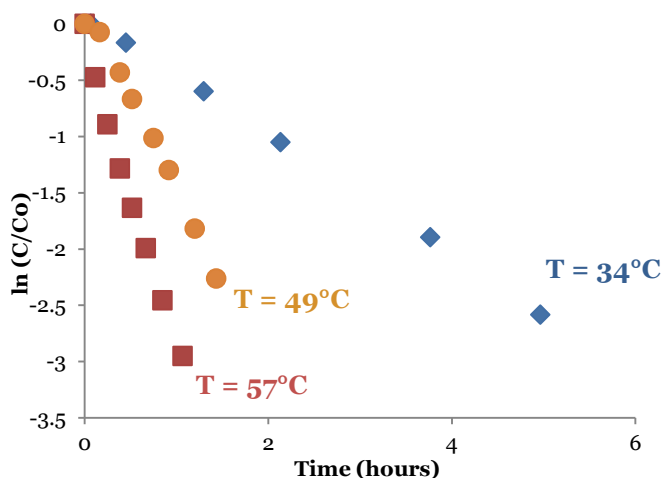


Figure 4-4. Temperature dependence of the degradation of dazomet as a function of time (h), conducted at four temperatures (34°C, 49°C and 57°C). The pH (when cooled to 21°C) was measured at 6.3. The reaction was performed under oxalic conditions with a starting concentration of 175  $\mu\text{M}$ .

Dazomet hydrolysis proves to be sensitive to changes in temperature, with an increase of 23°C quadrupling the hydrolysis rate. By using the Arrhenius equation (equation 2) where  $R$  is the molar gas constant,  $T$  is the absolute temperature and  $A$  is the pre-exponential factor, the activation energy or  $E_a$  can be calculated.

$$k_{obs} = A \cdot \exp\left(-\frac{E_a}{RT}\right) \quad \text{Eq. 3}$$

By plotting the linearized form of this equation in Figure 4-5 the  $E_a$  was estimated at 61 kJ/mol. An  $R^2$  of 1 indicates that the  $E_a$  is consistent over the temperature range of this experiment. This falls within the range of 50 to 100 kJ/mol given for the oxygen analogues, carbamates (Schwarzenbach et al., 2003).

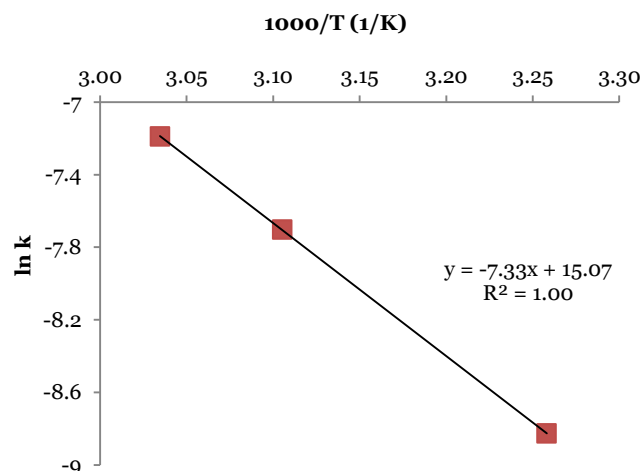


Figure 4-5. Plot of  $\ln k$  as a function of  $1000/T$  to estimate the activation energy of dazomet hydrolysis. The slope led to an estimated activation energy,  $E_a$  of 61 kJ/mol.

To summarize thus far, the results for these experiments are presented in Table 4-1.

Table 4-1. Pseudo first-order rate constant for the hydrolysis of dazomet under varying, pH, temperature dissolved iron (II), dazomet concentration, dissolved sodium and oxygen removal, along with the corresponding calculated lifetimes. Initial concentration for all experiments was 80  $\mu\text{M}$ , unless otherwise indicated.

Variable tested	Conditions	k ( $\text{h}^{-1}$ )	Half-life (h)
<b><i>Effect of pH</i></b>			
pH = 3.4	20°C, oxic conditions	0.082	8.5
pH = 4.1	20°C, oxic conditions	0.085	8.2
pH = 8.2	20°C, oxic conditions	0.19	3.6
pH = 9.5	20°C, oxic conditions	0.38	1.8
<b><i>Effect of temperature</i></b>			
T = 34°C	Oxic conditions, measured pH = 6.3	0.53	1.3
T = 49°C	Oxic conditions, measured pH = 6.3	1.6	0.43
T = 57°C	Oxic conditions, measured pH = 6.3	2.7	0.26
<b><i>Effect of dissolved Fe<sup>II</sup></i></b>			
[Fe <sup>II</sup> ] = 0 mM	20°C, anoxic conditions, pH = 3	0.12	5.8
[Fe <sup>II</sup> ] = 0.4 mM	20°C, anoxic conditions, pH = 3	0.20	3.4
[Fe <sup>II</sup> ] = 0.8 mM	20°C, anoxic conditions, pH = 3	0.35	2.0
<b><i>Effect of Dazomet concentration</i></b>			
[Dazomet] = 12 $\mu\text{M}$	Oxic conditions, measured pH = 6.3	0.22	3.2
[Dazomet] = 49 $\mu\text{M}$	Oxic conditions, measured pH = 6.3	0.23	3.0
[Dazomet] = 490 $\mu\text{M}$	Oxic conditions, measured pH = 6.3	0.21	3.4
<b><i>Effect of dissolved NaCl</i></b>			
[Na <sup>+</sup> ] = 0 mM	Oxic conditions, measured pH = 6.3	0.14	4.9

<b>Variable tested</b>	<b>Conditions</b>	<b>k (h<sup>-1</sup>)</b>	<b>Half-life (h)</b>
[Na <sup>+</sup> ] = 10 mM	Oxic conditions, measured pH = 6.3	0.14	5.1
[Na <sup>+</sup> ] = 100 mM	Oxic conditions, measured pH = 6.3	0.14	4.9

#### 4.4.5 *Catalysis due to oxidized and unoxidized pyrite*

For this experiment two distinct pyrite surfaces were tested to identify the effect of pyrite treatments. The first was oxygen exposed pyrite in oxygen-saturated water. The second was freshly cleaned (acid-washed) pyrite, in anoxic water. Both were performed at 20 g/L. The resulting degradation rates of dazomet relative to a control containing no pyrite are shown in Figure 4-6. All reactions were at 23°C. Interestingly, the clean pyrite surface has no perceptible effect on the degradation of dazomet relative to the control. However, the oxidized surface led to accelerated removal of the biocide, which degraded 5 times faster than the control. When measured using the ferrozine method, the concentrations of dissolved Fe<sup>II</sup> and Fe<sup>III</sup> in the oxidized sample were below the limit of detection, suggesting a surface reaction. To identify whether the reaction was due to the production of hydroxyl radicals ( $\bullet$ OH), 2-propanol, a hydroxyl radical scavenger was added to a separate vial containing pyrite. No significant change in the reaction rates was noted due to the addition.

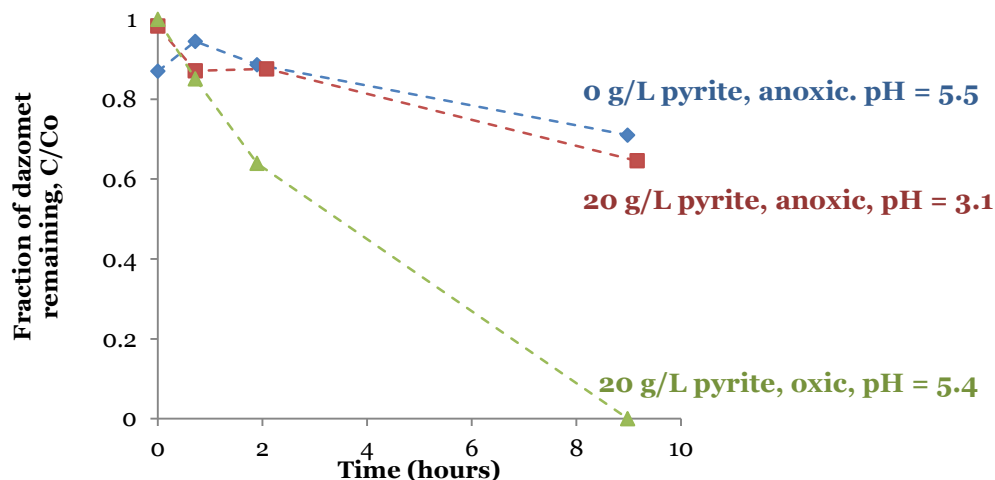


**Figure 4-6.** Fraction of dazomet remaining as a function of time (h), in aqueous suspensions of 0 g/L pyrite, 20 g/L unoxidized (acid washed) pyrite and 20 g/L of pyrite (FeS<sub>2</sub>). Reaction conditions: 23°C, using nitrogen-sparged water for the anoxic experiments and oxygen saturated water for the oxidic experiments. The initial dazomet concentration was 1mM.

#### 4.4.6 Analysis of hydrolysis products

A thorough assessment of the risks of dazomet should also consider the concentrations and behavior of the hydrolysis products. The major reaction products detected at pH 6.3, 18°C under oxidic conditions are shown in Figure 4-7. While methyl isothiocyanate (MITC) concentrations remained constant over the initial production, formaldehyde (HCHO) concentrations increase steadily over time. Small amounts of *n,n*-dimethylthiourea were also detected. These compounds account for 75% of the carbon lost from dazomet. With GC analysis, hexahydro-1,3,5-trimethyl-1,3,5-triazine-2-thione (see Figure 4-1) was detected, which is the compound observed by (Orem et al., 2014). Trace amounts of 5,6-dihydro-5-methyl-4H-1,3,5-dithiazine, trimethylthiourea and cyclic octaatomic sulfur were also detected with GC analysis. CO<sub>2</sub> and S<sup>2-</sup> levels were both below the instrument limit of detection (0.1 mg/L and 5 mg/L, respectively). With pyrite, formaldehyde, MITC and *n,n*-dimethylthiourea again emerged as the predominant products. An additional peak was found in solutions with pyrite which was

tentatively assigned as 4-methyl-5-methylimino-1,2,4-dithiazolidine-3-thione found in aged solutions (30-day hydrolysis) of dazomet (Subramanian et al., 1996).

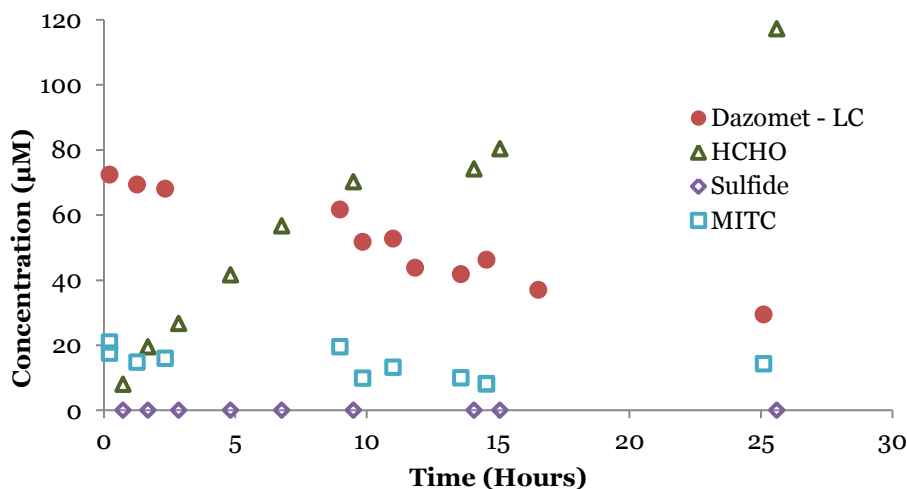


**Figure 4-7. Dazomet degradation and production of major hydrolysis products formaldehyde (HCHO), hydrogen sulfide, and methyl isothiocyanate as a function of time (h). Reaction was performed at pH 6.3, 18°C under oxic conditions. Initial dazomet concentration 80 µM.**

Table 2 reports the key physicochemical properties of these products, comparing them to those of dazomet. Toxicity values illustrate that formaldehyde and methyl isothiocyanate are significantly more toxic than the parent compound: dazomet is designed to act as a carrier for these compounds. The high vapor pressures indicate that exposure to these compounds can occur via inhalation, with both compounds causing irritation to the respiratory tract. Formaldehyde has been shown to be carcinogenic in humans resulting in cancer of the nasopharynx, nasal cavity and leukemia. It is also particularly toxic to aquatic life. Methyl isothiocyanate is a sensitizer that irritates the skin, eye and respiratory system (NIH TOXNET, 2015; NIH TOXNET, 2014). Unlike dazomet, abiotic degradation of these products is limited or very slow. Reports cite that MITC hydrolysis occurs on the order of months, formadehyde hydrolysis is unlikely as the aldehyde group is not susceptible to OH<sup>-</sup> attack. Instead, a major

elimination mechanism for formaldehyde would be its polymerization to form paraformaldehyde.

**Table 4-2. The key physicochemical properties and biodegradability of biocides used in hydraulic fracturing operations. Sources: US EPA, 2008; SciFinder 2016; NIH TOXNET, 2015; NIH TOXNET, 2014.**

Compound	Solubility (g/L)	Log P @ 25C	Vapor pressure (atm)	EC <sub>50</sub> (µg/L)	LC <sub>50</sub> (µg/L)	LD <sub>50</sub> (mg/kg)	Hydrolysis half-lives at pH 7
Dazomet	4.9	0.639	0.102	11,900	550	320	3-5 hours
Formaldehyde	198	0.350	3460	14,600	NR	100	(unlikely)
Methyl isothiocyanate	4.8	1.13	31.2	55	280	72	65 days
<i>n,n</i> -dimethyl thiourea	133	-0.285	14.5	NR	16,500	NR	NR

#### 4.5 Discussion

These results confirm that under the conditions of the Marcellus Shale, the persistence of dazomet will change when compared to its reactivity in surface water. Its half-life is strongly affected by the specific water chemistry as shown by experiments varying temperature, pH and dissolved cations content. Although direct comparisons are difficult to make due to differing reaction conditions, Figure 4-8 illustrates estimations of the relative change for temperature, pH and Fe<sup>II</sup>. The baseline for each case was taken to be the average value recorded for the shale or for produced water in Dilmore et al., 2015, Hayes, 2009 and Abualfara et al., 2014. The half-lives are approximations based on available data points from this study. Based on our data, temperature and dissolved Fe<sup>II</sup> are expected to have the greatest effect on the variability of dazomet degradation. This is due to the high sensitivity of dazomet to these variables and the wide ranges experienced in the Marcellus shale. This supports recommendations to use dazomet at low temperatures and shallower formations. It also suggests that the iron content of flowback water must be controlled when reusing produced water. It should be noted that concentrations

of Fe<sup>II</sup> as high as 10 mM have been recorded and that influence must be examined by further experimentation.

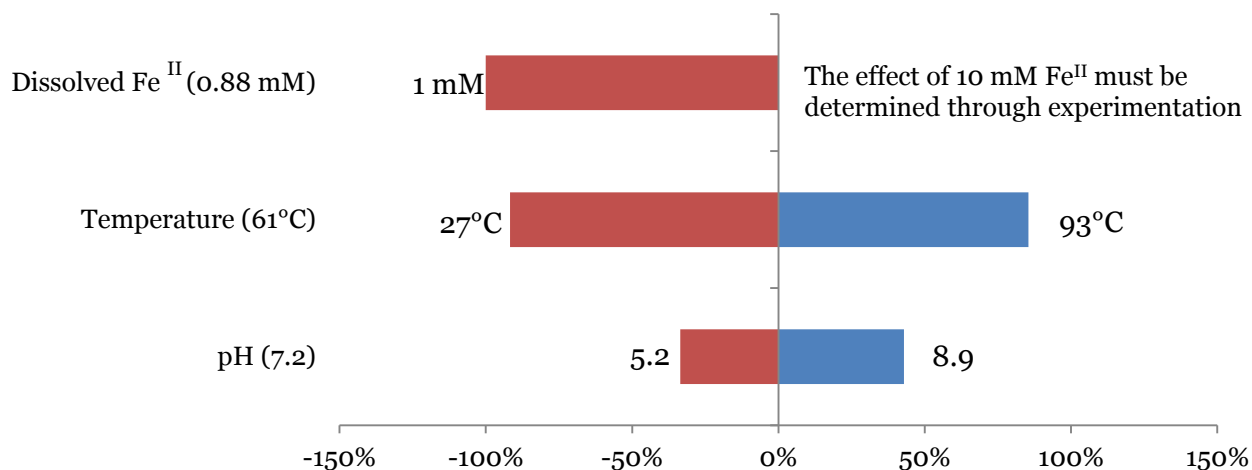


**Figure 4-8. Projected percentage decrease and increase of dazomet half-lives due to varying compositions of dissolved Fe<sup>II</sup>, temperature and pH. The median value used as the baseline is shown in parentheses, and the minimum and maximum values for each variable shown next to calculated percentages.**

The lack of acid-catalyzed hydrolysis indicates that hydrolysis occurs due to hydroxide (OH<sup>-</sup>) attack of the aminal group in dazomet, that is, the carbon atom between the two nitrogen groups. The exact half-lives of dazomet in reports vary widely, possibly due to the strong temperature dependence of dazomet or to interactions with the selected buffer. However, in general, the persistence of dazomet decreases as pH increases, Figure 4-9 (US EPA, 2008; Australian NRA, 1997; Subramanian et al., 1996). Organic compounds which degrade faster when protonated do so due to a shift in the electron density away from the central carbon atom on bonding with the proton. Although protonation of dazomet is estimated to occur between pH 4 and 6 (SciFinder, 2016; Pubchem), there is no corresponding increase in degradation. This implies that nucleophilic attack is far-removed from the likely site of protonation (at the C=S moiety) and occurs at a point surrounded by electron-withdrawing atoms. This conclusion agrees with the mechanism suggested by van der Kerk (Goksøyr et al., 1964).

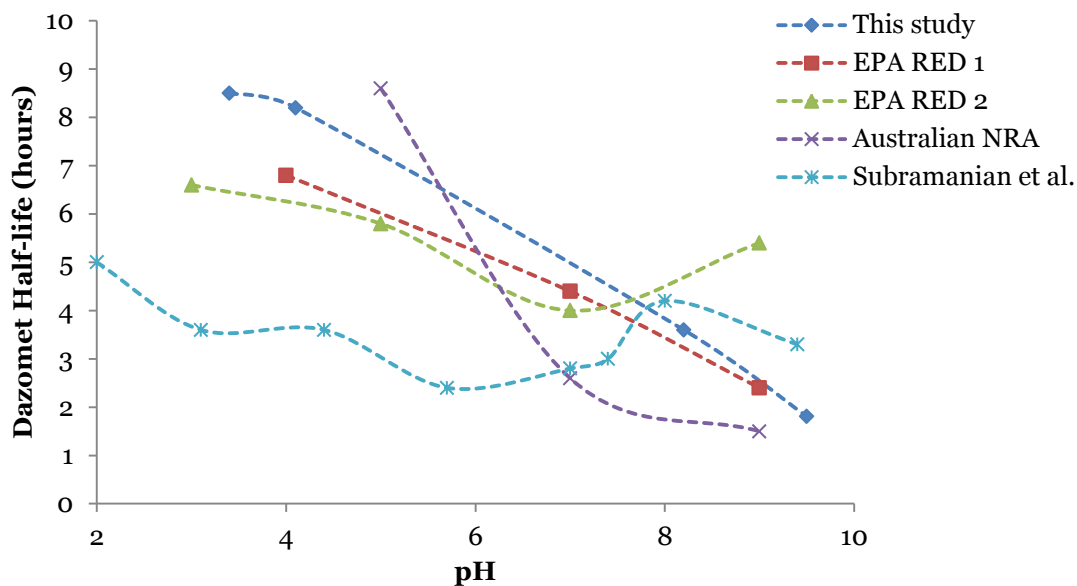
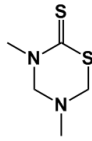
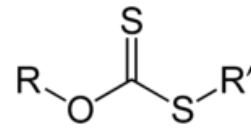


Figure 4-9. Comparison of hydrolysis half-lives determined in this study to those in previously published results as a function of pH.

On the other hand, complexation with the oxygen exposed pyrite surface does accelerate the degradation of dazomet. The evidence suggests that this is due to accelerated hydrolysis at the pyrite surface due to strong interactions with the surface. Dazomet possess structural groups that are similar to xanthate esters which are used as collectors for the flotation of pyrite, Figure 4-10 (Montalti et al., 1991). Chemisorption of xanthates occurs via the interaction of the negatively charged sulfur group with any oxidized iron-centered (sulfur-deficient) surface sites (Wang, 1995; Ahmed, 1978). This suggests that highly favorable interactions within the stern layer can occur between pyrite and the oxidized pyrite surface as well. This strong sorption is sufficient to cause a shift in the electronic distribution of the central aminal carbon atom, leaving the nucleus more prone to nucleophilic attack (Stone and Torrents, 1995, Smolen and Stone, 1997). Various studies have highlighted that pyrite can induce a Fenton-like mechanism leading to the production of  $\bullet\text{OH}$  radicals under oxic conditions (Pham et al., 2009). However, the degradation rate of dazomet due to pyrite was unaffected with the addition of 2-propanol (a  $\bullet\text{OH}$  scavenger), suggesting that this mechanism was not significant.



**Dazomet**



**Xanthate ester**

**Figure 4-10. The structure of dazomet, the Marcellus Shale biocide of interest and a generic xanthate, a common collector used for the flotation of pyrite. Both compounds display -C(=S)S groups which may lead to specific sorption between these organic compounds and the pyrite surface.**

The effect of Fe<sup>II</sup> is not as straight forward. Several hypotheses are put forward to explain the observed degradation of dazomet over time. The first is that the dissolved Fe<sup>II</sup> ions can complex with dazomet, thereby increasing its susceptibility to hydrolytic attack, much like the catalysis observed with pyrite above. Copper salts have been used as accelerants for dazomet degradation (Pope et al., 2016) and the interactions between Cu<sup>II</sup> and Fe<sup>II</sup>. However, this is debatable as the unoxidized Fe<sup>II</sup> groups of pyrite had no effect on the degradation of dazomet. The second is that Fe<sup>II</sup> can reduce dazomet, itself oxidized to Fe<sup>III</sup>. This reaction is not unlike the reduction of oxygen analogues, carbamates by Fe<sup>II</sup>, Cu<sup>I</sup>, and Cu<sup>II</sup> (Strathmann and Stone, 2001). The third is that over long periods (greater than five hours) the speciation of Fe<sup>II</sup> changes, resulting in a new, reactive iron specie. As this is the first study to present accelerated degradation of dazomet with Fe<sup>II</sup>, additional research is necessary to verify these proposed mechanisms. Additional experiments could look at the effect of the transition metals Ni<sup>II</sup>, Pb<sup>II</sup>, Zn<sup>II</sup> and Co<sup>II</sup> which possess very high complex formation constants, but no redox activity. Because produced waters rarely exhibit significant concentrations of these metal ions, they were not investigated in this study.

This work also points out that a true risk assessment of the chemicals used in hydraulic fracturing must consider any long-lived daughter compounds, as well as the parent products. While dazomet is notably toxic, it serves primarily as a vehicle for the delivery of the more

persistent fumigants: MITC and formaldehyde. As a result, the toxicity of dazomet actually increases as degradation proceeds. Despite its relatively short lifetime in aqueous solutions, dazomet can serve as a long-lasting preservative for shale formations due to the long half-lives of the daughter products. However, these compounds are also likely to be in flowback water that returns to surface, generating toxic fumes in the vicinity of produced water impoundments, particularly in warmer temperatures where vapor pressures will increase and solubility is likely to decrease. The observed reaction products agree with previous publications (Subramanian et al., 1996; Matolcsy et al., 1988; US EPA, 2008).

## 4.6 References

- Abualfaraj, N., Gurian, P.L., Olson, M.S., 2014. Characterization of Marcellus Shale Flowback Water. *Environmental Engineering Science* 31, 514–524. doi:10.1089/ees.2014.0001
- Ahmed, S.M., 1978. Electrochemical studies of sulphides, I. The electrocatalytic activity of galena, pyrite and cobalt sulphide for oxygen reduction in relation to xanthate adsorption and flotation. *International Journal of Mineral Processing* 5, 163–174. doi:10.1016/0301-7516(78)90013-3
- Analysis of Hydraulic Fracturing Fluid Data from the FracFocus Chemical Disclosure Registry (No. EPA/601/R-14/003), 2015. . U.S. Environmental Protection Agency (EPA).
- Atkins, P.W., De Paula, J., 2011. Accounting for the rate laws, in: *Physical Chemistry for the Life Sciences*. W.H. Freeman and Co. ; Oxford University Press, New York : Oxford.
- Barbot, E., Vidic, N.S., Gregory, K.B., Vidic, R.D., 2013. Spatial and Temporal Correlation of Water Quality Parameters of Produced Waters from Devonian-Age Shale following Hydraulic Fracturing. *Environmental Science & Technology* 47, 2562–2569. doi:10.1021/es304638h
- BASF, 2000. Water and oilfield biocides.
- Borda, M.J., Elsetinow, A.R., Strongin, D.R., Schoonen, M.A., 2003. A mechanism for the production of hydroxyl radical at surface defect sites on pyrite. *Geochimica et Cosmochimica Acta* 67, 935–939. doi:10.1016/S0016-7037(02)01222-X
- Carter, K.E., Hakala, J.A., Hammack, R.W., 2013. Hydraulic Fracturing and Organic Compounds – Uses, Disposal and Challenges. Presented at the SPE Eastern Regional Meeting, Society of Petroleum Engineers, Pittsburgh, PA.
- Carter, K.M., Harper, J.A., Schmid, K.W., Kostelnik, J., 2011. Unconventional natural gas resources in Pennsylvania: The backstory of the modern Marcellus Shale play. *Environmental Geosciences* 18, 217–257. doi:10.1306/eg.09281111008
- Che, H., Lee, W., 2011. Selective redox degradation of chlorinated aliphatic compounds by Fenton reaction in pyrite suspension. *Chemosphere* 82, 1103–1108. doi:10.1016/j.chemosphere.2010.12.002
- Dhanasekara, S.A.K.M., Attanayake, A.N.B., Herath, A.C., Nanayakkara, N., Senaratne, A., Indrarathne, S.P., Weerasooriya, R., 2015. Partial degradation of carbofuran by natural pyrite. *Environmental Nanotechnology, Monitoring & Management* 4, 51–57. doi:10.1016/j.enmm.2015.07.002
- Dilmore, R., Bruner, K., Wyatt, C., Romanov, V., Goodman, A., Hedges, S., McIntyre, D., Crandall, D., Gill, M., Disenhof, C., Jinesh, J., Lopano, C., Aminian, K., Zamirian, M., Mashayekhi, A., Sanguinito, S., Mroz, T., Soeder, D., 2015. Experimental Characterization of Marcellus Shale Outcrop Samples, and their Interactions with Carbon Dioxide and Methane, NETL Technical Report Series. U.S. Department of Energy, National Energy Technology Laboratory, Morgantown, WV.
- Dow Microbial Control, n.d. Selection Guide for Microbial Control Actives in Oil and Gas Operations.
- ECOTOXicology knowledgebase (ECOTOX), 2017. . Environmental Protection Agency, Duluth, MN.
- Elliott, E.G., Ettinger, A.S., Leaderer, B.P., Bracken, M.B., Deziel, N.C., 2016. A systematic evaluation of chemicals in hydraulic-fracturing fluids and wastewater for reproductive and developmental toxicity. *Journal of Exposure Science and Environmental Epidemiology*. doi:10.1038/jes.2015.81

- Facchini, M.C., Lind, J., Orsi, G., Fuzzi, S., 1990. Chemistry of carbonyl compounds in Po Valley fog water. *Science of The Total Environment* 91, 79–86. doi:10.1016/0048-9697(90)90289-7
- Fishman, M.J., Friedman, L.C. (Eds.), 1989. Methods for the Determination of Inorganic Substances in Water and Fluvial Sediments, in: Book 5, Chapter A1, Techniques of Water-Resources Investigations of the United States Geological Survey. United States Government Printing Office, Washington, DC.
- Gaspar, J., Mathieu, J., Yang, Y., Tomson, R., Leyris, J.D., Gregory, K.B., Alvarez, P.J.J., 2014. Microbial Dynamics and Control in Shale Gas Production. *Environmental Science & Technology Letters* 1, 465–473. doi:10.1021/ez5003242
- Goksøyr, J., Pilstrom, L., Johansson, L., Nihlgård, B., Nilsson, L., 1964. Chemical and Fungicidal Reactions of 3,5-Dimethyltetrahydro-1,3,5-thiadiazine-2-thione (3,5-D). A Comparison with Sodium N-Methyl Dithiocarbamate and Methyl Isothiocyanate. *Acta Chemica Scandinavica* 18, 1341–1352. doi:10.3891/acta.chem.scand.18-1341
- Hayes, T., 2009. Sampling and Analysis of Water Streams Associated with the Development of Marcellus Shale Gas. Gas Technology Institute, Des Plaines, IL.
- Hazardous Substances Data Bank: Formaldehyde (Hazardous Substances Databank Number: 164), 2015. . National Institute of Health (NIH) Toxicology Data Network (TOXNET).
- Hazardous Substances Data Bank: Methyl Isothiocyanate (Hazardous Substances Databank Number: 6396), 2014. . National Institute of Health (NIH) Toxicology Data Network (TOXNET).
- Jain, P., Sharma, M., Dureja, P., Sarma, P.M., Lal, B., 2017. Bioelectrochemical approaches for removal of sulfate, hydrocarbon and salinity from produced water. *Chemosphere* 166, 96–108. doi:10.1016/j.chemosphere.2016.09.081
- Kahrilas, G.A., Blotvogel, J., Stewart, P.S., Borch, T., 2015. Biocides in Hydraulic Fracturing Fluids: A Critical Review of Their Usage, Mobility, Degradation, and Toxicity. *Environmental Science & Technology* 49, 16–32. doi:10.1021/es503724k
- King, G.E., 2012. Hydraulic Fracturing 101: What Every Representative, Environmentalist, Regulator, Reporter, Investor, University Researcher, Neighbor, and Engineer Should Know About Hydraulic Fracturing Risk. Presented at the SPE Hydraulic Fracturing Technology Conference, Society of Petroleum Engineers, The Woodlands, TX, pp. 34–42.
- Lash, G.G., Blood, D.R., 2014. Organic matter accumulation, redox, and diagenetic history of the Marcellus Formation, southwestern Pennsylvania, Appalachian basin. *Marine and Petroleum Geology* 57, 244–263. doi:10.1016/j.marpetgeo.2014.06.001
- Lee, W., Batchelor, B., 2002. Abiotic Reductive Dechlorination of Chlorinated Ethylenes by Iron-Bearing Soil Minerals. 1. Pyrite and Magnetite. *Environmental Science & Technology* 36, 5147–5154. doi:10.1021/es025836b
- Liu, R., Wolfe, A.L., Dzombak, D.A., Horwitz, C.P., Stewart, B.W., Capo, R.C., 2008a. Electrochemical study of hydrothermal and sedimentary pyrite dissolution. *Applied Geochemistry* 23, 2724–2734. doi:10.1016/j.apgeochem.2008.06.005
- Liu, R., Wolfe, A.L., Dzombak, D.A., Stewart, B.W., Capo, R.C., 2008b. Comparison of dissolution under oxic acid drainage conditions for eight sedimentary and hydrothermal pyrite samples. *Environmental Geology* 56, 171–182. doi:10.1007/s00254-007-1149-0
- Luther, G.W., 1987. Pyrite oxidation and reduction: Molecular orbital theory considerations. *Geochimica et Cosmochimica Acta* 51, 3193–3199. doi:10.1016/0016-7037(87)90127-X
- Matolcsy, G., Nádasy, M., Andriska, V., Terényi, S., 1988. Dithiocarbamate acid derivatives, in: *Pesticide Chemistry, Studies in Environmental Science*. Elsevier ; Elsevier Science Pub. Co. [distributor], Amsterdam ; New York : New York, N.Y., USA.

- Montalti, M., Fornasiero, D., Ralston, J., 1991. Ultraviolet-visible spectroscopic study of the kinetics of adsorption of ethyl xanthate on pyrite. *Journal of Colloid and Interface Science* 143, 440–450. doi:10.1016/0021-9797(91)90278-G
- NRA special review of metham sodium, dazomet and methylisothiocyanate (MITC) Volume III, 1997. . Australian National Registration Authority for Agricultural and Veterinary Chemicals, Canberra, Australia.
- Orem, W., Tatu, C., Varonka, M., Lerch, H., Bates, A., Engle, M., Crosby, L., McIntosh, J., 2014. Organic substances in produced and formation water from unconventional natural gas extraction in coal and shale. *International Journal of Coal Geology* 126, 20–31. doi:10.1016/j.coal.2014.01.003
- Paschka, M.G., Dzombak, D.A., 2004. Use of Dissolved Sulfur Species to Measure Pyrite Dissolution in Water at pH 3 and 6. *Environmental Engineering Science* 21, 411–420. doi:10.1089/1092875041358502
- Pham, H.T., Suto, K., Inoue, C., 2009. Trichloroethylene Transformation in Aerobic Pyrite Suspension: Pathways and Kinetic Modeling. *Environmental Science & Technology* 43, 6744–6749. doi:10.1021/es900623u
- Pope, T., Herdman, D.J., Tham, P., 2016. Dazomet compositions. Reregistration Eligibility Decision for Dazomet (No. EPA 738-R-08-007), 2008. . U.S. Environmental Protection Agency, Washington, DC.
- Roberts, T.R., Hutson, D.H. (Eds.), 1999. Fungicides, in: *Metabolic Pathways of Agrochemicals*. Royal Society of Chemistry, Cambridge, pp. 937–960.
- Rogers, J.D., Burke, T.L., Osborn, S.G., Ryan, J.N., 2015. A Framework for Identifying Organic Compounds of Concern in Hydraulic Fracturing Fluids Based on Their Mobility and Persistence in Groundwater. *Environmental Science & Technology Letters* 2, 158–164. doi:10.1021/acs.estlett.5b00090
- Rowan, E., Engle, M.A., Kirby, C.S., Kraemer, T.F., 2011. Radium content of oil-and gas-field produced waters in the northern Appalachian Basin (USA)—Summary and discussion of data. US Geological Survey Scientific Investigations Report 5135, 2011.
- Schwarzenbach, R.P., Gschwend, P.M., Imboden, D.M., 2003. *Environmental organic chemistry*, 2. ed. ed. Wiley, New York.
- Scifinder, 2016. . Chemical Abstracts Service, Columbus, OH.
- Smolen, J.M., Stone, A.T., 1997. Divalent Metal Ion-Catalyzed Hydrolysis of Phosphorothionate Ester Pesticides and Their Corresponding Oxonates. *Environmental Science & Technology* 31, 1664–1673. doi:10.1021/es960499q
- Stone, A.T., Torrents, A., 1995. The role of dissolved metals and metal-containing surfaces in catalyzing the hydrolysis of organic pollutants, in: Huang, P.M. (Ed.), *Environmental Impact of Soil Component Interactions*. Lewis Publishers, Boca Raton.
- Strathmann, T.J., Stone, A.T., 2001. Reduction of the Carbamate Pesticides Oxamyl and Methomyl by Dissolved Fe II and Cu I. *Environmental Science & Technology* 35, 2461–2469. doi:10.1021/es001824j
- Subramanian, P., Teesch, L., Thorne, P.S., 1996. Degradation of 3,5-dimethyl-tetrahydro-2H-1,3,5-thiadiazine-2-thione in aqueous aerobic media. *Environmental Toxicology and Chemistry* 15, 503–513. doi:10.1002/etc.5620150415
- Tilton, F., Ladu, J., Vue, M., Alzarban, N., Tanguay, R., 2006. Dithiocarbamates have a common toxic effect on zebrafish body axis formation. *Toxicology and Applied Pharmacology* 216, 55–68. doi:10.1016/j.taap.2006.04.014
- Vengosh, A., Jackson, R.B., Warner, N., Darrah, T.H., Kondash, A., 2014. A Critical Review of the Risks to Water Resources from Unconventional Shale Gas Development and Hydraulic Fracturing in the United States. *Environmental Science & Technology* 48, 8334–8348. doi:10.1021/es405118y

- Viollier, E., Inglett, P., Hunter, K., Roychoudhury, A., Van Cappellen, P., 2000. The ferrozine method revisited: Fe(II)/Fe(III) determination in natural waters. *Applied Geochemistry* 15, 785–790. doi:10.1016/S0883-2927(99)00097-9
- Wang, W., Qu, Y., Yang, B., Liu, X., Su, W., 2012. Lactate oxidation in pyrite suspension: A Fenton-like process in situ generating H<sub>2</sub>O<sub>2</sub>. *Chemosphere* 86, 376–382. doi:10.1016/j.chemosphere.2011.10.026
- Wolfe, A.L., Liu, R., Stewart, B.W., Capo, R.C., Dzombak, D.A., 2007. A method for generating uniform size-segregated pyrite particle fractions. *Geochemical Transactions* 8, 9. doi:10.1186/1467-4866-8-9
- Zhang, H., Xiong, Z., Ji, F., Lai, B., Yang, P., 2017. Pretreatment of shale gas drilling flowback fluid (SGDF) by the microscale Fe<sub>0</sub>/persulfate/O<sub>3</sub> process (mFe<sub>0</sub>/PS/O<sub>3</sub>). *Chemosphere* 176, 192–201. doi:10.1016/j.chemosphere.2017.02.122
- Zhang, Y., Zhang, K., Dai, C., Zhou, X., 2014. Performance and mechanism of pyrite for nitrobenzene removal in aqueous solution. *Chemical Engineering Science* 111, 135–141. doi:10.1016/j.ces.2014.02.029

**Chapter 5      Pyrite-induced reduction of four hydraulic  
fracturing biocides: the effect of selected functional  
groups on reactivity**

## 5.1 Abstract

Although pyrite has been shown to reduce organic compounds, there is a need to investigate how this mineral may affect the fate of the different classes of biocides used in hydraulic fracturing. This work investigates the hydrolysis of a subset of the biocides and their reduction by pyrite: 1,2-dibromo-2,4-dicyanobutane (DBDCB), methylene bis(thiocyanate) (MBT), methylisothiazolinone (MIT) and benzisothiazolinone (BIT). The goal is to explore the mechanism of degradation of specific functional groups found in biocide compounds. Although considered stable against hydrolysis at low pH, DBDCB and MBT degraded over the course of the experiment at pH = 2.7, with half-lives estimated at 39 day and 24 days, respectively. This was due to the presence of hydrolysable bromo (-Br) and thiocyanate (-SCN) functional groups. The isothiazolinones MIT and BIT showed no significant degradation under the same conditions. This was attributed to the stabilizing effect of the carbonyl (-C=O) group. Significant reduction due to the addition of pyrite was only observed with DBDCB: The approximate surface area-normalized rate constant was calculated to be  $7 \times 10^{-3} \text{ Lm}^{-2}\text{day}^{-1}$ . The resulting product was the debrominated compound 2-methyleneglutaronitrile. This is due to the ease of reducing bromo groups (standard redox potential for the  $\text{Br}_{2(g)}-2\text{Br}^-$  couple,  $E^\circ = 1.1 \text{ V}$ ). The results show that by investigating the reactivity of specific functional groups, we can gain insight into the reactivity of the different classes of biocides used by the industry.

## 5.2 Introduction

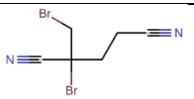
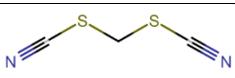
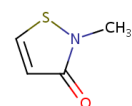
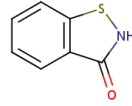
Several studies have demonstrated that pyrite can reduce organic compounds, and this may affect the fate of biocides used in hydraulic fracturing. Theoretical examinations demonstrate that pyrite can donate electrons to organic compounds (Luther, 1987). Laboratory results confirm this hypothesis, showing that chlorinated compounds (Lee and Batchelor, 2002; Kriegman-King and Reinhard, 1994) and nitro-containing compounds (Oh et al., 2008) can be reduced by natural pyrite. Much of this work was motivated by the need to identify abiotic methods to transform these contaminants into less toxic compounds in the subsurface environment. These results suggest that pyrite may also undergo redox reactions with some organic biocides used in hydraulic fracturing and likely decrease the persistence of these biocides.

However, unlike the organic compounds represented in literature, the biocides used in hydraulic fracturing span a wider range of functional groups. In fact, few of the biocides possess chlorinated or nitro groups. Because of the dearth of information, there is a need to experimentally determine how the reactivity of organic compounds will change on addition of pyrite. The outcome will inform our knowledge of the behavior of biocides in hydraulic fracturing, and contribute fundamental knowledge to our understanding of the reactivity of pyrite with other classes of organic compounds, as well.

To understand the reactivity of these biocides with pyrite, four biocides were selected from the 22 organic biocides used in hydraulic fracturing fluids: 1,2-dibromo-2,4-dicyanobutane (DBDCB), methylene bis(thiocyanate) (MBT), methylisothiazolinone (MIT) and benzisothiazolinone (BIT). The structures and key physicochemical properties are in Table 5-1 below. A primary feature of this group of biocides is that they are expected to be stable against

hydrolysis at low pH. As pyrite dissolves to produce H<sup>+</sup> ions, little to no reactivity under acidic conditions will make it simpler to identify the effect of pyrite on the reactivity of each biocide.

**Table 5-1. The abbreviation, structural and physical properties of biocides selected for this chapter. Note: log P is the logarithm of the partitioning between octanol and water as modeled by SciFinder (2016) and LD<sub>50</sub> is the median lethal dose as cited in EPA reregistration eligibility decision for the respective biocide (US EPA, 1995; US EPA, 1996; US EPA, 1997; US EPA, 1998).**

Biocide	DBDCB	MBT	MIT	BIT
Structure				
MW (g/mol)	256.93	130.19	115.15	151.19
Solubility (g/L)	0.82	23	24	0.56
Log P	1.515	0.630	0.119	1.953
pK <sub>a</sub> (basic)	none	none	-2.03	-1.97
LD <sub>50</sub> (mg/kg) rat, oral	643	77	105	727

This small sample of biocides captures many of the important physicochemical properties and functional groups found in the wider class. Their solubilities range from moderate to highly soluble (0.56 g/L to 24 g/L). All of these biocides are considered neutral biocides under the conditions of hydraulic fracturing, although some small percentage ( $\approx 0.01\%$ ) of MIT and BIT is expected to be protonated at pH 2, which allows for detection with liquid chromatography-mass spectrometry. Some of the most common functional groups and structures are represented, among them the heterocyclic ring, bromo groups (-Br), and carbonyl groups (-C=O).

All of these biocides are all preservatives that protect vital organic compounds in fracking fluid from undergoing microbial degradation. They fall into category II and III for oral acute toxicity, as they cause harm and possibly death if swallowed. In humans, DBDCB, MIT and BIT can cause sensitization to individuals who are repeatedly exposed to these compounds (Wilkinson et al., 2002; Jensen et al., 2004). Data also suggest that MIT may be a neurotoxin and cytotoxin, even at low concentrations (He et al., 2006). However, the primary health

concern for these biocides is to fish and invertebrates in receiving waters as they range from highly toxic to moderately toxic to these organisms (US EPA, 1995; US EPA, 1996; US EPA, 1997; US EPA, 1998).

Although EPA risk assessments suggest that these biocides are stable to hydrolysis for many days under low to neutral pH, multiple elimination mechanisms exist in the environment. For example, although MBT is expected to remain unaltered in aqueous solutions for over 30 days at pH 5, under alkaline conditions (pH 9) it hydrolyzes with a half-life of 2.2 hours producing thiocyanate ions,  $-\text{[SCN]}^-$  (US EPA, 1997). DBDCB is rapidly debrominated in soils and on fruit, with half-lives ranging from 4 to 8 days. The major product identified was 2-methyleneglutaronitrile, but the mechanism of degradation is not clear (Liu et al., 2014). The biocides MIT and BIT are often used as preservatives in paint and consequently, they can leach from buildings and enter the surrounding soils. Measurements of the biocides from building facades show that MIT and BIT are degraded in soils with half-lives of less than 1 day. The degradation products were not identified (Bollmann et al., 2017). Although these studies offer some insight into the persistence of these biocides under surface conditions, none of them have explicitly explored whether abiotic reduction of these compounds by natural minerals can play a role in their elimination.

The objective of this chapter is to identify the reactivity of various biocide functional groups due to the addition of pyrite. To do this, the four selected biocides will be added to identical solutions of pyrite. The task is then to determine the mechanism of degradation for these specific biocides at the pyrite-fluid interface, in particular distinguishing between two elimination mechanisms: hydrolysis and reduction. From this work, the reactivity of specific functional groups can be explored which can be extended to other biocides used in hydraulic fracturing as well.

## 5.3 Methods and Materials

### 5.3.1 Materials

The chemicals used in this study were dibromodicyanobutane (analytical standard grade, Aldrich), methylene bis(thiocyanate) (98%, AK Scientific), benzisothiazolinone (97%, Alfa Chemistry), methyl isothiazolinone (95%, AK Scientific), methanol (98%, BDH Chemicals), ethanol (200 proof ACS/USP grade, Pharmoco-Aaper), acetonitrile (99.8% EMD), hydrochloric acid (36.5 - 38%, BDH), formic acid (96+%, Alfa Aesar), acetone (99.5%, EM Science). All chemicals were used as received. Research grade pyrite (Zacatecas, Mexico) was obtained from Wards chemical. Methanol stock solutions of organics were prepared and the reaction initiated within a day. Water was obtained from a Barnstead 18.1 M $\Omega$  water system and oxygen was removed for anoxic experiments by purging with N<sub>2</sub>.

### 5.3.2 Preparation of pyrite

Large pyrite aggregates greater than 10 mm in diameter were first crushed by using a ceramic mortar and pestle, then further size-reduced with an 8530 Shatterbox. The fraction between 20 and 38  $\mu$ m was retained by wet-sieving in 70% ethanol (Wolfe et al. 2007). The surface was then cleaned to dissolve iron oxide layer that forms on the pyrite surface due to prolonged exposure to air. This was done by the rinsing in boiling acid, followed by deionized water and then acetone (Paschka and Dzombak, 2004). The acetone was removed by placing the pyrite in 105°C oven for 5 mins. This method resulted in minimal oxidation of the surface. The pyrite was cooled and stored under vacuum. Sedimentary pyrite was not available during the period of this study. Hydrothermal pyrite is a suitable proxy for probing the fundamental degradation mechanisms as in this study (Liu et al., 2008a) However, as sedimentary pyrite is

often more varied in chemistry than the hydrothermal variety, additional experiments may be needed to accurately translate these results to shale formations (Liu et al., 2008b).

### 5.3.3 *Batch experiments*

Batch experiments were performed in amber vials (50 mL) sealed with polypropylene screw caps fitted with polytetrafluoroethylene (PTFE) and silicone septa. All the experiments were anoxic, set up and sampled in a glove box under nitrogen atmosphere with 2% hydrogen. Exactly 4.5 g of pyrite was added to each vial resulting in a 100 g/L solution of pyrite to investigate the reductive effect of the mineral. Each experiment was initiated by adding a known amount of biocide stock solution to each vial, yielding a final concentration of about 1 mM. Solutions involving pyrite were then placed on an end-over-end tumbler to ensure adequate mixing. Samples investigating the effect of acidic conditions were performed by adding 0.1% formic acid to pyrite-free solutions, resulting in pH 2.7 for each sample. Aliquots were taken from each batch reactor, placing 0.5 mL of the filtered solutions of MBT, MIT and BIT into autosampler filter vials and immediately analyzed over the course of 10 to 15 days. For DBDCB, 2 mL of each solution was removed and prepared for liquid-liquid extraction. The pH of each of these solutions was taken at the end of each experiment.

### 5.3.4 *Analysis of dibromodicyanobutane.*

The analytical procedure was adapted from Pellegrini, et al. (2011). Dibromocyanobutane was extracted from aqueous samples into equal volumes of ethyl acetate. Analysis of the organic portion was then performed with an Agilent GCMS system (7890B/5977A G), equipped with an HP5-MS column (30 m x 0.25 mm x 0.25  $\mu$ m). Exactly 1  $\mu$ L was injected in splitless mode at 250°C. The carrier gas was ultra-high purity helium at 1 mL/min, constant flow. The oven was held at 80°C for 1 minute and then ramped up to 290°C

at 10°C/min. The MS transfer line, quadrupole and source temperatures were set to 280°C, 150°C and 230°C, respectively. Mass spectroscopy was done in scan mode ( $m/z$  40 – 350). It was discovered that for solutions of over 1 mM, three peaks were identified for dibromocyanobutane. This is likely due to dimerization of triple bonds to 5,6,6-tribromo-5-(bromomethyl)-3,4,5,6-tetrahydro-2-pyridinamine, under the high temperatures of the GC, as suggested by Fritz et al. (1976). Thus, the sum of these three peaks were used for calibration instead of the peak suggested by Pellegrini, et al. (2011) This greatly improved the calibration fit from,  $R^2 = 0.967$  to  $R^2 = 0.993$ .

#### 5.3.5 Analysis of methylene bis(thiocyanate)

The analysis of methylene bis(thiocyanate) was performed by direct injection of the filtered sample into an Agilent 1100 HPLC, equipped with Zorbax Eclipse C18 column (4.6 x 150 mm, 5  $\mu$ m) and a variable wavelength detector. Isocratic separation was performed with 15% acetonitrile and water, both acidified with 0.1 vol% formic acid at a flowrate of 1 mL/min. The column temperature was 30°C. Detection was done at 252 nm (Borisova-Jan et al., 2011).

#### 5.3.6 Analysis of benzisothiazolinone and methyl isothiazolinone

This analytical procedure was adapted from Wittenberg et al., 2015 and Alvarez-Rivera et al., 2012. The isothiazolinones were analyzed with an Agilent 1100 liquid chromatograph and Agilent 6430 tandem mass spectrometer (LC-MS/MS). The separation was done on the Zorbax Eclipse C18 column (4.6 x 150 mm, 5  $\mu$ m) at a flowrate of 0.5 mL/min. A gradient of water acidified with 0.1 vol% formic acid (A) and methanol (B) was used, starting at 30% B for 4 minutes, ramped up to 90% B for 2 minutes. The injection volume was 5  $\mu$ L and the column temperature was 30°C. Detection was also done with the UV-visible detector, set to 274 nm. The mass spectrometer was operated in multiple reaction monitoring (MRM) mode, using the

product ions and collision energies as mentioned in Alvarez-Rivera et al. (2012). The mass spectrometer source parameters were the following: gas temperature of 250°C; 10 L/min N<sub>2</sub> gas flow at 60 psi; capillary voltage at 3000 V. Of the two detection methods, UV-visible spectrometry was determined to be more precise.

## 5.4 Results

### 5.4.1 Degradation of DBDCB

The degradation rate of DBDCB under anoxic conditions was shown to be affected by pH. Previous studies found that DBDCB hydrolyzes rapidly under alkaline conditions (US EPA, 1996). The reported half-life decreased from 190 days at pH 5 to 13 days at pH 9. In Figure 5-1, DBDCB degradation was imperceptible at pH 5.1, confirming that the biocide is relatively stable in water at this pH. This work also shows that DBDCB degradation rates increase as the pH was lowered to 2.7 (without pyrite). Because less than 30% of the DBDCB reacted over the course of the experiment, only a rough approximate of the half-life could be obtained. Assuming pseudo-first order degradation rate with respect to DBDCB ( $R^2 = 0.93$ ), the half-life time was estimated at 39 days.

The addition of pyrite resulted in an increase in the degradation of DBDCB as indicated in Figure 5-1. In a solution of 100 g/L pyrite, with a final pH of 2.1, the half-life time of DBDCB is approximately an order of magnitude faster. The half-life was estimated at 4 to 5 days (assuming pseudo-first order degradation rates with respect to DBDCB,  $R^2 = 0.97$ ). Assuming a pyrite surface area of 0.2 m<sup>2</sup>/g (Pham et al., 2008), the approximate surface area-normalized rate constant was calculated to be  $7 \times 10^{-3}$  Lm<sup>-2</sup>day<sup>-1</sup>. This is two orders of magnitude slower than measured in this work for 2,2-dibromo-3-nitrilopropionamide (DBNPA) but two orders of magnitude faster than measured for chlorinated ethenes by Lee and Batchelor (2002).

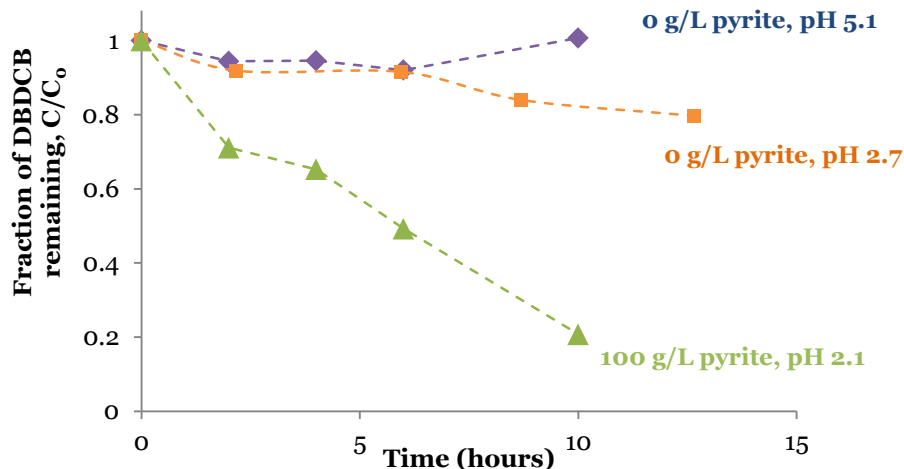
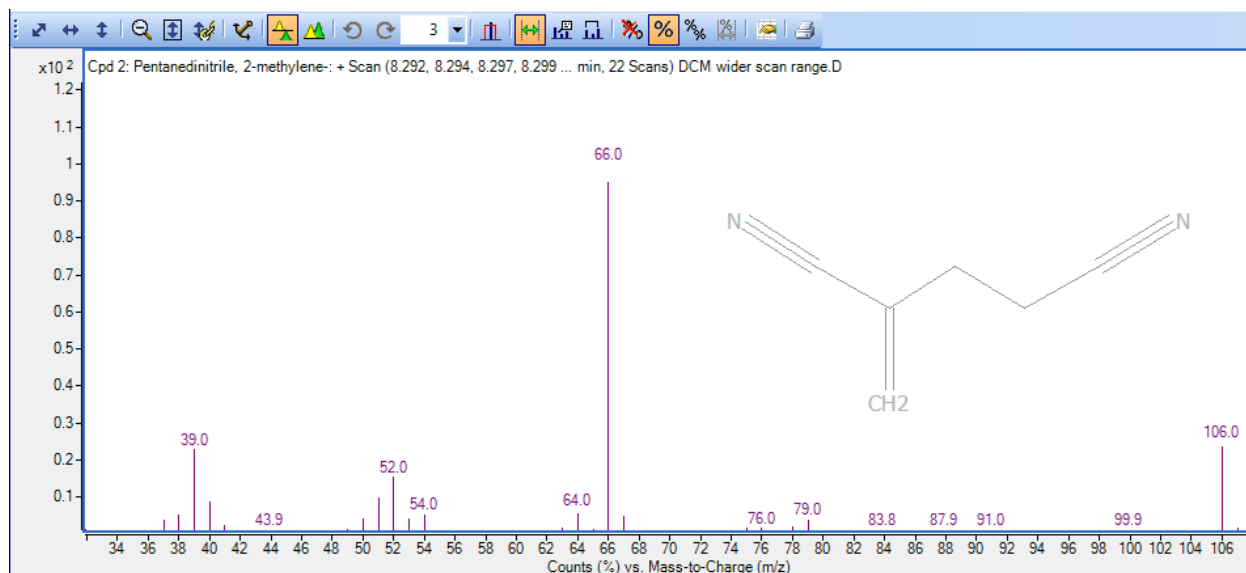


Figure 5-1. Fraction of DBDCB remaining as a function of time (h), in aqueous suspensions of 0 g/L, 5 g/L, 10 g/L and 15 g/L of pyrite (FeS<sub>2</sub>). The experiment was performed in nitrogen-sparged water, with an initial DBDCB concentration of 0.4 mM. The hydrolysis (no pyrite) experiments were performed at pH 5.1 and 2.7. The final pH was measured at 2.1 for the solution with pyrite

The debrominated product, 2-methyleneglutaronitrile (or 2-methylenepentanedinitrile) was identified by GCMS analysis and HPLC-MS analysis. As no standard was available, the MS electron ionization (EI) spectra (Figure 5-2) was matched to spectra from the NIST Mass Spectrometry Data Center (2017). The molecular ion (M<sup>+</sup>) peak of m/z 106 corresponds to the monoisotopic mass of 2-methyleneglutaronitrile (106.053 g/mol). The base peak, m/z of 66 is due to loss of CN<sub>2</sub> (Pellegrini et al., 2011). The aqueous extract was also injected into the HPLC with mass spectroscopy in scan mode. This is considered a “soft” ionization technique so there is little fragmentation of the molecular ion. Three separate compounds were identified, and one possesses a molecular weight of 106 g/mol, also corresponding to 2-methyleneglutaronitrile. The other two yet unidentified products had molecular weights of 99.9 g/mol and 148.0 g/mol. Simple analytical techniques also confirm that Br<sup>-</sup> was released from the solution containing pyrite. The addition of AgNO<sub>3</sub> led to the precipitation of a white precipitate, which was soluble in a strong base. This was likely AgBr<sub>(s)</sub>, formed from free Br<sup>-</sup> ions released due to reduction of DBDCB on exposure to pyrite.



**Figure 5-2. EI-MS spectrum of the main product of DBDCB, 2-methyleneglutaronitrile (or 2-methylenepentanedinitrile). The structural formula of 2-methyleneglutaronitrile is also illustrated.**

The results suggest that the debromination of DBDCB is accelerated by pyrite. The nitrile group ( $\text{-C}\equiv\text{N}$ ), however, seems to be unaffected by the presence of pyrite. Nitriles are not easily reduced (Rao and Hoz, 2012). Therefore, on transferring electrons to the DBDCB, the bromo functionality is the most likely group to be lost.

#### 5.4.2 Degradation of MBT

The degradation of MBT under anoxic conditions is unaffected by the addition of pyrite, but hydrolysis is expected to be a significant elimination mechanism for this biocide at low pH. Although cited as being stable at low pH, the results show that hydrolysis is significant under acidic conditions, with a half-life of about 24 days. The hydrolysis product that evolved under these conditions is expected to be the same as that reported at higher pH: thiocyanate ions,  $[\text{SCN}]^-$ . Negligible degradation was observed due to the addition of pyrite, as reduction of the thiocyanate group is particularly difficult, requiring strong reducing agents such as nitrogenase (Rasche and Seefeldt, 1997). Thus, MBT is unlikely to be reduced by pyrite.

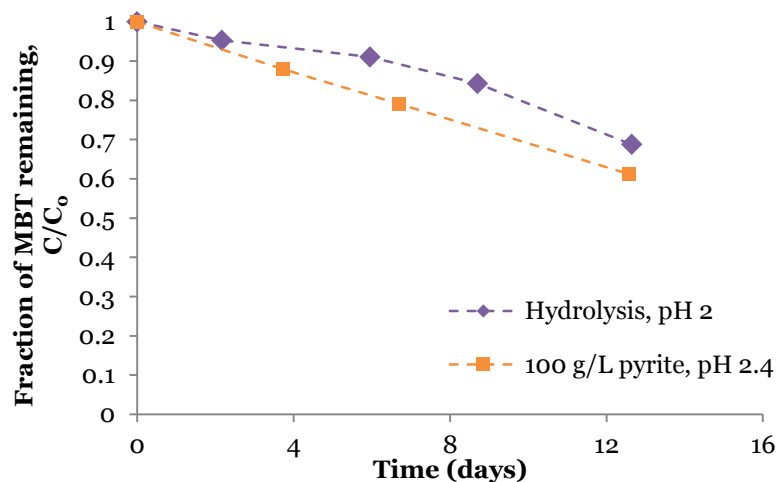


Figure 5-3. Fraction of MBT remaining as a function of time (h), in aqueous suspensions of 0 g/L and 100 g/L of pyrite ( $\text{FeS}_2$ ). The experiment was performed in nitrogen-sparged water, with an initial MTC concentration of 0.9 mM. The hydrolysis (no pyrite) experiments were performed at pH 2.7. The final pH was measured between 2.5 and 2.9 for pyrite solutions and 2.4 for the solution with pyrite.

#### 5.4.3 Degradation of the isothiazoliones: BIT and MIT

Pyrite has very little effect on the degradation of the isothiazolinones under anoxic conditions, Figure 5-4. Of the four biocides studied, MIT and BIT were the most stable at low pH, with negligible hydrolysis at any pH (Krzeminski et al., 1975; Park and Kwon, 2016). This agrees with data showing that BIT is stable under reducing conditions (Gillatt, 1997).

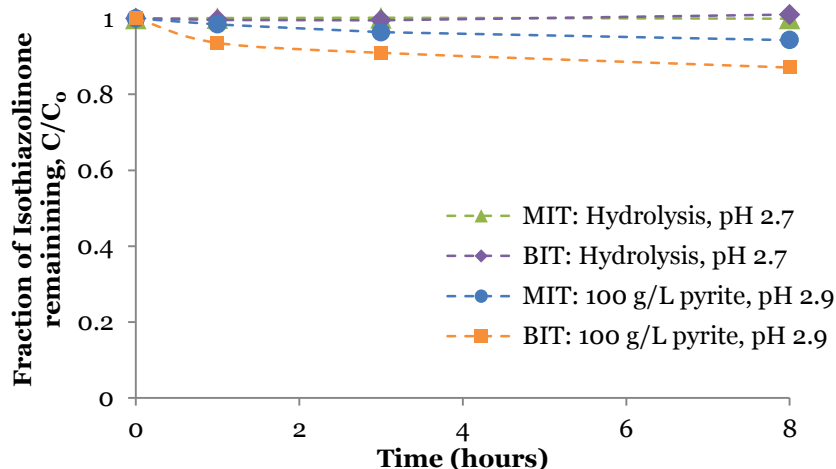


Figure 5-4. Fraction of MIT and BIT remaining as a function of time (h), in aqueous suspensions of 0 g/L and 100 g/L of pyrite ( $\text{FeS}_2$ ). The experiment was performed in nitrogen-sparged water, with initial MIT and BIT concentrations of 0.9 mM. The hydrolysis (no pyrite) experiments were performed at pH 2.7. The final pH was measured between 2.5 and 2.9 for pyrite solutions and 2.4 for the solution with pyrite.

## 5.5 Discussion

The biocides used in hydraulic fracturing undergo various elimination mechanisms in aqueous solutions. While the environmental fate of these biocides has been studied under ambient surface conditions, their behavior under the specific conditions of the Marcellus Shale is largely unknown. Although it is possible to run experiments on each biocide, a fundamental understanding of the reactivity of the relevant functional groups will be more useful, as this will allow for quantitative prediction of reactivity, and save on costly laboratory experiments. In this chapter we investigated the hydrolysis of selected biocides and their reduction by pyrite, with a focus on the effect of each elimination process on specific functional groups.

Even at low pH, the hydrolysis of many biocides may be significant. As pH increases, the hydrolysis rate of many organic compounds also increases. This is due to more hydroxyl groups available for nucleophilic attack. In this work, the rate of hydrolysis at a given pH depends on whether the biocide possesses a good leaving group, that is, an anion that is stable in aqueous solutions. A good quantitative proxy for this is the acid dissociation constant or  $\text{pK}_a$ . As shown in

Table 5-2, HBr and HSCN possess fairly low  $pK_a$ , making the conjugate bases  $-Br$  and  $-SCN$  good leaving groups. As a result, biocides with these functional groups are likely to hydrolyze in water. However HCN has a very high  $pK_a$  making  $-CN$  a poor leaving group. This functional group is therefore less likely to hydrolyze in water. The implication is that biocides with functional groups that are good leaving groups will experience hydrolysis, particularly at high pH. Likewise, the stability of the isothiazolinones stems from a very specific functional group. Donor-acceptor interactions between the carbonyl group ( $-C=O$ ) and metal cations included in the formula are responsible for the stability of these ringed structures (Krzeminski, et al., 1975).

**Table 5-2. The functional groups of DBDCB and MBT, and the acid dissociation constant ( $pK_a$ ) of the conjugate acids.**

Biocide	Functional groups	$pK_a$ of conjugate acid
DBDCB	-Br	-9.0
	-CN	9.4
MBT	-SCN	4.0

Of the biocides investigated, significant reduction was only noted for DBDCB with pyrite under anoxic conditions. The other biocides showed little to no reduction in the presence of pyrite. The ease of reduction of any functional group can be quantified by its redox potential. Here, the redox potential of the dimeric species is a good proxy for the redox potential of the relevant functional group. Table 5-3 illustrates that the reduction of the  $-Br$  groups in DBDCB is the more thermodynamically favorable under standard condition than the  $-CN$  in the same compound and of  $-SCN$  in MBT. Likewise other biocides containing  $-Br$  or  $-Cl$  groups are likely to be reduced as well (standard redox potential for the  $Cl_2(g)-2Cl^-$  couple,  $E^\circ = 1.36 V$ ).

**Table 5-3. The functional groups of DBDCB and MBT, and the standard redox potential for the corresponding dimer.**

Biocide	Half-life in water (days)	Half-life in pyrite solutions (days)	Functional groups	Standard Reduction Half Equation	$E^\circ$ (V)
DBDCB	39	4.5	-Br	$Br_2 + 2e^- = 2 Br^-$	+1.1
			-CN	$(CN)_2 + 2e^- = 2 CN^-$	+0.373
MBT	24	24	-SCN	$(SCN)_2 + 2e^- = 2 (SCN)^-$	+0.77

This work investigated the hydrolysis and reduction by pyrite of several functional groups: -Br, -CN, -SCN, and the isothiazolinone heterocyclic ring. The results show that by investigating the reactivity of specific functional groups, we can gain insight into rate limiting factors affecting the reactivity of these and other biocide compounds. Based on these results, future research can focus on testing the reduction of a homologous series of organic compounds with pyrite. By isolating the effect of the rate limiting step (that is, keeping the leaving group the same), experiments can further increase the understanding of fundamental mineral interactions with biocides and their degradation mechanisms.

## 5.6 References

- Alvarez-Rivera, G., Dagnac, T., Lores, M., Garcia-Jares, C., Sanchez-Prado, L., Lamas, J.P., Llompert, M., 2012. Determination of isothiazolinone preservatives in cosmetics and household products by matrix solid-phase dispersion followed by high-performance liquid chromatography–tandem mass spectrometry. *Journal of Chromatography A* 1270, 41–50. doi:10.1016/j.chroma.2012.10.063
- Bollmann, U.E., Fernández-Calviño, D., Brandt, K.K., Storgaard, M.S., Sanderson, H., Bester, K., 2017. Biocide Runoff from Building Facades: Degradation Kinetics in Soil. *Environmental Science & Technology* 51, 3694–3702. doi:10.1021/acs.est.6b05512
- Borisova-Jan, L., Jönsson, S., Fransson, D., Tammela, M., Johansson, M., 2011. Screening procedure for determination of preservatives in commercial skin-care products. Läkemedelsverket Medical Products Agency, Uppsala, Sweden.
- Fritz, H., Weis, C.D., Winkler, T., 1976. Halogenierte Pyridine I. Die Herstellung von 3-Halogenmethylpyridinen aus dimerem Acrylnitril. *Helvetica Chimica Acta* 59, 179–190. doi:10.1002/hlca.19760590121
- Gillatt, J., 1997. The effect of redox chemistry on the efficacy of biocides in polymer emulsions. *Surface Coatings International* 80, 172–177. doi:10.1007/BF02692638
- He, K., Huang, J., Lagenaur, C.F., Aizenman, E., 2006. Methylisothiazolinone, A Neurotoxic Biocide, Disrupts the Association of Src Family Tyrosine Kinases with Focal Adhesion Kinase in Developing Cortical Neurons. *Journal of Pharmacology and Experimental Therapeutics* 317, 1320–1329. doi:10.1124/jpet.106.103044
- Jensen, C.D., Johansen, J.D., Menne, T., Andersen, K.E., 2004. Methylidibromoglutaronitrile in rinse-off products causes allergic contact dermatitis: an experimental study. *British Journal of Dermatology* 150, 90–95. doi:10.1111/j.1365-2133.2004.05727.x
- Kriegman-King, M.R., Reinhard, M., 1994. Transformation of Carbon Tetrachloride by Pyrite in Aqueous Solution. *Environmental Science & Technology* 28, 692–700. doi:10.1021/es00053a025
- Krzeminski, S.F., Brackett, C.K., Fisher, J.D., 1975. Fate of microbicidal 3-isothiazolone compounds in the environment. Modes and rates of dissipation. *Journal of Agricultural and Food Chemistry* 23, 1060–1068. doi:10.1021/jf60202a053
- Lee, W., Batchelor, B., 2002. Abiotic Reductive Dechlorination of Chlorinated Ethylenes by Iron-Bearing Soil Minerals. 1. Pyrite and Magnetite. *Environmental Science & Technology* 36, 5147–5154. doi:10.1021/es025836b
- Liu, H., Guo, B., Wang, H., Li, J., Zheng, L., 2014. Determination of Bromothalonil Residues and Degradation in Apple and Soil by QuEChERS and GC–MS/MS. *Bulletin of Environmental Contamination and Toxicology* 92, 451–454. doi:10.1007/s00128-014-1224-7
- Liu, R., Wolfe, A.L., Dzombak, D.A., Horwitz, C.P., Stewart, B.W., Capo, R.C., 2008a. Electrochemical study of hydrothermal and sedimentary pyrite dissolution. *Applied Geochemistry* 23, 2724–2734. doi:10.1016/j.apgeochem.2008.06.005
- Liu, R., Wolfe, A.L., Dzombak, D.A., Stewart, B.W., Capo, R.C., 2008b. Comparison of dissolution under oxic acid drainage conditions for eight sedimentary and hydrothermal pyrite samples. *Environmental Geology* 56, 171–182. doi:10.1007/s00254-007-1149-0
- Luther, G.W., 1987. Pyrite oxidation and reduction: Molecular orbital theory considerations. *Geochimica et Cosmochimica Acta* 51, 3193–3199. doi:10.1016/0016-7037(87)90127-X

- NIST Mass Spec Data Center, 1997. Mass Spectra, in: Linstrom, P.J., Mallard, W.G. (Eds.), NIST Chemistry WebBook, NIST Standard Reference Database Number 69. National Institute of Standards and Technology. doi:10.18434/T4D303
- Oh, S.-Y., Chiu, P.C., Cha, D.K., 2008. Reductive transformation of 2,4,6-trinitrotoluene, hexahydro-1,3,5-trinitro-1,3,5-triazine, and nitroglycerin by pyrite and magnetite. *Journal of Hazardous Materials* 158, 652–655. doi:10.1016/j.jhazmat.2008.01.078
- Park, S.-K., Kwon, J.-H., 2016. The fate of two isothiazolinone biocides, 5-chloro-2-methylisothiazol-3(2H)-one (CMI) and 2-methylisothiazol-3(2H)-one (MI), in liquid air fresheners and assessment of inhalation exposure. *Chemosphere* 144, 2270–2276. doi:10.1016/j.chemosphere.2015.10.136
- Paschka, M.G., Dzombak, D.A., 2004. Use of Dissolved Sulfur Species to Measure Pyrite Dissolution in Water at pH 3 and 6. *Environmental Engineering Science* 21, 411–420. doi:10.1089/1092875041358502
- Pellegrini, M., Bossù, E., Rotolo, M.C., Pacifici, R., Pichini, S., 2011. Simple and rapid analysis of methyl dibromo glutaronitrile in cosmetic products by gas chromatography mass spectrometry. *Journal of Pharmaceutical and Biomedical Analysis*. doi:10.1016/j.jpba.2011.07.046
- Pham, H.T., Kitsuneduka, M., Hara, J., Suto, K., Inoue, C., 2008. Trichloroethylene Transformation by Natural Mineral Pyrite: The Deciding Role of Oxygen. *Environmental Science & Technology* 42, 7470–7475. doi:10.1021/es801310y
- Rao, C.N., Hoz, S., 2012. Photostimulated Reduction of Nitriles by SmI<sub>2</sub>. *The Journal of Organic Chemistry* 77, 4029–4034. doi:10.1021/jo300383r
- Rasche, M.E., Seefeldt, L.C., 1997. Reduction of Thiocyanate, Cyanate, and Carbon Disulfide by Nitrogenase: Kinetic Characterization and EPR Spectroscopic Analysis †. *Biochemistry* 36, 8574–8585. doi:10.1021/bi970217e
- Reregistration eligibility decision for 1,2-Benzisothiazolin-3-one (BIT) (Case 3026), 1995. . U.S. Environmental Protection Agency (EPA).
- Reregistration eligibility decision for Dibromodicyanobutane (Case 2780), 1996. . U.S. Environmental Protection Agency (EPA).
- Reregistration eligibility decision for Methylene bis(thiocyanate) (Case 2415), 1997. . U.S. Environmental Protection Agency (EPA).
- Reregistration eligibility decision for Methylisothiazolinone (Case 3092), 1998. . U.S. Environmental Protection Agency (EPA).
- Scifinder, 2016. . Chemical Abstracts Service, Columbus, OH.
- Wilkinson, J.D., Shaw, S., Andersen, K.E., Brandao, F.M., Bruynzeel, D.P., Bruze, M., Camarasa, J.M.G., Diepgen, T.L., Ducombs, G., Frosch, P.J., Goossens, A., Lachappelle, J.-M., Lahti, A., Menné, T., Seidenari, S., Tosti, A., Wahlberg, J.E., 2002. Monitoring levels of preservative sensitivity in Europe. A 10-year overview (1991-2000). *Contact Derm.* 46, 207–210.
- Wittenberg, J.B., Canas, B.J., Zhou, W., Wang, P.G., Rua, D., Krynitsky, A.J., 2015. Determination of methylisothiazolinone and methylchloroisothiazolinone in cosmetic products by ultra high performance liquid chromatography with tandem mass spectrometry: Liquid Chromatography. *Journal of Separation Science* 38, 2983–2988. doi:10.1002/jssc.201500365
- Wolfe, A.L., Liu, R., Stewart, B.W., Capo, R.C., Dzombak, D.A., 2007. A method for generating uniform size-segregated pyrite particle fractions. *Geochemical Transactions* 8, 9. doi:10.1186/1467-4866-8-9

**Chapter 6**

**Conclusions and recommendations for  
future work**

## 6.1 Overall conclusions

The overall goal of this study was to understand the effect of pyrite on biocide reactivity in hydraulic fracturing. This work explored the hydrolysis and transformation of several biocides, focusing on their interaction with pyrite. Pyrite oxidizes readily in air and in aqueous solutions. As a result, this work looked at the effect of these different reactive sites on a range of biocides. These results also offer fundamental insight into the reactivity of natural pyrite by exploring the role it plays in the degradation of reactive and recalcitrant compounds. This work can also help to inform stakeholders of the organic compounds returning in flowback fluids, so that the appropriate wastewater treatment methods can be adopted prior to reuse or disposal.

The conclusions for each of the specific objectives are outlined below.

*Objective 1. To demonstrate the effect of pyrite and pyrite reaction products on the degradation of the bromine-containing biocide, DBNPA.*

For this objective, experimental work was done to quantify the degradation rates of 2,2-dibromo-3-nitrilopropionamide (or DBNPA) with pyrite and to identify the reaction products. In addition, the products were analyzed to determine the mechanism of degradation. On the addition of pyrite to DBNPA, degradation rates of the doubly brominated compound were found to increase significantly, specifically catalyzing the debromination (or reduction) of DBNPA. The intermediate product was the monobrominated analogue, 2-monobromo-3-nitrilopropionamide (or MBNPA). The amide group and nitrile groups were unaffected by pyrite. The reduction was proposed to occur via a two-electron transfer. The surface area-normalized first-order degradation rate constant was estimated at  $5.1 \text{ L}\cdot\text{m}^{-2}\cdot\text{day}^{-1}$ .

The dissolution and oxidation products of pyrite ( $\text{Fe}^{\text{II}}$ ,  $\text{S}_2\text{O}_3^{2-}$  and  $\text{SO}_4^{2-}$ ) are known reducing agents, but their reaction rates with DBNPA suggest that these species do little to contribute to the reduction of the biocide.  $\text{Fe}^{\text{II}}$  is produced on the dissolution of pyrite but had

negligible effects on the degradation of DBNPA, possibly due to a stabilizing coordination to the amide group (as in Huang and Stone, 1999). Thiosulfate ( $S_2O_3^{2-}$ ) results in the rapid reduction of DBNPA. However, concentrations of  $S_2O_3^{2-}$  are expected to be low and this strong reducing agent is too quickly depleted by DBNPA and any other oxidants to contribute to the rates observed with pyrite. Sulfate ( $SO_4^{2-}$ ) had no discernible effect on DBNPA. Taken together, the results illustrate that a surface reaction with pyrite has the ability to reduce the persistence of DBNPA, and as a consequence change the distribution of reaction products.

*Objective 2. To quantify the influence of water chemistry and interactions with pyrite on the degradation of the sulfur-containing biocide, dazomet.*

For this objective, experimental work was done to quantify the degradation rates of dazomet under a variety of conditions found in the Marcellus Shale. Dazomet readily hydrolyses in aqueous solutions and this occurs at faster rates with high temperature and dissolved  $Fe^{II}$  concentrations. The activation energy of dazomet was estimated at 60 kJ/mol. Experiments increasing  $Fe^{II}$  concentrations to 0.8 mM (roughly the average recorded Fe concentration in produced water) resulted in an increase of 190% over iron-free solutions. As concentrations as high as 10 mM have been reported, this factor has significant ability to increase the degradation of dazomet. Dazomet was found to be base-catalyzed, with half-lives ranging from 8.5 hours at pH 4.1 to 3.4 hours at pH 8.2.

In experiments with pyrite, dazomet was not degraded by the pristine pyrite surface, but rather by the oxidized pyrite surface. In solutions with the oxidized pyrite, dazomet was removed from the solution 5 times faster than the (pyrite-free) control. When measured, the concentrations of dissolved  $Fe^{II}$  and  $Fe^{III}$  from the oxidized surface were below the limit of detection, suggesting a surface reaction. The products measured were identical to those identified on hydrolysis (methyl isothiocyanate and formaldehyde). This suggests the

dithiocarbamate group in dazomet was able to chemisorb onto the oxidized pyrite surface, resulting in accelerated hydrolysis of the biocide.

*Objective 3. To identify the reactivity of various biocide functional groups due to the addition of pyrite.*

For this objective, experimental work was done to compare the degradation of dibromodicyanobutane (DBDCB), methylene bis(thiocyanate), benzisothiazolinone and methyl isothiazolinone in the presence of pyrite, under identical experimental conditions. Where possible, the degradation products of the biocides was identified or inferred. This resulted in a comparison of the hydrolysis and pyrite-induced reduction of several distinct functional groups: the bromo group, -Br; the thiocyanate groups, -SCN, the nitrile group -CN and the isothiazolinone group (heterocyclic compounds containing, nitrogen, sulfur and a carbonyl, -C=O group).

Several elimination mechanisms were identified, and tied to the reactivity of the specific functional group involved. For dibromodicyanobutane and methylene bis(thiocyanate), hydrolysis was found to be a significant elimination mechanism. Although considered stable at neutral pH, the half-lives of both biocides were roughly 30 days at pH 2. This was attributed to the fact that -Br and -SCN are good leaving groups, and dissociate from the parent compounds in aqueous solutions over time. Conversely, hydrolysis of benzisothiazolinone and methyl isothiazolinone was negligible due to the stabilizing effect of donor-acceptor interactions between the -C=O group of the isothiazolinones and cations in the solution. Pyrite was shown to reduce one of the biocides, dibromodicyanobutane with the consequent production of its debrominated daughter molecule, 2-methyleneglutaronitrile. The lability of this compound with pyrite is attributed to the ease at which the -Br group is reduced (standard redox potential for the  $\text{Br}_{2(g)}-2\text{Br}^-$  couple,  $E^\circ = 1.1 \text{ V}$ ).

## 6.2 Summary of novel contributions

Consistent with the overall goal of this work, these results contribute to our knowledge of pyrite-biocide interactions. These are summarized below:

1. *A pyrite surface-controlled reduction mechanism can transform brominated biocides used in the Marcellus Shale, reducing their persistence.*

The degradation of DBNPA and DBDCB was accelerated in the presence of pyrite. With DBNPA, it was clear that pyrite caused an increase in reduction rates but had no effect on the hydrolysis rates of this compound. For both compounds, Br<sup>-</sup> ions are released into the solution. This study is the first to illustrate that pyrite can reduce brominated compounds, due to the oxidizing potential of the organic compounds.

2. *Reaction with pyrite can alter the product distribution of biocides, and as a result change the efficacy and risks of these products.*

Pyrite may also influence the distribution of reaction products. This will be especially true for biocides that possess multiple competing elimination mechanisms or are stable in aqueous solutions. For example, DBNPA's reduced product was identified as less toxic than the parent biocide or the alternative hydrolysis product. These new or different products complicate the assessment of the efficacy of, and risk due to the use these biocides for hydraulic fracturing. However, it is important to note that the experiments with pyrite were performed at low pH where hydrolysis is relatively slow. At higher pH, hydrolysis for some compounds may outcompete reduction by pyrite. As a result, further work will be needed to extend this to higher pH.

- 3. The Fe<sup>III</sup> surface groups of pyrite accelerate the degradation of hydrolysable compounds.*

The rapid oxidation of pyrite results in Fe<sup>III</sup> groups on the surface of the mineral. In the case of dazomet, these groups were shown to catalyze the hydrolysis of the biocide. This may be a factor for other biocides possessing functional groups that coordinate to Fe<sup>III</sup>, causing a redistribution of the electrons in the molecule that leaves it open to nucleophilic attack. However, as shown, many of these organic compounds hydrolyze faster at higher pH. Therefore, the contribution of this mechanism is likely to diminish as pH increases.

- 4. The reactivity of the biocides in the Marcellus Shale can be anticipated by investigating the specific functional groups of each biocide.*

The utility of predicting reactivity based on the functionality of a compound has been exploited in the fields of chemical synthesis and pharmacology. However, exposure assessments for risk assessment rely heavily on costly and often time-consuming experiments. The experimental work in this dissertation has supplied evidence that well-established chemical properties such as the acid dissociation constant (pK<sub>a</sub>) of the conjugate acid and the standard reduction potential (E<sup>o</sup>) of the corresponding dimer can describe the reactions of these functional groups under new environmental conditions.

### **6.3 Suggestions for future work**

While this dissertation has generated some fundamental findings on biocide-pyrite interactions, the following are suggestions to further our understanding of the mechanisms occurring in this complex system.

1. *Investigation of the effect of pH on the removal of biocides from solution in the presence of pyrite.*

The effect of pH is two-fold: it may affect the hydrolysis rate of organic compounds, and may also affect the pyrite-induced reduction rates. As pyrite dissolves, the pH of the solution drops, due to dissolution of the mineral. In this work, no buffer was used as this may have affected the degradation rates observed with pyrite. As a result, all studies with pyrite were performed at low pH where hydrolysis is limited. Fracking fluid in carbonate-rich formations very quickly becomes alkaline, with pH up to 8.4 being recorded (Barbot et al., 2013). Thus, it is important to consider the importance of alkaline conditions to the pyrite-biocide interactions. At higher pH, the hydrolysis rates of organic compounds will increase significantly. But research suggests that reduction rates will increase as well (Weerasooriya and Dharmasena, 2001; Oh et al., 2008). Future work is needed to investigate the effect of pH on the contribution of pyrite as an elimination mechanism.

2. *Characterization of the mineral phases leading to catalysis of dazomet hydrolysis.*

In this work, the oxidized pyrite surface was shown to catalyze the hydrolysis of dazomet. Studies suggest that pyrite is oxidized to form ferric (hydroxy)sulfate and ferric oxyhydroxide (Todd et al., 2002; Dos Santos et al., 2016). In this study, characterization of the surface using techniques such as X-ray absorption spectroscopy (XAS) was not possible. However, surface characterization will give insight into the iron-bearing phases that are responsible for the observed increase in the rate of hydrolysis. This in turn can be used to discern the conditions that favor this reaction.

3. *Investigation of the effect of salinity on the reduction of biocides.*

The produced water generated from the Marcellus Shale is hypersaline, with a median salinity of 250,000 mg/L from the Marcellus Shale (Rowan et al., 2011). Salinity affects both the

mineral surface and the activity of the organic biocides. Increasing the ionic strength of the surrounding fluid generally compresses the double layer. This could greatly decrease the accessibility of reactive pyrite sites to the organic compounds (Su and Puls, 2004). On the other hand, dissolved metal cations may enhance the interaction of the organic species with the pyrite surface (Bebié and Schoonen, 2000). Furthermore, high ionic strengths decrease the aqueous solubility of organic compounds (Burant et al., 2017), which further complicates our ability to predict biocide-mineral interactions at high ionic strengths

#### *4. Examination of the effect of reducing organic compounds on the pyrite surface.*

This work has focused on the influence of pyrite on the persistence of biocides and has shown that pyrite can accelerate the degradation of certain biocides. However, additional work is needed to characterize the reciprocal effect on the pyrite surface. Molecular orbital theory posits that when pyrite reduces a dissolved ion or organic compound, it is itself oxidized to form thiosulfate,  $S_2O_3^{2-}$  (Luther, 1987). Kriegman-King and Reinhard (1994) investigated the pyrite surface using x-ray photoelectron spectroscopy (XPS) after a small amount of carbon tetrachloride had been reduced by pyrite. Under anoxic conditions, they found no change to the sulfur groups, although calculations indicate that the concentration of reacted surface sites may have been too low to be detected. They did note significant leaching of the iron from the surface, which increased the S:Fe<sup>II</sup> ratio from 2.1 to 4. Changes to the shale minerals can have a pronounced effect on the permeability of the shale (Harrison, 2017). Therefore a more thorough investigation of effect of organic compounds on the pyrite surface can aid in predicting how the formation will change over time.

#### *5. Evaluation of the competition and inhibition by O<sub>2</sub> and other oxidizing compounds*

These experiments have been performed largely under anoxic conditions. However, in real systems, biocides are expected to face significant competition for pyrite reactive surfaces

due to the presence of other organics additives. Some organics such as petroleum distillates may simply sorb to the shale, protecting the pyrite surface. Others such as persulfates are strong oxidizing agents and consequently, they may oxidize reactive pyrite sites (Tasker, 2016). In addition, if the fracking fluid contains dissolved oxygen during the shut-in period, molecular oxygen will compete for these reactive groups as well.

#### *6. Experimentation with sedimentary and amorphous pyrite.*

Because of its commercial availability, these studies used framboidal hydrothermal pyrite to as an initial step in determining possible interactions with organic biocides and pyrite. A logical next step would be to perform similar experiments on sedimentary pyrite, specifically samples from the Marcellus Shale or another producing shale gas formation. In particular, the ratios of trace elements (for example, Cu, Ni, Zn) may differ between samples and this may have small, but noticeable effects on pyrite induced degradation rates (Huang et al., 2015; Liu et al., 2008).

In addition to the source of pyrite, pyrite morphology should also be considered. Pyrite morphology varies as a function of the conditions under which it was produced (Alonso-Azcárate et al., 2001; Wang and Morse, 1996). Various crystal morphologies and aggregates may be present within one shale formation (such as in Wignall and Newton, 1998). The non-framboidal pyrite may have different dissolution and reaction rates (Liu et al., 2008). Thus, experimental work should be done to investigate the effect alternate pyrite textures on other biocide reactivity.

#### *7. Understanding the contribution of pyrite in complex and changing shale matrices.*

To understand the mechanisms of degradation of organics due to pyrite, this work was performed under very controlled conditions to isolate the effect of pyrite. However, as highlighted in Chapter 2, the shale mineral interface is a complex mixture of minerals. The rock

composition varies significantly between shale formations and even within the same shale play (Chalmers et al., 2012; Chermak and Schreiber, 2014). In addition to this, on exposure to the hydraulic fracturing fluid, mineral dissolution and precipitation occurs, changing the distribution of minerals from that of pristine shale samples (Jew et al., 2017; Marcon et al., 2017). Experiments with real shale samples can be optimized to investigate the reactivity of biocides to determine the extent to which pyrite contributes to the transformation of these organic compounds used in hydraulic fracturing.

*8. Development of analytical methods to measure biocides and their degradation products at relevant concentrations.*

Biocides, in general, are harmful to human and ecological health at very low concentrations. However, for many of these compounds the limit of detection is very high (particularly for compounds that rely on HPLC with UV-visible detection) or their detection requires multiple steps (that is, compounds that need to be derivatized). For these biocides, there is a need to develop rapid and simple ways to quantify them at concentrations near to the quoted toxicity values. One interesting approach may to develop and validate assays that can measure non-specific toxicity. This will be especially useful for the complex produced water matrices and will enable rapid detection in the field, without expensive analytical instruments.

## 6.4 References

- Alonso-Azcárate, J., Rodas, M., Fernández-Díaz, L., Bottrell, S.H., Mas, J.R., López-Andrés, S., 2001. Causes of variation in crystal morphology in metamorphogenic pyrite deposits of the Cameros Basin (N Spain): Crystal Morphology in Pyrite Deposits. *Geological Journal* 36, 159–170. doi:10.1002/gj.889
- Barbot, E., Vidic, N.S., Gregory, K.B., Vidic, R.D., 2013. Spatial and Temporal Correlation of Water Quality Parameters of Produced Waters from Devonian-Age Shale following Hydraulic Fracturing. *Environmental Science & Technology* 47, 2562–2569. doi:10.1021/es304638h
- Bebié, J., Schoonen, M.A.A., 2000. Pyrite surface interaction with selected organic aqueous species under anoxic conditions. *Geochemical Transactions* 1, 47. doi:10.1039/b005581f
- Burant, A., Lowry, G.V., Karamalidis, A.K., 2017. Measurement and Modeling of Setschenow Constants for Selected Hydrophilic Compounds in NaCl and CaCl<sub>2</sub> Simulated Carbon Storage Brines. *Accounts of Chemical Research* 50, 1332–1341. doi:10.1021/acs.accounts.6b00567
- Chalmers, G.R., Bustin, R.M., Power, I.M., 2012. Characterization of gas shale pore systems by porosimetry, pycnometry, surface area, and field emission scanning electron microscopy/transmission electron microscopy image analyses: Examples from the Barnett, Woodford, Haynesville, Marcellus, and Doig units. *AAPG Bulletin* 96, 1099–1119. doi:10.1306/10171111052
- Chermak, J.A., Schreiber, M.E., 2014. Mineralogy and trace element geochemistry of gas shales in the United States: Environmental implications. *International Journal of Coal Geology* 126, 32–44. doi:10.1016/j.coal.2013.12.005
- Dos Santos, E.C., de Mendonça Silva, J.C., Duarte, H.A., 2016. Pyrite Oxidation Mechanism by Oxygen in Aqueous Medium. *The Journal of Physical Chemistry C* 120, 2760–2768. doi:10.1021/acs.jpcc.5b10949
- Harrison, A.L., Jew, A.D., Dustin, M.K., Thomas, D.L., Joe-Wong, C.M., Bargar, J.R., Johnson, N., Brown, G.E., Maher, K., 2017. Element release and reaction-induced porosity alteration during shale-hydraulic fracturing fluid interactions. *Applied Geochemistry* 82, 47–62. doi:10.1016/j.apgeochem.2017.05.001
- Huang, C.-H., Stone, A.T., 1999. Hydrolysis of Naptalam and Structurally Related Amides: Inhibition by Dissolved Metal Ions and Metal (Hydr)Oxide Surfaces. *Journal of Agricultural and Food Chemistry* 47, 4425–4434. doi:10.1021/jf990423o
- Huang, X.-W., Gao, J.-F., Qi, L., Zhou, M.-F., 2015. In-situ LA-ICP-MS trace elemental analyses of magnetite and Re–Os dating of pyrite: The Tianhu hydrothermally remobilized sedimentary Fe deposit, NW China. *Ore Geology Reviews* 65, 900–916. doi:10.1016/j.oregeorev.2014.07.020
- Jew, A.D., Dustin, M.K., Harrison, A.L., Joe-Wong, C.M., Thomas, D.L., Maher, K., Brown, G.E., Bargar, J.R., 2017. Impact of Organics and Carbonates on the Oxidation and Precipitation of Iron during Hydraulic Fracturing of Shale. *Energy & Fuels* 31, 3643–3658. doi:10.1021/acs.energyfuels.6b03220
- Kriegman-King, M.R., Reinhard, M., 1994. Transformation of Carbon Tetrachloride by Pyrite in Aqueous Solution. *Environmental Science & Technology* 28, 692–700. doi:10.1021/es00053a025
- Liu, R., Wolfe, A.L., Dzombak, D.A., Stewart, B.W., Capo, R.C., 2008. Comparison of dissolution under oxic acid drainage conditions for eight sedimentary and hydrothermal pyrite samples. *Environmental Geology* 56, 171–182. doi:10.1007/s00254-007-1149-0

- Luther, G.W., 1987. Pyrite oxidation and reduction: Molecular orbital theory considerations. *Geochimica et Cosmochimica Acta* 51, 3193–3199. doi:10.1016/0016-7037(87)90127-X
- Oh, S.-Y., Chiu, P.C., Cha, D.K., 2008. Reductive transformation of 2,4,6-trinitrotoluene, hexahydro-1,3,5-trinitro-1,3,5-triazine, and nitroglycerin by pyrite and magnetite. *Journal of Hazardous Materials* 158, 652–655. doi:10.1016/j.jhazmat.2008.01.078
- Marcon, V., Joseph, C., Carter, K.E., Hedges, S.W., Lopano, C.L., Guthrie, G.D., Hakala, J.A., 2017. Experimental insights into geochemical changes in hydraulically fractured Marcellus Shale. *Applied Geochemistry* 76, 36–50. doi:10.1016/j.apgeochem.2016.11.005
- Rowan, E., Engle, M.A., Kirby, C.S., Kraemer, T.F., 2011. Radium content of oil-and gas-field produced waters in the northern Appalachian Basin (USA)—Summary and discussion of data. US Geological Survey Scientific Investigations Report 5135, 2011.
- Su, C., Puls, R.W., 2004. Nitrate Reduction by Zerovalent Iron: Effects of Formate, Oxalate, Citrate, Chloride, Sulfate, Borate, and Phosphate. *Environmental Science & Technology* 38, 2715–2720. doi:10.1021/es034650p
- Tasker, T.L., Piotrowski, P.K., Dorman, F.L., Burgos, W.D., 2016. Metal Associations in Marcellus Shale and Fate of Synthetic Hydraulic Fracturing Fluids Reacted at High Pressure and Temperature. *Environmental Engineering Science* 33, 753–765. doi:10.1089/ees.2015.0605
- Todd, E., Sherman, D., Purton, J., 2003. Surface oxidation of pyrite under ambient atmospheric and aqueous (pH = 2 to 10) conditions: electronic structure and mineralogy from X-ray absorption spectroscopy. *Geochimica et Cosmochimica Acta* 67, 881–893. doi:10.1016/S0016-7037(02)00957-2
- Wang, Q., Morse, J.W., 1996. Pyrite formation under conditions approximating those in anoxic sediments I. Pathway and morphology. *Marine Chemistry* 52, 99–121. doi:10.1016/0304-4203(95)00082-8
- Weerasooriya, R., Dharmasena, B., 2001. Pyrite-assisted degradation of trichloroethene (TCE). *Chemosphere* 42, 389–396.
- Wignall, P.B., Newton, R., 1998. Pyrite framboid diameter as a measure of oxygen deficiency in ancient mudrocks. *American Journal of Science* 298, 537–552. doi:10.2475/ajs.298.7.537

**Appendix A      Supporting information for Chapter 3**

Table A-1. Data for Figures 3-2 and 3-4

<b>Time Elapsed (hours)</b>	<b>Concentration of MBNPA (mM)</b>	<b>Moles of DBNPA reacted (mM)</b>
<b>15 g/L pyrite</b>		
0.0	0.032	0.013
0.6	0.177	0.226
1.6	0.287	0.391
3.2	0.390	0.546
<b>10 g/L pyrite</b>		
1.4	0.121	0.130
3.8	0.309	0.410
4.3	0.327	0.569
<b>5g/L pyrite</b>		
0.9	0.077	0.062
3.3	0.195	0.223
5.8	0.290	0.361
8.0	0.448	0.449
<b>0 g/L pyrite</b>		
0.3	n.d.	-
2.7	n.d.	-
4.5	n.d.	-
6.7	n.d.	-
9.4	n.d.	-

Table A-2. Data for Figure 3-5.

<b>Time elapsed (Hours)</b>	<b>Concentration DBNPA (mM)</b>
<b>0 mM Fe (II)</b>	
0.8	1.062
2.1	1.046
3.4	1.031
5.2	1.046
8.1	1.047
10.9	1.057
21.4	1.024
29.0	0.968
33.8	0.978
38.7	0.993
43.5	0.895
48.3	0.920
<b>1 mM Fe (II)</b>	
0.3	1.063
2.9	1.078
4.7	1.052
7.5	1.055
10.3	1.091
13.2	1.087
17.0	1.058
20.8	1.054
24.7	1.036
28.5	1.042
33.3	1.038
38.1	1.042
42.9	1.023
47.8	1.024

Table A-3. Data for control/blank and NaCl samples in Figures 3-6, 3-7, and 3-8

<b>Time Elapsed (hours)</b>	<b>Concentration of DBNPA (mM)</b>	<b>Concentration of MBNPA (mM)</b>	<b>Concentration of DBAN (mM)</b>
<b>Control (no added salt)</b>			
0.0	1.67	n.d.	0.07
1.5	1.61	n.d.	0.06
3.3	1.60	n.d.	n.d.
5.1	1.59	n.d.	0.10
8.3	1.48	0.08	0.05
14.4	1.41	0.11	0.09
20.2	1.30	0.14	0.09
35.2	1.02	0.21	0.12
65.0	0.63	0.29	0.12
64.7	0.70	0.29	0.14
49.9	0.83	0.25	0.11
<b>2 mM NaCl</b>			
0.0	1.67	n.d.	0.05
1.5	1.67	n.d.	0.04
3.3	1.59	n.d.	0.09
5.1	1.63	n.d.	0.07
8.3	1.53	0.07	0.10
14.4	1.39	0.11	0.10
20.1	1.30	0.13	0.09
35.2	1.05	0.20	0.13
49.9	0.82	0.25	0.11
64.7	0.67	0.30	0.12

Table A-4. Data for Figures 3-6 and 3-7

<b>Time Elapsed (hours)</b>	<b>Concentration of DBNPA (mM)</b>	<b>Concentration of MBNPA (mM)</b>	<b>Concentration of DBAN (mM)</b>
<b>1 mM CuCl<sub>2</sub></b>			
0.0	1.60	n.d.	0.52
0.7	1.52	0.05	0.41
1.8	1.35	0.10	0.45
2.4	1.25	0.11	0.41
3.7	1.05	0.20	0.47
4.2	1.02	0.19	0.42
5.6	0.76	0.25	0.46
6.0	0.70	0.27	0.41
8.8	0.29	0.36	0.47
9.2	0.23	0.37	0.44
15.0	n.d.	0.24	0.60
15.3	n.d.	0.24	0.52
36.1	n.d.	0.00	0.84
<b>1 mM NiCl<sub>2</sub></b>			
1.6	1.66	n.d.	0.04
3.6	1.65	n.d.	0.06
5.4	1.65	n.d.	0.05
8.6	1.57	n.d.	0.09
14.8	1.43	0.05	0.06
20.7	1.33	0.09	0.09
35.5	1.11	0.13	0.09
50.5	0.91	0.19	0.11
65.3	0.72	0.29	0.11

Table A-5. Data for Figure 3-8

<b>Time Elapsed (hours)</b>	<b>Concentration of DBNPA (mM)</b>	<b>Concentration of MBNPA (mM)</b>	<b>Concentration of DBAN (mM)</b>
<b>1 mM NaSO<sub>4</sub></b>			
0.0	1.71	0.00	0.00
0.9	1.68	0.00	0.00
1.9	1.67	0.00	0.00
2.5	1.67	0.00	0.00
3.9	1.63	0.00	0.00
5.7	1.65	0.00	0.00
8.9	1.58	0.00	0.00
15.1	1.43	0.08	0.00
21.2	1.37	0.11	0.00
35.9	1.18	0.17	0.00
51.0	1.00	0.22	0.00
65.7	0.83	0.26	0.00
<b>1 mM Na<sub>2</sub>S<sub>2</sub>SO<sub>3</sub></b>			
0.0	0.47	0.82	0.06
0.3	0.37	0.92	0.14
0.6	0.39	0.87	0.11
0.9	0.37	0.87	0.09
1.3	0.37	0.88	0.10
1.9	0.37	0.87	0.14
2.5	0.33	0.88	0.03
3.9	0.37	0.91	0.13
4.5	0.36	0.91	0.14
5.7	0.34	0.90	0.13
6.3	0.34	0.93	0.12
9.5	0.33	0.93	0.13
12.3	0.28	0.97	0.15

**Appendix B      Supporting information for Chapter 4**

Table B-1. Data for Figure 4-2

Time elapsed (Hours)	Concentration of Dazomet ( $\mu\text{m}$ )			
	pH 3	pH 4.1	pH 8.2	pH 9.5
0.00	83.68	78.16	71.43	62.93
0.48	87.02	80.88	68.43	55.61
1.23	84.63	78.37	61.74	43.17
1.98	81.54	75.09	54.60	33.09
2.98	74.75	68.19	44.60	22.76
3.97	68.72	63.22	37.03	15.42
4.97	63.45	57.85	30.21	10.29
6.22	56.04	50.91	23.17	6.33
7.47	50.37	46.02	18.35	3.82
8.70	46.00	41.50	14.39	2.43
9.95	41.23	37.36	11.24	1.46

Table B-2. Data for Figure 4-3

<b>Time Elapsed (hours)</b>	<b>Concentration dazomet (<math>\mu\text{m}</math>)</b>
<b>0 mM Fe(II) Cl</b>	
0.2	69.84
0.8	65.66
1.3	62.48
2.2	56.96
4.1	46.78
6.0	37.75
8.0	30.01
9.9	24.02
14.8	13.59
19.7	8.86
<b>0.4 mM Fe(II) Cl</b>	
0.1	70.83
0.6	61.68
1.2	53.76
2.1	45.00
4.0	37.27
5.9	29.75
7.8	20.58
9.8	19.60
14.7	9.01
19.6	4.37
<b>0.8 mM Fe(II) Cl</b>	
0.0	59.34
0.5	59.96
1.1	62.55
2.0	48.36
3.9	26.75
5.8	11.13
7.7	5.80
9.6	6.25
14.5	3.77
19.5	3.61

Table B-3. Data for Figure 4-4

<b>Time elapsed (hours)</b>	<b>Concentration of dazomet(<math>\mu\text{m}</math>)</b>
<b>Temperature = 34C</b>	
0.00	
0.07	179.56
0.45	151.58
1.30	98.55
2.13	62.60
3.77	26.95
4.97	13.52
5.77	2.42
<b>Temperature = 49C</b>	
0.00	170.42
0.17	158.23
0.38	110.63
0.52	87.29
0.75	61.64
0.92	46.43
1.20	27.61
1.43	17.70
<b>Temperature = 49C</b>	
0.00	174.17
0.12	109.56
0.25	73.32
0.38	50.63
0.52	36.77
0.67	26.71
0.85	18.13
1.07	12.40

Table B-4. Data for Figure 4-6

<b>Time elapsed (hours)</b>	<b>Concentration of pyrite</b>
<b>Control, 0 g/L pyrite</b>	
0.0	0.870
0.7	0.945
1.9	0.886
9.0	0.710
<b>Oxidized pyrite, 20 g/L</b>	
0.0	0.837
0.7	0.713
1.9	0.535
9.0	n.d.
<b>Unoxidized pyrite, 20 g/L</b>	
0.0	0.983
0.7	0.871
2.1	0.876
9.2	0.646

**Appendix C      Supporting information for Chapter 5**

Table C-1. Data for Figure 5-1

<b>Time Elapsed (days)</b>	<b>Concentration (mM)</b>
<b>0 g/L pyrite, pH = 2.7</b>	
0	0.307
2	0.282
6	0.281
9	0.257
13	0.244
<b>0 g/L pyrite, pH = 5.1</b>	
0	0.376
2	0.355
4	0.356
6	0.346
10	0.379
<b>100 g/L pyrite, pH = 2.1</b>	
0	0.376
2	0.355
4	0.356
6	0.346
10	0.379

Table C-2. Data for Figure 5-3.

<b>Time elapsed (days)</b>	<b>Concentration MBT (mM)</b>
<b>100 g/L Pyrite, pH = 2.1</b>	
0.0	0.865
3.7	0.764
6.7	0.689
12.6	0.538
<b>0 g/L Pyrite, pH = 2.1</b>	
0.0	0.896
2.2	0.854
6.0	0.816
8.7	0.755
12.6	0.616

Table C-3. Data for Figure 5-4

<b>Time elapsed (days)</b>	<b>BIT Concentration (mM)</b>		<b>MIT Concentration (mM)</b>	
	0 g/L pyrite, pH = 2.7	100 g/L pyrite, pH = 2.9	0 g/L pyrite, pH = 2.7	100 g/L pyrite, pH = 2.9
0	0.689	0.665	0.895	0.879
1	0.644	0.663	0.881	0.879
3	0.669	0.664	0.802	0.879
8	0.659	0.675	0.956	0.877

**Appendix D    Structure-reactivity relationships to predict  
pyrite induced reduction of organic compounds**

## D.1 Background on structure-activity relationships

A useful tool may lie in developing a structure-activity relationship to describe the reactivity of these biocides with pyrite. These relationships assume a correlation between the structural and physicochemical properties of a molecule and its environmental reactivity (Walker et al., 2003; Tropsha et al., 2003; Nirmalakhandan & Spence, 1988). Structure-activity relationships have been established for other abiotic transformations in the environment. Zhao et al. (2001) found  $E_{LUMO}$  to be a significant descriptor in developing a structure-activity relationship between the first order reduction kinetics of 13 halogenated aliphatics in anoxic sediment slurries, explaining 81% in the variability of the rates. The compound's molecular weight and average molecular polarizability also contributed to the variation of the reduction rates. Conversely, the energy of the highest occupied molecular orbital,  $E_{HOMO}$ , was the variable that was most able to predict the oxidation rates of 78 aromatic compounds by hydroxyl radical reaction (Kušić et al., 2009). These studies highlight the insight gained by using structure-activity relationships in connecting our theoretical understanding of electron transfer between molecular orbitals to observable redox reactions in the environment.

Such relationships have yet to be published for pyrite reactivity. Our greatest insight comes from data published by Lee and Batchelor (2002) who investigated the rate of the abiotic reductive dechlorination of homologous chlorinated ethenes by pyrite. To explore the quantum chemical parameters which can be used to predict the reactivity of these organic compounds with pyrite, we modeled each of these compounds to obtain electronic descriptors with the semi-empirical computational software package MOPAC2016 (Stewart Computational Chemistry, CO). For this model we included the following keywords: GNORM=0.0, BAR=0.03, RELSCF=0.01, STATIC, AM1. The results in Figure D-1 show that  $E_{LUMO}$  explains 93% of the variability in the rates of dechlorination of tetrachloroethylene (perchloroethylene, PCE),

trichloroethylene (TCE), *cis*- dichloroethylene (*cis*-DCE) and chloroethene (vinyl chloride, VC). Thus,  $E_{LUMO}$  shows significant potential as a variable that is able to account for variations in the observed reduction rates of organic compounds.

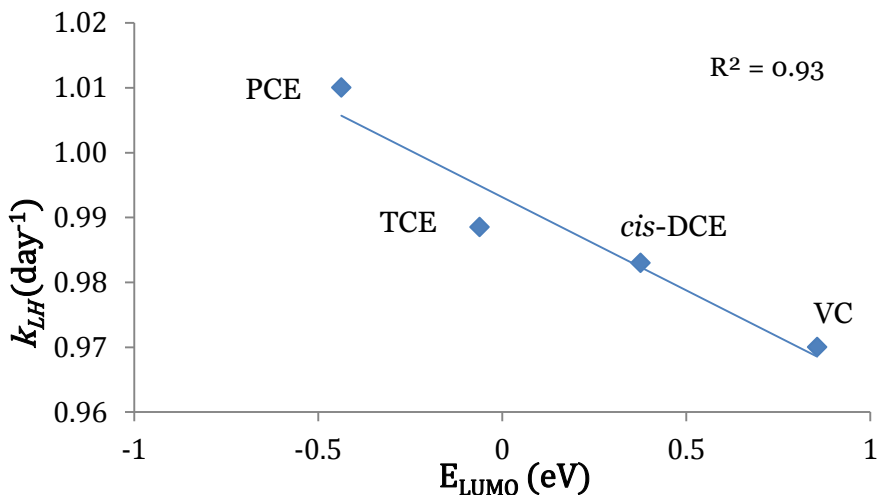


**Figure D-1. Best fit for the Langmuir-Hinshelwood (LH) reduction rate constant of chlorinated ethenes with pyrite as a function the  $E_{LUMO}$  of the chlorinated ethenes (AM1 semi-empirical method).**

In the body of this work, the pyrite-induced reduction rates of several biocides were compared. This research showed that structure-activity relationships are likely only applicable to compounds in which the transfer of electrons to the compound is the rate-limiting step. For example, homologous chlorinated compounds such as those shown in (Figure D-1) are more likely to correlate as the chlorine group is easily reduced (standard redox potential,  $E^{\circ}_H = 1. \text{ V}$  for the  $\text{Na}_2\text{SO}_4\text{- Na}_2\text{S}_2\text{O}_3$  couple). In this case, the transfer of electrons to the compound (quantified by  $E_{LUMO}$  is the rate-limiting step). Thus,  $E_{LUMO}$  describes the overall rate. However, for groups such as the thiocyanate (-SCN) functionality in methylene bis(thiocyanate) (Table 5-3), the rate limiting factor is the reduction of the specific group, so the rate of these reactions is governed by the standard reduction potential ( $E^{\circ}$ ) of the functional group, in this case, -SCN.

To summarize, our literature review has shown that there are no studies investigating the effect of pyrite on biocides in the Marcellus Shale, and very little information to offer insight into the possible reactions. Pyrite was identified as a significant factor affecting the fate of organic

compounds. Two possible mechanisms are suggested for the transformation of organics in the presence of pyrite. The first is a transfer of electrons between the S<sub>2</sub> dimer and the organic compound. This results in reduction or oxidation of the organic. The second mechanism is the *in situ* production of hydroxyl radicals due to the transformation of pyrite Fe defects. This would lead to oxidation of the organic. Most of these published experiments were performed on recalcitrant chloride-containing compounds. And while structure-activity relationships have been proposed for other abiotic transformations (for example Colón et al., 2006; Zhao et al., 2001; Kušić et al., 2009), none have yet been presented to predict the degradation of organics due to pyrite nor have shed light on pyrite interactions with hydraulic fracturing biocides. Additionally, at a more fundamental level, they have yet to ascertain the molecular factors that drive the degradation of organic compounds with pyrite.

## D.2 References

- Colón, D., Weber, E.J., Anderson, J.L., 2006. QSAR study of the reduction of nitroaromatics by Fe (II) species. *Environmental science & technology* 40, 4976–4982.
- Kušić, H., Rasulev, B., Leszczynska, D., Leszczynski, J., Koprivanac, N., 2009. Prediction of rate constants for radical degradation of aromatic pollutants in water matrix: A QSAR study. *Chemosphere* 75, 1128–1134. doi:10.1016/j.chemosphere.2009.01.019
- Lee, W., Batchelor, B., 2002. Abiotic Reductive Dechlorination of Chlorinated Ethylenes by Iron-Bearing Soil Minerals. 1. Pyrite and Magnetite. *Environmental Science & Technology* 36, 5147–5154. doi:10.1021/es025836b
- MOPAC2016, [HTTP://OpenMOPAC.net/](http://OpenMOPAC.net/), Version 16.299W, J.J.P. Stewart, Stewart Computational Chemistry, Colorado Springs, CO, USA
- Nirmalakhandan, N., Speece, R.E., 1988. ES Critical Review: Structure-activity relationships. Quantitative techniques for predicting the behavior of chemicals in the ecosystem. *Environmental Science & Technology* 22, 606–615. doi:10.1021/es00171a002
- Tropsha, A., Gramatica, P., Gombar, V.K., 2003. The importance of being earnest: validation is the absolute essential for successful application and interpretation of QSPR models. *QSAR & Combinatorial Science* 22, 69–77.
- Walker, J.D., Jaworska, J., Comber, M.H.I., Schultz, T.W., Dearden, J.C., 2003. Guidelines for Developing and Using Quantitative Structure-Activity Relationships. *Environmental Toxicology and Chemistry* 22, 1653. doi:10.1897/01-627
- Zhao, H., Chen, J., Quan, X., Yang, F., Peijnenburg, W., 2001. Quantitative structure–property relationship study on reductive dehalogenation of selected halogenated aliphatic hydrocarbons in sediment slurries. *Chemosphere* 44, 1557–1563.